

**EXPERIMENTAL EXAMINATION OF PARTIAL
OCCLUSION ACUTE MYOCARDIAL
ISCHEMIA**

by
Brian Zenger

A dissertation submitted to the faculty of
The University of Utah
in partial fulfillment of the requirements for the degree of

Doctor of Philosophy

Department of Biomedical Engineering
The University of Utah
August 2021

Copyright © Brian Zenger 2021

All Rights Reserved

The University of Utah Graduate School

STATEMENT OF DISSERTATION APPROVAL

The dissertation of Brian Zenger
has been approved by the following supervisory committee members:

<u>Robert S. MacLeod</u> ,	Chair(s)	<u>5/29/2021</u> Date Approved
<u>Frank B. Sachse</u> ,	Member	<u>5/26/2021</u> Date Approved
<u>Ravi Ranjan</u> ,	Member	<u>5/26/2021</u> Date Approved
<u>Lucas Timmins</u> ,	Member	<u>5/26/2021</u> Date Approved
<u>Vikas Sharma</u> ,	Member	<u>5/27/2021</u> Date Approved

by David W. Grainger , Chair/Dean of
the Department/College/School of Engineering
and by David B. Kieda , Dean of The Graduate School.

ABSTRACT

The most common reason for a patient to visit the emergency department is chest pain caused by myocardial ischemia. Myocardial ischemia develops from inadequate perfusion of myocardial tissue and indicates the presence of surprising range of conditions, including coronary artery disease, coronary microvascular dysfunction, Takotsubo cardiomyopathy, and coronary artery dissection, and other potentially fatal cardiac diseases. If left untreated, the long-term effects of these diseases can lead to significant decreases in quality of life and increased mortality. Current noninvasive tests to detect ischemia may be limited by an incomplete understanding of the mechanisms used to induce the stress (exercise or pharmacological agents) or the limited understanding of how ischemic signals change over time. These limitations increase the risk for failed detection of deadly cardiac diseases and explain the unsatisfactory accuracy of current diagnostic and monitoring approaches.

The goal of this dissertation was to leverage recent experimental findings and breakthroughs about the onset and progression of ischemia as the basis for a comprehensive re-evaluation of acute myocardial ischemia. First, we refined our experimental model to include comprehensive electrical measurements sampled simultaneously from within the myocardium, on the heart surface, and on the torso surface. We then built on our experience with our novel large-animal experimental models of ischemia to measure and characterize the electrical changes that arise during acute myocardial ischemia created from various types of ischemic stress. We also explored possible mechanistic drivers for these differences. Finally, we assessed the transient changes common to ischemic signatures, including the appearance and disappearance of ischemic potentials as recorded from epicardial and torso surface measurements.

For all who have supported me

CONTENTS

ABSTRACT	iii
LIST OF TABLES	vii
CHAPTERS	
1. INTRODUCTION	1
1.1 Motivation for Research	1
1.2 Introduction to Doctoral Research	3
1.3 References	6
2. BACKGROUND	10
2.1 Electrical Sources and Volume Conductors: A Cardiac Application .	10
2.2 Changes to the Cardiac Source and Volume Conductor During Acute Myocardial Ischemia	15
2.3 Experimental Models of Acute Myocardial Ischemia	22
2.4 Electrical Detection of Acute Myocardial Ischemia in the Clinical Setting	25
2.5 References	28
3. NOVEL EXPERIMENTAL MODEL FOR STUDYING THE SPATIOTEMPORAL ELECTRICAL SIGNATURE OF ACUTE MYOCARDIAL ISCHEMIA: A TRANSLATIONAL PLATFORM	35
3.1 Abstract	36
3.2 Introduction	36
3.3 Methods	37
3.4 Results	41
3.5 Discussion	44
3.6 Acknowledgements	47
3.7 Author Contributions	47
3.8 Grant Support	48
3.9 References	48
4. PHARMACOLOGICAL AND SIMULATED EXERCISE CARDIAC STRESS TESTS PRODUCE DIFFERENT ISCHEMIC SIGNATURES IN HIGH-RESOLUTION EXPERIMENTAL MAPPING STUDIES	52
4.1 Abstract	52
4.2 Introduction	53
4.3 Methods	55

4.4	Results	64
4.5	Discussion	71
4.6	Conclusion	78
4.7	References	79
5.	TRANSIENT RECOVERY OF EPICARDIAL AND TORSO ST-SEGMENT ISCHEMIC SIGNALS DURING CARDIAC STRESS TESTS: A POSSIBLE PHYSIOLOGICAL MECHANISM	83
5.1	Abstract	83
5.2	Introduction	84
5.3	Methods.....	86
5.4	Results	90
5.5	Discussion	95
5.6	Limitations	102
5.7	Acknowledgments	102
5.8	Grant Support	103
5.9	References	103
6.	CONCLUDING REMARKS	106
6.1	Development of a Translational Experimental Model	106
6.2	Contributions to Knowledge of Acute Myocardial Ischemia Development.....	109
6.3	Providing Meaningful Clinical Insights From Experimental Studies .	111
6.4	Future Work	112
6.5	References	114

LIST OF TABLES

3.1	Recorded torso potentials prior to sternotomy, with no sock or needle electrodes placed, compared to those acquired after placement of the cardiac electrodes and closure of the chest. Values were the mean and standard deviations across all torso electrodes.	45
3.2	Recorded epicardial sock potentials before, 30 minutes after, and 90 minutes after placement of needle electrodes. Values were the mean and standard deviations across all sock electrodes	45
3.3	Table showing the recorded voltages separated by canine, porcine, and different recording surfaces. S and AP stand for Sinus and Atrial Paced recordings, respectively, QRS Amp and VRange stand for QRS peak to peak amplitude and voltage range across all electrodes, respectively. Each metric was derived from each individual electrode . .	45
3.4	Table showing the recorded time intervals in canine vs. porcine subjects. Each metric was derived from the from a manual marking of the root-mean-squared (RMS) signal.	46
4.1	Dobutamine infusion rates and heart rate increase by stage within an intervention	60

CHAPTER 1

INTRODUCTION

1.1 Motivation for Research

The most common reason for a visit to the emergency department is chest pain caused by myocardial ischemia [1], [2]. These acute ischemic events cause the stereotypical crushing chest pain that ceases after rest, i.e., after removal of the cardiac stress [3], [4]. A surprising range of pathologies can cause acute transient ischemia, including coronary artery disease, coronary microvascular dysfunction, Takotsubo cardiomyopathy, and coronary artery dissection [1], [5]–[7]. Each carries a significant risk of short- and long-term mortality that can be reduced substantially by early detection [6]. Therefore, detecting myocardial ischemia early is paramount to prevent long-term negative consequences [1], [8], [9].

Ischemia develops when the perfusion to a specific region of the heart is inadequate [10], [11]. Such inadequate perfusion, in combination with cardiac stress, leads to acute changes in the tissue that eventually result in cell death. Well before this cell death, an insufficient supply of oxygen and other nutrients in combination with poor metabolite removal creates a toxic extracellular milieu that prevents cardiomyocytes from functioning normally [3], [12]. However, the individual and collective effects of the mode of cardiac stress, the timing of development, and signal manifestations of these acute ischemic events have not been fully elucidated.

The first step to improving detection of acute ischemia is to understand the associated electrical sources. Experimental models used previously have documented the cellular, tissue, and whole organ manifestations of myocardial ischemia [13]–[20]. Holland and Brooks et al. performed the first detailed and comprehensive animal studies in the late 1970s and documented the electrical changes that occurred during myocardial ischemia at the tissue and organ scales [13], [14], driving much of the conventional clinical thinking, including the idea that ischemia

first develops near the endocardial border and progresses radially toward the epicardium [3], [13], [14]. Recently, our group has improved this experimental model by increasing the temporal sampling and recording electrode density in the myocardium and on the heart surface [21]–[23]. Our studies have shown distinctly different patterns of ischemia that initiate throughout the myocardial wall, which has motivated a complete reevaluation of the electrical sources created during ischemia. However, limits to the translational potential of our recent experimental models include, first, the lack of body-surface ECG recordings during controlled ischemia and, second, the absence of clinically relevant ischemic induction. We addressed these limitations in the first aim of this dissertation, the result of which is the most detailed and translational model of acute ischemia to date. In our model, we measured realistic ischemic sources simultaneously within the heart, on the heart surface, and on the body surface.

Detecting acute myocardial ischemia clinically requires provoking some form of carefully controlled cardiac stress to expose inadequate perfusion with an induced increase in cardiac metabolic demand of a region of the heart [24]. In most circumstances, the safest method to induce myocardial ischemia is to increase metabolic demand by having the patient exercise or by administering a pharmacological infusion to increase heart rate and contractility [1], [9], [25]. Pharmacological stimulation is used in situations in which the patient is unable to exercise or when body motion is disruptive. However, studies have suggested that exercise and pharmacological stimulation may result in different electrocardiographic findings [26]–[28]. These studies were limited to examination of 12-lead ECG and were unable to compare the ischemic region created within the myocardium [26]–[28]. Complementary comparisons of ischemic zones detected with nuclear medicine techniques did not measure the electrical signs of ischemia within the heart and were unable to capture their temporal development [29]. In the second aim of this dissertation, we addressed these limitations and test the underlying hypothesis that the ischemic zone created depends on the method of ischemic induction, as revealed through comprehensive electrical measurements in large-animal models.

Finally, little is understood about the transient and dynamic nature of ischemic

signals during a partial occlusion event. Often, patients present to the emergency department complaining of significant chest pain; however, no ischemic electrical biomarkers can be detected [30]–[32]. In other circumstances, there is spontaneous recovery of ischemic electrical signals thought to be a recovery of the myocardial tissue [33]. However, the mechanism, progression, and temporal development of this spontaneous recovery are poorly defined. Previous studies have examined ischemia following a full occlusion of a coronary artery, simulating a myocardial infarction by completely arresting blood flow to a region of myocardial tissue, and correlated a decrease in ischemic signatures on the epicardial or torso surfaces with cell-to-cell uncoupling [34]–[39]. The timing and progression of these potentials is mixed, but most studies observe cellular uncoupling beginning around 10–15 minutes after occlusion [38], [39]. However, these studies examined full occlusion events without intramural sampling and without added cardiac stress. The goal of the third aim of this dissertation was to assess the transient recovery of ST-segment deviations on remote recording electrodes during a partial occlusion cardiac stress test.

1.2 Introduction to Doctoral Research

The needs and challenges in understanding and detecting acute myocardial ischemia motivated a set of specific aims that resulted in the following studies and chapters/manuscripts in this dissertation:

1.2.1 Chapter 3: Novel Experimental Model for Studying the Spatiotemporal Electrical Signature of Acute Myocardial Ischemia: A Translational Platform

The goal of this aim was to extend an animal model of ischemia to measure electrical potentials within the myocardium, on the heart surface, and on the body surface during controlled ischemic stress. We designed the experimental preparation with three important characteristics: 1) enable comprehensive and simultaneous high-resolution electrical recordings within the myocardial wall, on the heart surface, and on the torso surface; 2) develop techniques to visualize these recorded electrical signals in time and space; and 3) accurately and controllably simulate

ischemic stress within the heart by modulating the supply of blood, the demand for perfusion, or a combination of both. To achieve these goals, we designed a comprehensive system that includes 1) custom electrode arrays, 2) signal acquisition and multiplexing units, 3) a surgical technique to place electrical recording and myocardial ischemic control equipment, and 4) an image-based modeling pipeline to acquire, process, and visualize the results. With this setup, we are uniquely able to capture simultaneously and continuously the electrical signatures of acute myocardial ischemia within the heart, on the heart surface, and on the body surface. This novel experimental preparation enables investigation of the complex and dynamic nature of acute myocardial ischemia that should lead to new, clinically translatable results.

1.2.2 Chapter 4: Pharmacological and Simulated Exercise Cardiac Stress Tests Produce Different Ischemic Signatures in High-Resolution Experimental Mapping Studies

The goal of the second aim in this dissertation was to test the hypothesis that exercise and dobutamine infusion create different regions of myocardial ischemia. We used a porcine model of acute myocardial ischemia in which animals were instrumented with transmural plunge-needle electrodes, an epicardial sock array, and torso surface arrays to simultaneously measure within the heart wall, on the epicardial surface, and on the torso surface, respectively. Three-dimensional geometric models with electrode locations were created from postmortem magnetic resonance imaging. Ischemic stress by means of simulated exercise and pharmacological stimulation was created with rapid electrical pacing and dobutamine infusion, respectively, and applied in five escalating stages of 3 minutes each. Perfusion to the myocardium was regulated by a variable hydraulic occluder around the left anterior descending coronary artery. Electrical markers of ischemia were measured as deflections to the ST-segment, gradients of ST-segment potentials, and the intramyocardial volume that showed suprathreshold ST levels.

Across eight experiments with 30 ischemic interventions (14 simulated exercise and 16 dobutamine), the spatial correlations between exercise and pharmacological stress were initially high but diverged significantly toward the end of the

interventions (stages 3–5) in all recording domains ($p < 0.05$ for all). We found significantly more detectable ST40 changes on the epicardial surface during simulated exercise than with dobutamine at stages 4 and 5 ($p < 0.05$). The intramyocardial ischemia formed during simulated exercise had significantly larger ST40 potential gradient magnitudes ($p < 0.05$). We found no significant difference between intervention types in the overall intramyocardial volume of ischemic zones. A possible mechanism for these differences was the larger ST40 potential gradient magnitudes seen within the myocardium during simulated exercise. The presence of microvascular dysfunction during simulated exercise and its absence during dobutamine testing may explain these differences.

1.2.3 Chapter 5: Temporal Recovery of Electrical Ischemic Signatures During Cardiac Stress Tests: An Experimental Examination

The goal of the third aim in this dissertation was to assess the transient recovery of ST-segment deviations on remote recording electrodes during a partial occlusion cardiac stress test and compare them to intramyocardial ST-segment deviations. Acute myocardial ischemia has several characteristic ECG findings, including clinically detectable ST-segment deviations. However, the sensitivity and specificity of ECG-based ST-segment changes are low. Furthermore, ST-segment deviations have been shown to be transient and spontaneously recover without any indication the ischemic event has subsided. We used a previously validated experimental model of acute myocardial ischemia with controllable ischemic load and measurement electrodes within the heart wall, on the epicardial surface, and on the torso surface. Simulated cardiac stress tests were induced by occluding a coronary artery while simultaneously pacing or infusing dobutamine to stimulate cardiac function. Postexperimental imaging created anatomical models for data visualization and quantification. Markers of ischemia were identified as deviations in the potentials measured at 40% of the ST-segment. Intramural cardiac conduction speed was also determined using the inverse gradient method. Changes in intramyocardial ischemic volume proportion, conduction speed, clinical presence of ischemia on remote recording arrays, and regional changes to intramyocardial ischemia were assessed. Peak deviation response time was the time interval after onset of is-

chemia that maximum ST-segment deviation was achieved and ST-recovery time was the interval when ST deviation returned to below 1mV of ST elevation.

In both epicardial and torso recordings, the peak ST-segment deviation response time was 4.9 ± 1.1 min and the ST-recovery time was approximately 7.9 ± 2.5 min, both well before the termination of the ischemic stress. At peak response time, conduction speed was reduced by 50% and returned to near baseline at ST-recovery. The overall ischemic volume proportion initially increased to 37% at peak response time; however, it recovered to only 30% at the ST-recovery time. By contrast, the subepicardial region of the myocardial wall showed 40% ischemic volume at peak response time and recovered much more strongly to 25% as epicardial ST-segment deviations returned to baseline. Our data show that remote ischemic signal recovery correlates with a recovery of the subepicardial myocardium, while subendocardial ischemic development persists.

1.3 References

- [1] B. Safdar, P. Ong, and P. G. Camici, "Identifying myocardial ischemia due to coronary microvascular dysfunction in the emergency department: introducing a new paradigm in acute chest pain evaluation," *Clin. Therapeutics*, pp. 1–11, Nov. 2018. doi: <http://dx.doi.org/10.1016/j.clinthera.2018.09.010>.
- [2] F. A. Bhuiya, S. R. Pitts, and L. F. McCaig, "Emergency department visits for chest pain and abdominal pain: United States, 1999-2008," *NCHS Data Brief*, no. 43, pp. 1–8, Sep. 2010.
- [3] A. M. Katz, *Physiology of the Heart*. Lippincott Williams & Wilkins, 2010.
- [4] B. Surawicz, "Ventricular repolarization in myocardial ischemia and myocardial infarction: Theory and practice," in *Comprehensive Electrocardiology*, 2nd ed., P. Macfarlane, A. van Oosterom, O. Pahlm, P. Kligfield, M. Janse, and J. Camm, Eds. London, England: Springer-Verlag, 2011, ch. 18, pp. 803–831.
- [5] L. Jespersen, S. Z. Abildstrøm, A. Hvelplund, and E. Prescott, "Persistent angina: highly prevalent and associated with long-term anxiety, depression, low physical functioning, and quality of life in stable angina pectoris," *Clin. Res. in Cardiol.*, vol. 102, no. 8, pp. 571–581, Aug. 2013. doi: <http://dx.doi.org/10.1007/s00392-013-0568-z>.
- [6] B. M. C. Noel, P. C. J., W. M. Norine, F. J. L., C. P. G., C. W. M., C. J. Austin, C. L. S., C. Filippo, D. C. Marcelo, D. P. S., G. Z. S., G. Paul, H. E. M., H. Ahmed, H. J. A., H. J. S., I. Erin, K. Ruth, L. G. N., L. Peter, L. Joao, M. Puja, D.-N. Patrice, O. Michelle, P. G. D., Q. A. A., R. Harmony, R. British, S. George,

- T. Viviany, W. Janet, and W. Nanette, "Ischemia and no obstructive coronary artery disease (INOCA)," *Circ.*, vol. 135, no. 11, pp. 1075–1092, Mar. 2017. doi: <http://dx.doi.org/10.1161/CIRCULATIONAHA.116.024534>.
- [7] L. Jespersen, A. Hvelplund, S. Z. Abildstrøm, F. Pedersen, S. Galatius, J. K. Madsen, E. Jørgensen, H. Kelbæk, and E. Prescott, "Stable angina pectoris with no obstructive coronary artery disease is associated with increased risks of major adverse cardiovascular events," *Europ. Heart J.*, vol. 33, no. 6, pp. 734–744, Mar. 2012.
- [8] M. Kontos, F. Anderson, K. Schmidt, J. Ornato, J. Tatum, and R. Jesse, "Early diagnosis of acute myocardial infarction in patients without ST-segment elevation," *Am. J. Cardiol.*, vol. 83, no. 2, pp. 155–158, Jan. 1999.
- [9] J. Knuuti, H. Ballo, L. E. Juarez-Orozco, A. Saraste, P. Kolh, A. W. S. Rutjes, P. Jüni, S. Windecker, J. J. Bax, and W. Wijns, "The performance of non-invasive tests to rule-in and rule-out significant coronary artery stenosis in patients with stable angina: A meta-analysis focused on post-test disease probability," *Europ. Heart J.*, vol. 39, no. 35, pp. 3322–3330, Sep. 2018. doi: <http://dx.doi.org/10.1093/eurheartj/ehy267>.
- [10] D. Hearse, "Myocardial ischaemia: Can we agree on a definition for the 21st century?" *Cardiovasc. Res.*, vol. 28, pp. 1737–1744, 1994.
- [11] E. Falk, P. Shah, and P. de Feyter, *Ischemic Heart Disease*, 1st ed. London, England: Manson Publishing, 2007.
- [12] H. Fozzard and M. Arnsdorf, "Cardiac electrophysiology," in *The Heart and Cardiovascular System*, H. Fozzard, Ed. New York, NY, USA: Raven Press, 1986, pp. 1–30.
- [13] R. Holland and H. Brooks, "Spatial and nonspatial influences on the tq-st segment deflection of ischemia," *J. Clin. Invest.*, vol. 60, no. 1, pp. 197–214, Jul. 1977.
- [14] —, "TQ-ST segment mapping: Critical review and analysis of current concepts," *Am. J. Cardiol.*, vol. 40, no. 1, pp. 110–129, Jul. 1977.
- [15] A. Kléber, M. Janse, F. van Capelle, and D. Durrer, "Mechanism and time course of ST- and TQ-segment changes during acute regional myocardial ischemia in the pig heart determined by extracellular and intracellular recordings," *Circ. Res.*, vol. 42, pp. 603–613, May 1978.
- [16] M. Janse, F. van Capelle, H. Morsink, A. Kleber, F. Wilms-Schopman, R. Cardinal, C. d Alnoncourt, and D. Durrer, "Flow of "injury" current and patterns of excitation during early ventricular arrhythmias in acute regional myocardial ischemia in isolated porcine and canine hearts," *Circ. Res.*, vol. 47, no. 2, pp. 151–165, Aug. 1980.

- [17] J. Cinca, M. J. Janse, H. Morena, J. Candell, V. Valle, and D. Durrer, "Mechanism and time course of the early electrical changes during acute coronary artery occlusion," *Chest*, vol. 77, no. 4, pp. 499–505, Apr. 1980. doi: <http://dx.doi.org/10.1378/chest.77.4.499>.
- [18] W. Chang, T. Akitama, J. Richeson, R. Faillace, and P. Serrino, "Origin of the giant R wave in acute transmural myocardial infarctions in the pig." *Jap. Heart J.*, vol. 30, no. 6, pp. 863–883, Nov. 1989.
- [19] R. MacLeod, B. Taccardi, and R. Lux, "Mapping of cardiac ischemia in a realistic torso tank preparation," in *Building Bridges: International Congress on Electrocardiology Meeting*, Sep. 1995, pp. 76–77.
- [20] R. MacLeod, R. Lux, and B. Taccardi, "A possible mechanism for electrocardiographically silent changes in cardiac repolarization," *J. Electrocardiol.*, vol. 30, no. Suppl, pp. 114–121, Apr. 1997.
- [21] S. Shome, R. Lux, B. Punske, and R. MacLeod, "Ischemic preconditioning protects against arrhythmogenesis through maintenance of both active as well as passive electrical properties in ischemic canine hearts," *J. Electrocardiol.*, vol. 40, no. 4, pp. S5–S6, Nov. 2007.
- [22] K. Aras, S. Shome, D. Swenson, J. Stinstra, and R. MacLeod, "Electrocardiographic response of the heart to myocardial ischemia," in *Computers in Cardiology 2009*, Sep. 2009, pp. 105–108.
- [23] K. Aras, B. Burton, D. Swenson, and R. MacLeod, "Spatial organization of acute myocardial ischemia," *J. Electrocardiol.*, vol. 49, no. 3, pp. 689–692, May 2016.
- [24] E. Pueyo, J. Garcia, G. Wagner, R. Bailón, L. Sörnmo, and P. Laguna, "Time course of ECG depolarization and repolarization changes during ischemia in PTCA recordings," *Meth. of Inf. in Med.*, vol. 43, no. 01, pp. 43–46, Jan. 2004.
- [25] S. Stern, "State of the art in stress testing and ischaemia monitoring." *Card. Electrophysiol. Rev.*, vol. 6, no. 3, pp. 204–208, Sep. 2002.
- [26] J. Shadeen, "Diagnostic value of 12-lead electrocardiogram during dobutamine echocardiographic studies," *Am. Heart J.*, vol. 136, no. 6, pp. 1061–1064, Dec. 1998. doi: [http://dx.doi.org/10.1016/S0002-8703\(98\)70163-2](http://dx.doi.org/10.1016/S0002-8703(98)70163-2).
- [27] M. R. Dhond, T. Nguyen, T. B. Whitley, K. Donnell, and W. J. Bommer, "Prognostic value of 12-Lead electrocardiogram during dobutamine stress echocardiography," *Echocardiography*, vol. 17, no. 5, pp. 429–432, Jul. 2000. doi: <http://dx.doi.org/10.1111/j.1540-8175.2000.tb01158.x>.
- [28] G. H. Mairesse, T. H. Marwick, J. L. J. Vanoverschelde, T. Baudhuin, W. Wijns, J. A. Melin, and J. M. R. Detry, "How accurate is dobutamine stress electrocardiography for detection of coronary artery disease? Comparison with two-dimensional echocardiography and technetium-99m methoxyl isobutyl isonitrile (mibi) perfusion scintigraphy," *J. Am. Coll. Cardiol.*, vol. 24, no. 4, pp. 920–927, Oct. 1994. doi: [http://dx.doi.org/10.1016/0735-1097\(94\)90850-8](http://dx.doi.org/10.1016/0735-1097(94)90850-8).

- [29] G. M. Santoro, R. Sciagra, P. Buonamici, N. Consoli, V. Mazzoni, F. Zeraushek, G. Bisi, and P. F. Fazzini, "Head-to-head comparison of exercise stress testing, pharmacologic stress echocardiography, and perfusion tomography as first-line examination for chest pain in patients without history of coronary artery disease," *J. of Nucl. Cardiol.*, vol. 5, no. 1, pp. 19–27, Jan. 1998. doi: [http://dx.doi.org/10.1016/S1071-3581\(98\)80006-8](http://dx.doi.org/10.1016/S1071-3581(98)80006-8).
- [30] E. K. Aslanger, P. H. Meyers, and S. W. Smith, "STEMI: A transitional fossil in MI classification?" *J. Electrocardiol.*, vol. 65, pp. 163–169, Mar. 2021. doi: <http://dx.doi.org/10.1016/j.jelectrocard.2021.02.001>.
- [31] R. J. Myerburg, "Non-atherosclerotic causes of myocardial ischemia: With emphasis on spontaneous dissection of coronary arteries," *Trends in Cardiovas. Med.*, Feb. 2021. doi: <http://dx.doi.org/10.1016/j.tcm.2021.02.003>.
- [32] J. M. Di Diego and C. Antzelevitch, "Acute myocardial ischemia: Cellular mechanisms underlying ST segment elevation," *J. Electrocardiol.*, vol. 47, no. 4, pp. 486–490, Jul. 2014. doi: <http://dx.doi.org/10.1016/j.jelectrocard.2014.02.005>.
- [33] G.-X. Yan, A. Joshi, D. Guo, T. Hlaing, J. Martin, X. Xu, and P. R. Kowey, "Phase 2 reentry as a trigger to initiate ventricular fibrillation during early acute myocardial ischemia," *Circ.*, vol. 110, no. 9, pp. 1036–1041, Aug. 2004. doi: <http://dx.doi.org/10.1161/01.CIR.0000140258.09964.19>.
- [34] A. Kléber, C. Riegger, and M. Janse, "Electrical uncoupling and increase of extracellular resistance after induction of ischemia in isolated, arterially perfused rabbit papillary muscle," *Circ. Res.*, vol. 61, pp. 271–279, Aug. 1987.
- [35] A. Kléber, M. Janse, F. Wilms-Schopmann, A. Wilde, and R. Coronel, "Changes in conduction velocity during acute ischemia in ventricular myocardium of the isolated porcine heart," *Circ.*, vol. 73, pp. 189–198, Jan. 1986.
- [36] A. G. Kleber, M. J. Janse, F. J. L. van Capelle, and D. Durrer, "Mechanism and time course of st- and tq-segment changes during acute regional myocardial ischemia in the pig heart determined by extracellular and intracellular recordings," *Circ. Res.*, vol. 42, pp. 603–613, May 1978.
- [37] J. Degroot and R. Coronel, "Acute ischemia-induced gap junctional uncoupling and arrhythmogenesis," *Circ. Res.*, vol. 62, no. 2, pp. 323–334, May 2004. doi: <http://dx.doi.org/10.1016/j.cardiores.2004.01.033>.
- [38] D. C. Russell, J. S. Lawrie, R. A. Riemersma, and M. F. Oliver, "Mechanisms of phase 1a and 1b early ventricular arrhythmias during acute myocardial ischemia in the dog," *Am. J. Cardiol.*, vol. 53, no. 2, pp. 307–312, Jan. 1984. doi: [http://dx.doi.org/10.1016/0002-9149\(84\)90444-2](http://dx.doi.org/10.1016/0002-9149(84)90444-2).
- [39] W. T. Smith, W. F. Fleet, T. A. Johnson, C. L. Engle, and W. E. Cascio, "The Ib phase of ventricular arrhythmias in ischemic in situ porcine heart is related to changes in cell-to-cell electrical coupling," *Circ.*, vol. 92, pp. 3051–3060, Nov. 1995.

CHAPTER 2

BACKGROUND

2.1 Electrical Sources and Volume Conductors: A Cardiac Application

Fundamentally, we can think of the cells and tissues within the heart as a bioelectric source, placed in a volume conductor, the thoracic cavity. The culmination of all the electrical sources and volume conductor creates electrical potentials that can be measured with electrodes, either directly on or in the heart, or, more often on the torso surface, the ubiquitous ECG. In the context of this research and understanding the electrical consequences of ischemia, this description provides a useful framework that we develop here, acknowledging that it is by no means the only way to consider the hierarchical organization of membranes, cells, tissues, and organs.

An electrical source is an active source of electric current, much like a battery or current generator [1], [2]. Using the analogy of a battery, one can represent the electrical source in different ways depending on the scale of a particular application. The lowest scale is the chemical reactions within each battery “cell,” generating potential energy (voltage) that can be released as electrical current. Going up in scale, the entire, multicellular battery itself becomes the source of current flowing between positive to negative contacts. At an even larger scale, the batteries can be connected and summed to create a source with even more energy. Each representation of these electrical sources is called a different “source model” [1]–[7].

A volume conductor is a conductive space that surrounds the electrical source [1], [2]. In a simple case, a volume conductor could be a bucket filled with electrolytic solution into which we place the battery as the source. We can then measure the electrical current from the battery or source at distinct points throughout

the bucket. In this simple case, the recorded signals near the battery would likely produce a strong current that is easily detected. If we measured at the edge of the bucket, the current would be significantly diminished, depending on the distance away from the battery and the conductivity of the electrolytic fluid inside the bucket.

The same fundamental theory of sources and volume conductors can be applied to cardiac electrophysiology [1], [2]. Importantly, we can examine the cardiac electrical source and volume conductors at different scales and locations. From a source perspective, electrically active membranes, cardiomyocytes, and collections of linked cardiomyocytes (tissues) are examples of possible source models [1], [2]. The relevant cardiac volume conductors include the extracellular space and the torso with surrounding organs. The representation of the sources and volume conductors changes depending on the scale and the application. Here, we review cardiac electrophysiology from the perspective of cardiac sources, anatomical volume conductors, and the measurements made at each location from smallest to largest or from cell to whole organ descriptions. This perspective is ideally suited to the context of the studies of acute ischemia and the resulting electrical signatures viewed across multiple scales.

2.1.1 Cellular View

At the cellular level, the cardiac source is the cellular membrane and the active currents that pass through the membrane in ion channels [8]. In this case, concentration gradients across the membrane created from the cellular conversion of ATP to electrochemical energy result in electrochemical gradients that drive current flow during the action potentials [8]. The action potential is the product of different ion channels, each of which conducts specific ions across the membrane. The electrical characteristics of each ion channel can be modified, e.g., by chemical agents, drugs, or by pathologies, with a resulting change in action potential. Measurements of individual ion channels are made by isolating small sections of the membrane with a small number of embedded ion channels using a patch electrode [8].

The action potential captures the integrated behavior of all the ion channels and represents the electrical source from each cell—a time-varying battery [1], [2]. Healthy cardiomyocytes have a typical action potential shape with five unique phases, 0 through 4 as shown in Panel A of Figure 2.1 [8]. We can measure these currents across the membrane using glass microelectrodes [9].

The physiological volume conductor for the single cell is the small interstitial space in which the cell is surrounded by electrolyte and the volume of neighboring cells to which each myocyte is coupled through gap junctions. The resulting electrical loading of the cell can change action potential shape from that which arises when a cell is fully isolated and placed in a bath. This scenario of an isolated cell in a bath is the standard measurement scenario used to study individual myocytes but it is rare to measure the resulting potential distribution within the bath [10].

2.1.2 Tissue View

At the myocardial tissue scale, cardiomyocytes link together through specialized channels called gap junctions, and the result is a syncytium, which rapidly conducts cardiac action potentials from cell to cell and throughout the tissue [8]. At this scale, the source model is the electrical potential and currents that arise from a piece of this syncytium. Internally, these are currents that flow between cells (intracellular) and the return currents outside the cells (extracellular). From some distance, the source can behave as a network of batteries connected in a sequence, in the simplest case with a positive and a negative terminal at the ends. Because the piece of tissue can assume very complex shapes, a more realistic source model is a surface, some portion of which emits current (the equivalent of the positive pole of a battery), another portion that absorbs it (the negative pole), and a third that is electrically neutral, i.e., that neither emits nor absorbs current. The results potentials are also time-varying and can take on very complex shapes depending on the tissue and the location of the measurement electrodes. An example of these recordings is shown in Figure 2.1 panel B.

Depending on the perspective, the volume conductor at the tissue scale can be seen as the extracellular space that forms between cells or the electrolyte in which

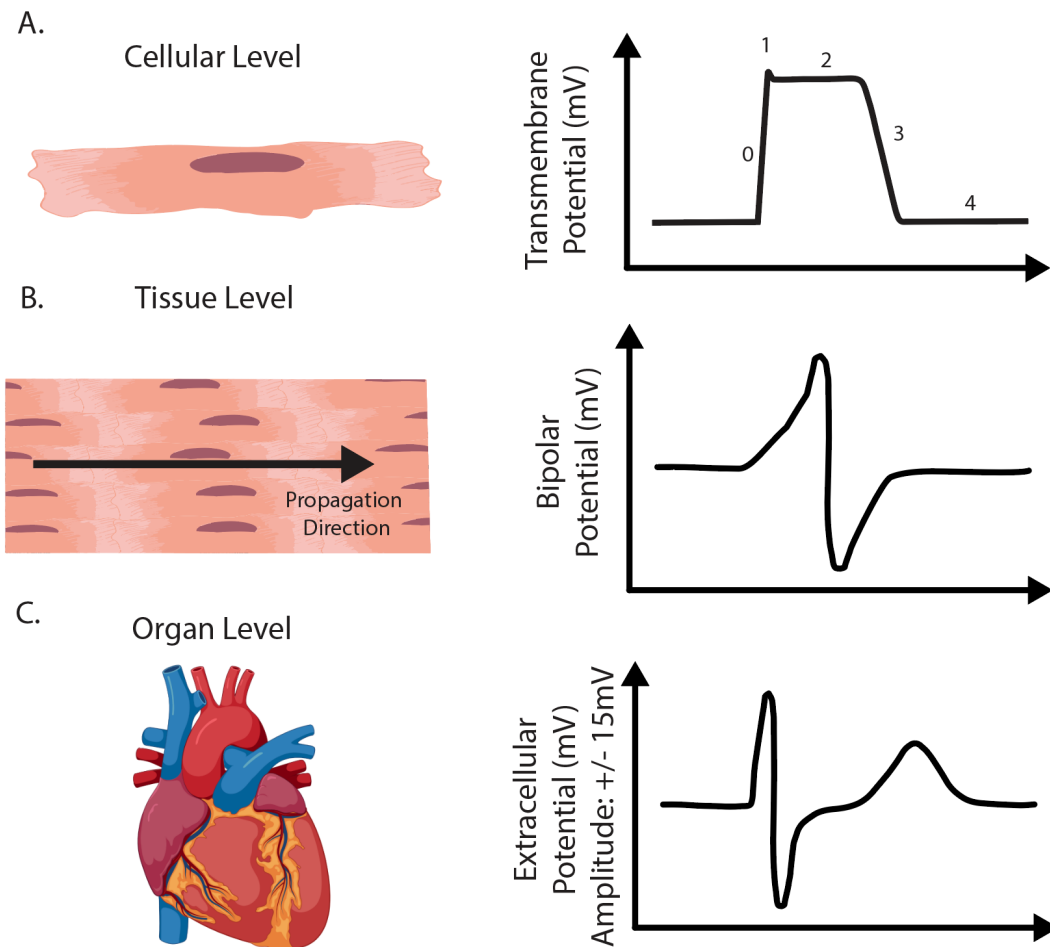


Figure 2.1: Example of observation scales within cardiac electrophysiology. The panels show three levels of the cell, tissue, and whole organ with their respective electrical recordings as extracellular or transmembrane potentials.

the piece of tissue is suspended. The cardiac extracellular space contains fluid with ions, proteins, and cellular scaffold components, which contribute to the electrical properties of the volume conductor [8].

Measurements at this scale are no longer transmembrane but consist of capturing extracellular potentials within a region of tissue or the bath in which the tissue sits. The resulting recordings are summed manifestations of local cellular action potentials and the potential differences they generate between cells. The individual action potentials are thus obscured, and only potential differences between regions of tissue are discernible.

2.1.3 Organ-Level View

From the perspective of the whole heart, the source is the entire set of electric potentials in or on the heart, which can be described in a number of ways. The simplest and most common formulation for clinical interpretation is the single ‘heart vector’, a single, moving, current dipole that formed the basis for Einthoven’s limb leads and his eventual Nobel Prize [11]. The heart vector direction and magnitude depend on the average current direction and strength throughout the heart during a normal heartbeat and obviously represent an extreme simplification, albeit a very useful one.

Other representations of the heart source are both more sophisticated and more challenging to capture and represent. The set of potentials on any closed surface that surrounds the heart is one of the most common representations that offers the option of direct measurements, as we describe below. It is also the target of the most common form of ECG imaging, a reconstruction technique that estimates cardiac sources from body-surface ECGs [2]. Other source models capture the volumetric distribution of potentials, or multiple, local current dipoles throughout the heart, a much more challenging measurement and reconstruction proposition.

Just as the cardiac source gains complexity at the whole organ scale, so too does the volume conductor, which is the entire thorax. This massive expansion means the volume conductor now includes the lungs, bones, skeletal muscles, and other thoracic organs. Fortunately, all these components are electrically passive (other

than possibly skeletal muscle) and do not actively contribute significant source current to the extracellular potentials recorded on the torso surface [1], [2]. These elements do, however, contribute an added electrical resistance, which decreases the current at the torso surface and consequentially the amplitude of recorded torso surface extracellular potentials, which are typically an order of magnitude smaller than those recorded directly from the heart [1], [2].

The measurement approaches at the organ level reflect the associated source. One can place electrodes directly on the heart surface (both endocardial and epicardial) or insert electrodes within the heart volume. The resulting signals represent an aggregate of all the cardiomyocyte potentials within that region [8]. An example extracellular recording is shown in Figure 2.1 panel C. The number of cells contributing to the signal at a single recording site can range to several thousands, which creates a blurring of the activity at the cellular scale. The torso surface provides another, noninvasive means to measure electrical potentials from the whole heart, the ECG that plays such a key role in clinical medicine. However, the ECG is a product of both the source and the volume conductor, whose complexity and inhomogeneity not only attenuate but also blur the resulting signals. The main challenge of electrocardiography then becomes to infer or estimate cardiac electrical sources from measurements on the torso surface in the face of this attenuation and distortion.

2.2 Changes to the Cardiac Source and Volume Conductor During Acute Myocardial Ischemia

2.2.1 Cellular-Level View

Acute myocardial ischemia has been shown to have specific and significant effects on the cardiomyocyte ion channels and action potential. Through a complex series of events, including metabolite build-up, energy depletion, and ion channel disturbances, ischemia creates an environment that significantly alters the cardiomyocyte action potential [8], [12]–[16]. Specifically, ischemia results in an increase in resting potential, a decrease in the upstroke velocity, and a decrease in the plateau phase potential, as shown in Figure 2.2 [8], [12]–[16]. As the resting

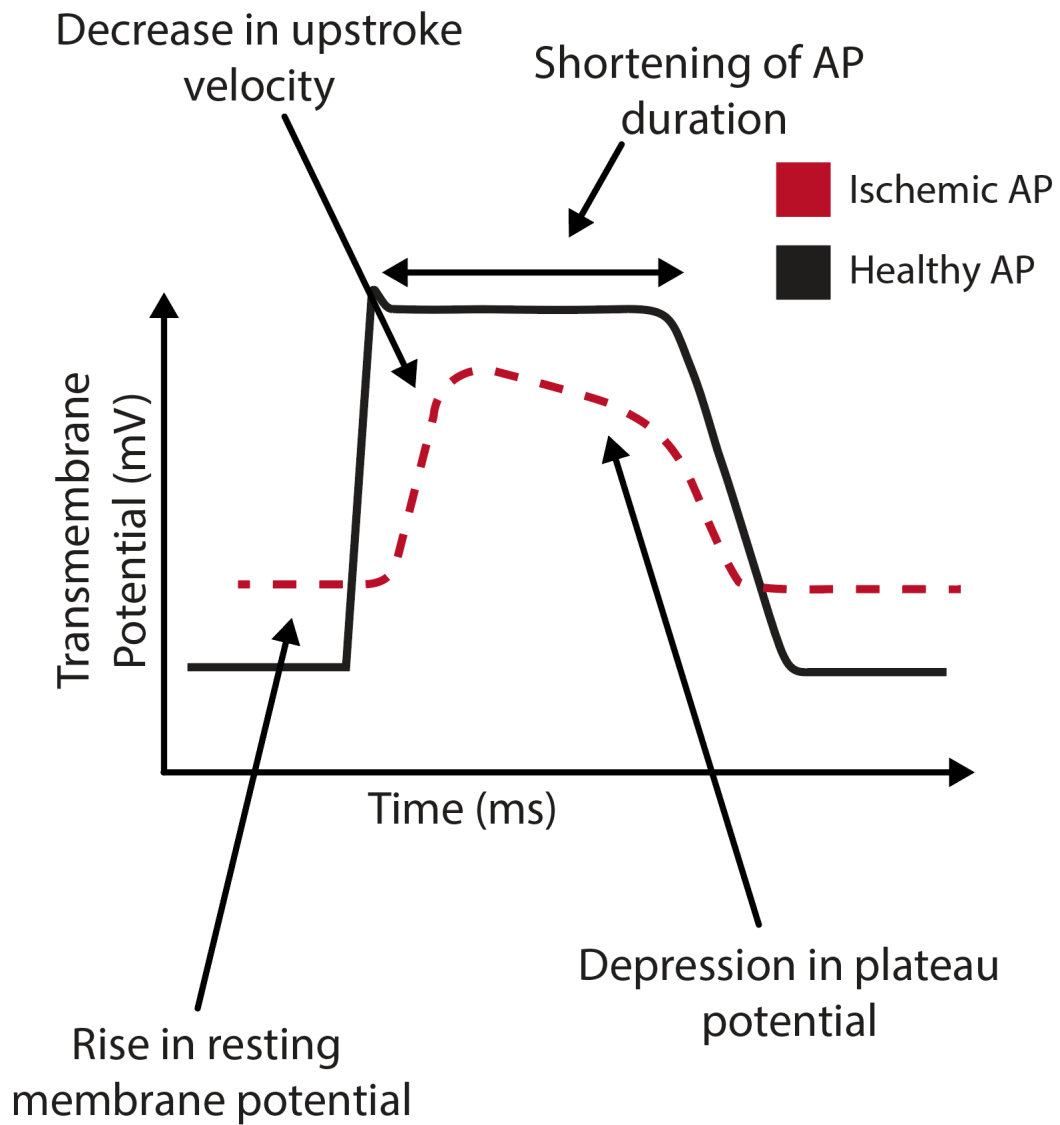


Figure 2.2: Schematic cardiac action potential under normal and ischemic conditions. Note the rise in resting membrane potential, decrease in upstroke velocity, depression of plateau potential, and shortening of the AP duration.

membrane potential becomes more positive, voltage-gated Na-channel function begins to degrade [8]. The action potential upstroke velocity also decreases, i.e., the depolarization of the entire cell takes significantly more time [8]. Additionally, the plateau phase potential and duration is significantly reduced compared to a normal action potential [8].

2.2.2 Tissue-Level View

At the tissue level, acute ischemia develops new regional gradients of potential between locally homogeneous healthy and ischemic cells. The gradient of potential forms first during the resting and plateau phases of action potentials and drives passive current flow, called injury current [13]–[15], [17]. Figure 2.3 shows this scenario during the plateau phase, when intracellular currents flow from healthy cells to nearby ischemic cells and extracellular currents close the loop. Seen as a macroscopic electrical source, this arrangement forms a battery or current dipole with the positive pole (or current source) over the ischemic tissue. [13]–[15], [17]. An example of these injury currents is found in Figure 2.3. These currents can then be measured by extracellular electrode recordings and are an indicator of ischemic formation.

The volume conductor also changes at the tissue level during acute myocardial ischemia. The arrest of perfusion to regional tissue areas reduces the vascular volume—blood vessels may even collapse—and drives a significant osmotic imbalance [8]. Osmotic gradients then push fluid from the extracellular space to the vascular space to correct the decreased vascular volume, which significantly shrinks the extracellular volume [8]. The decrease in extracellular volume increases the resistance throughout the extracellular space and alters passive current flow.

A later, tissue-level change induced by ischemia is the reduction in cell-to-cell coupling during prolonged ischemic events (around 15 minutes) [12], [14], [18]. Such long periods without perfusion result in the build-up of toxic metabolites, shut-down of cellular energy production, and a drop in tissue pH. These pH changes will drive gap junction proteins to begin to dissociate and separate [12],

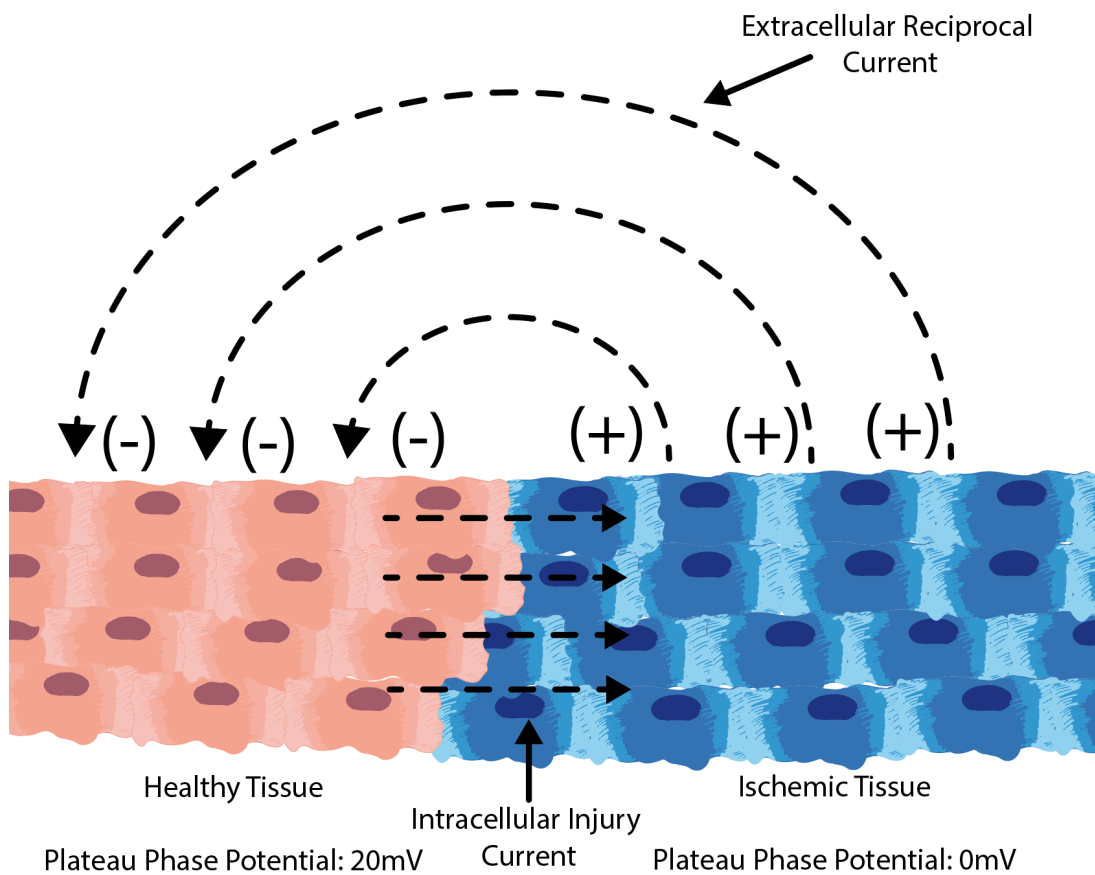


Figure 2.3: Example of tissue-level injury current flow. Blue cells are ischemic tissue, red cells are healthy. Intracellular injury current flows from healthy to ischemic tissue, and reciprocal extracellular current flows from ischemic to healthy tissue.

[14], [18], leading to a significant increase in intracellular resistance [18], [19]. This increase in bulk intracellular resistance has effects on both the source and the volume conductor action of the myocardium. Propagation of excitation becomes delayed, which alters the time course of the source, at the same time that passive currents, such as injury currents, fail to flow throughout the ischemic region [18], [19].

Electrical measurements in the tissue are of extracellular potentials, which are the product of both source and volume conductor effects and can detect the flow of injury currents. The polarity and amplitude of the resulting time-varying signals depend on electrode location relative to ischemic zone and manifest as positive or negative deflections in the ST-segment [13]–[15], [17]. Proximity to ischemia tissue, which acts like the positive pole of the source, results in ST-segment elevations and provides a means to probe the myocardium and localize the ischemia region. If sufficient time under ischemia has passed, cell-to-cell uncoupling occurs, injury currents are reduced, and ST-segment potentials will become significantly smaller than during the acute phase [15], [16], [18]–[22]. Furthermore, the speed of propagation through the ischemic tissue drops, resulting in substantial prolongations of the QRS duration [12], [14], [19].

2.2.3 Organ-Level View

The consequences of ischemia at the organ-level are limited to the electrical source model and represent the integrated effects from the tissue. Figure 2.4 captures the effects of myocardial ischemia in different regions of the ventricles as they are captured on the epicardial surface. The red regions of ischemia cause intracellular injury currents during the ST segment, indicated by the arrows in the Figure. Extracellular currents flow in the opposite directions so that the ischemic regions represent positive potentials (or current sources). The resulting epicardial potential distributions reflect proximity to these sources. A special case of note is in panel C of Figure 2.4, in which the ischemic zone is completely embedded by healthy tissue so that all the resulting injury currents balance and the epicardial potential is unaltered. The result is ischemia that does not contribute to the

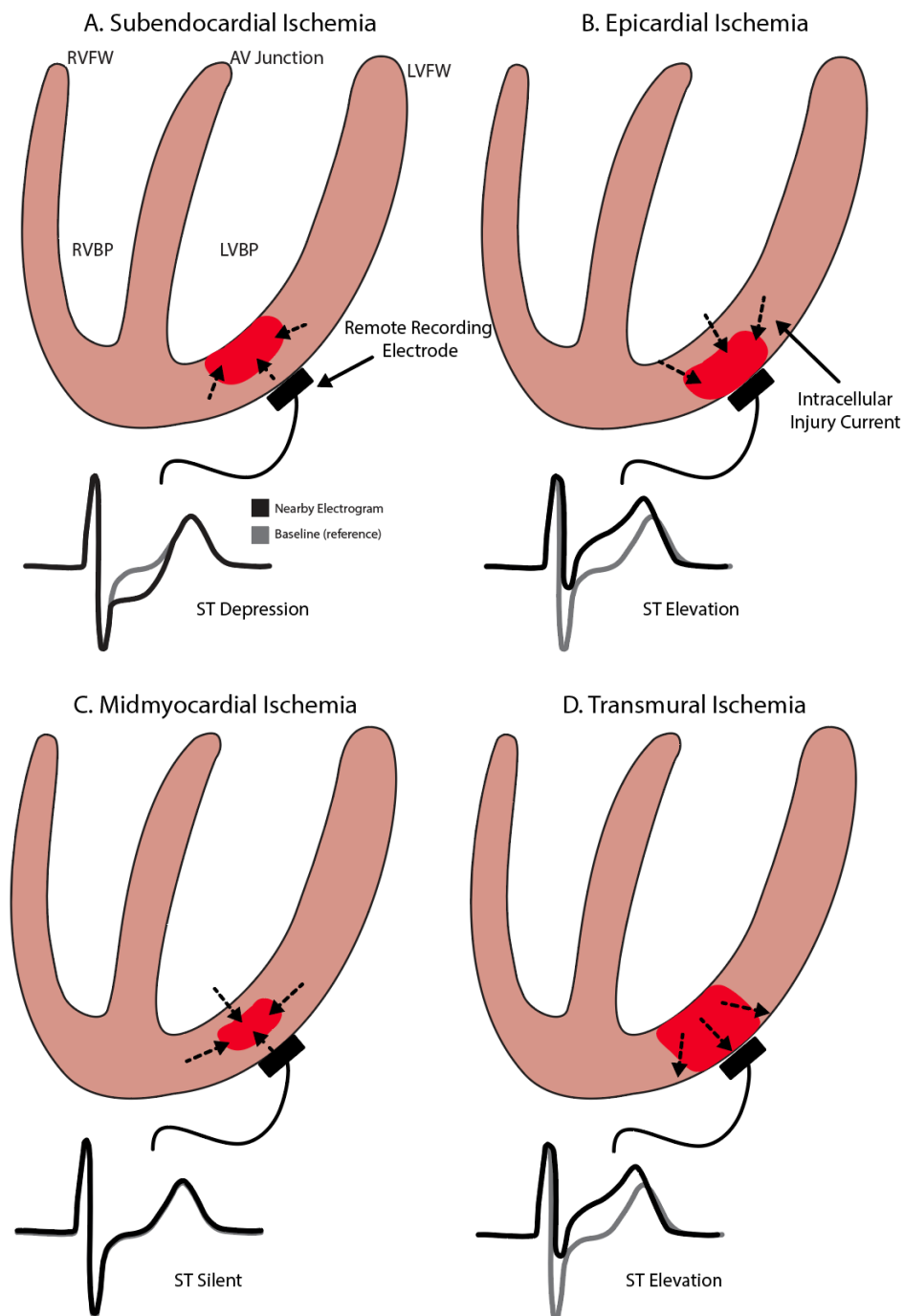


Figure 2.4: Example of ST-segment depression, elevation, and ST-silent ischemia. The panel examples are four typical situations including subendocardial, epicardial, midmyocardial, and transmural ischemia. Each creates a type of ST-segment change.

organ-level source and so becomes invisible to remote detection.

The volume conductor at this scale—the torso volume—does not change because of ischemia, and so its effects are, as described above, to enable extracellular current to flow outside the heart and generate smoothed, attenuated potential distributions on the body surface, which makes detection, and especially localization, of these sources extremely challenging [23].

Measurements of organ-level electrical activity is, as described above, by means of electrodes placed on or in the heart and also on the torso surface. The specific features that characterize the response to ischemia arise from injury currents, which drive ST-segment depressions or elevations, depending on electrode location relative to the ischemic region(s) [13]–[15], [17]. The time signals (electrogram) in Figure 2.4 demonstrate the results, with deflections of ST-segment potentials. Similar ECG signals arise on the torso surface. Injury currents also flow during the resting phase of the action potential, oppositely oriented from those during the depolarized phase, and so it would be natural to expect these to result in deflections during the (normally isopotential) T-Q segment of the electrogram (or ECG). One can, indeed, measure such potentials but only with amplifiers that offer direct-current (DC) coupling. However, contemporary amplifiers are almost ubiquitously AC coupled so that the long-lasting T-Q deflections are filtered away.

ST-segment deflections on the torso are challenging to detect because of their relatively low amplitude compared to cardiac electrograms [24]. The low amplitude means that ST-segments are particularly susceptible to blurring by the volume conductor or noise from internal or external sources. To combat the resulting poor signal-to-noise, we and others have implemented electrocardiographic imaging (ECGI) techniques to reconstruct the epicardial potentials or transmembrane potentials from torso surface recordings [2], [5], [25]–[27]. ECGI leverages known information about the volume conductor, including torso conductivities and anatomical geometries, to reconstruct cardiac sources [2], [5], [25]–[27].

2.3 Experimental Models of Acute Myocardial Ischemia

The two primary forms of ischemia that experimental models emulate involve either full or partial occlusion of a major coronary artery [13], [15], [20], [28]–[32]. Full-occlusion experimental models of ischemia simulate a myocardial infarction and have a long and storied history of contributing to our understanding of the progression, detection, and management of one the most common clinical events [13], [15], [20], [28]–[32]. These models can be created both using an isolated, perfused heart or the intact heart and the chest exposed. The former case offers complete access and a high degree of control over the heart but removes any physiologic regulation by means of the autonomic nervous system. The in situ preparation represents a more physiologically complete situation, with the heart beating into an intact vasculature and responding to both local and remote influences. Whereas experiments involving full occlusion remove blood flow entirely from some or all of the heart and thus emulate very well the condition of a myocardial infarction, they cannot capture the more subtle conditions that arise when blood supply and demand are marginally out of balance. Experimental models that create ischemic conditions by means of partial occlusion allow for these subtle conditions to be replicated. Clinically, such conditions resemble the effect of exercise in a patient with underlying compromised coronary circulation. Other conditions similarly bring about reduction in coronary flow that compromise cardiac perfusion and performance []. Significantly fewer studies have focused on partial occlusion experimental models despite their obvious translational and clinical implications.

In both experimental models, the hearts are instrumented with local recording electrodes applied on or within the heart, often arranged near and within anticipated zones of ischemia; they capture extracellular potentials that form the electrical sources described above [28], [29]. Some studies have included cellular recordings of transmembrane potentials by means of floating glass microelectrodes [33]. Simultaneous measurements from the cells, the tissue, and the whole heart have created the basis for our understanding of the interplay of ischemic changes across

the scales described above. Key features of the measurement that differentiate past studies include the number and location of the electrodes, e.g., whether they capture the epicardial or endocardial surfaces or are able to penetrate the heart and record potentials in the myocardial volume. A consistent technological limitation is the number of separate channels of signals that can be captured simultaneously at adequate sample rates. Progress in this domain has been dramatic, from a few separate channels in the 1960s to over 1000 in contemporary acquisition systems [34], technology that has enabled the progress in our group.

Motivated by past studies with only limited numbers of electrodes and incomplete experimental control, over the past 15 years, our lab has leveraged—and also developed—novel technology in electrodes, acquisition systems, medical image processing, signal and image processing, and computing to improve all aspects of our experimental models [35]–[40]. For example, improvements in the electrodes and acquisition systems we construct have allowed sampling resolution and coverage to significantly increase. Our custom intramural plunge needle arrays have 10 distinct electrodes to sample the depth of the myocardial wall, and we apply up to 50 needles in a single experiment. An epicardial sock array with 247 individual electrodes can sample the entire ventricular epicardial surface. Finally, a variable hydraulic occluder placed around the left anterior descending coronary artery can regulate blood flow to specific heart regions [39]. With the combination of these recording arrays, variable levels of controlled occlusion, and control over heart rate using pacing electrodes, we can create nontransmural regions of ischemia throughout the myocardial wall (Figure 2.5). To process the resulting signals, we have created a custom suite of signal processing tools called PFEIFER [41]. To reconstruct and align the geometry of image based models and the entire set of recording electrodes for each individual experiment, we have constructed a complete image-based modeling pipeline [42].

This suite of technology and a well-controlled animal model have enabled some of the most detailed explorations reported in the literature of the characteristics of partial occlusion ischemic events. Our recent studies showed that acute myocardial ischemia arises in a distributed pattern throughout the myocardial wall, [39]

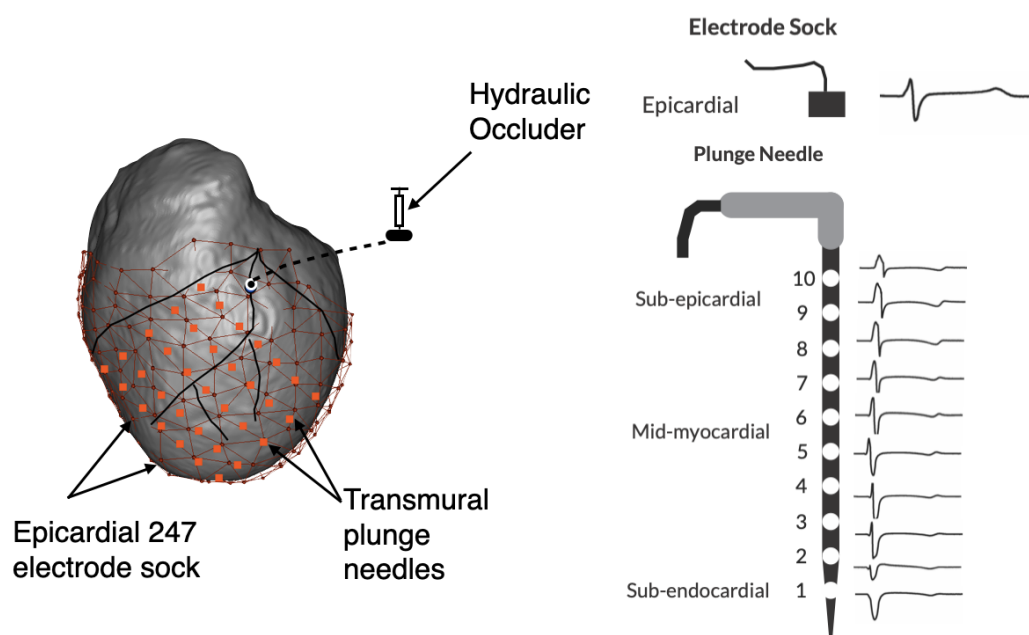


Figure 2.5: Previous experimental setup including location of the occlusion, epicardial sock electrodes, and transmural plunge needle electrodes. Also example recordings from the epicardial and intramural electrode arrays.

rather than solely anchored to the subendocardium, as previously assumed, which is a substantial shift from the clinical dogma that insisted ischemia developed only on the endocardial regions of the cardiac tissue [28], [29], [43]. Furthermore, we showed that it is possible to simulate the source model associated with ischemia and predict epicardial potentials, as long as precise, anatomically accurate ischemic zones are available [44]. However, the translational potential of these studies to noninvasive clinical measurements is lacking. Specifically, we have no torso surface recordings from these experimental models. Additionally, the stress protocols used to induce ischemia were different from those used during clinical cardiac stress tests. The first aim of this dissertation research will address these previous experimental shortcomings and further refine an experimental model of partial flow acute myocardial ischemia.

2.4 Electrical Detection of Acute Myocardial Ischemia in the Clinical Setting

Chest pain is the most common chief complaint of a patient arriving at the emergency department, with acute myocardial ischemia being the most worrisome underlying cause [45], [46]. A common clinical etiology includes a patient performing some type of atypical exercise, such as shoveling a large amount of snow, climbing significantly more stairs than usual, or overexerting themselves during exercise [8], [47]. The patients have thereby significantly increased the overall demand for perfusion throughout the heart to provide oxygen and remove metabolites. However, perfusion is limited for some pathological reasons, including coronary artery disease (CAD), coronary spasms, or other perfusion dysfunctions, limiting the available coronary blood flow [45], [48]–[50]. At this point, patients will begin to notice significant chest discomfort, usually described as a crushing pain. In an ideal scenario, an ECG would be immediately applied, and signal changes would provide a clear diagnosis, steps that require a trip to the emergency department.

Upon arrival to the emergency department, patients are quickly assessed to determine the root cause of their chest pain. Two coronary vascular pathologies

are generally the cause: full occlusion myocardial infarction and partial occlusion stable angina [8]. Several tests can rule out acute myocardial infarction, such as biochemical assays, computed tomography imaging, or coronary catheterization [51]. Assuming myocardial infarction is ruled out and partial occlusion ischemia is suspected, patients are usually sent home from the emergency department, with scheduled follow-up appointments and cardiac stress testing.

A cardiac stress test aims to determine if partial occlusion ischemia is the cause of the exercise-induced chest pain, a condition that requires long-term treatment and management. A cardiac stress test increases the overall cardiac stress while recording cardiac activity for evidence of ischemia [45], [52], [53]. Cardiac stress is induced via two primary methods, exercise with regulated interval training or a pharmacological challenge with dobutamine infusion [45], [52], [53]. During this episode of stress, the heart activity is measured by means of a 12-lead ECG or using ultrasound imaging, called an echocardiogram [45], [52], [53].

To better understand the mechanisms and interpret the results of a cardiac stress test, we must examine the cardiac stressors. In the exercise scenario, patients are asked to undergo regulated activity with 12-lead ECG monitoring. Exercise is the preferred cardiac stress type because it replicates the cardiovascular demand of normal life. This demand is by means of graded exercise, usually performed on a treadmill or stationary bike, in 3-minute intervals for a total of 15 minutes [54]. Exercise stimulates the heart by decreasing systemic vagal tone and increasing sympathetic tone [8]. Additionally, the venous return or pre-load increases [8]. These changes result in a significant increase in heart rate and a modest increase in cardiac contractility [8]. The other cardiac stressor is pharmacological stimulation via dobutamine infusion, chosen when patients cannot exercise because of safety concerns, previous cardiac abnormalities, or other personal preferences. Dobutamine is primarily a beta-1 agonist with off-target beta-2 effects [55]. Beta-1 receptors are primarily located on cardiomyocytes and increase calcium release within the cell during normal cardiac cycles, which leads to an increase in the contraction of cardiomyocytes by perpetuating and increasing the hydrolyzation of ATP to ADP [8]. Additionally, beta-1 receptors on the sino-atrial node stimulate

an ion channel that passes what is known as the ‘funny current’, which increases heart rate [55]. The net effect of dobutamine infusion is a significant increase in heart contraction and a moderate increase in heart rate [55], [56].

Despite the mechanistic and observed physiological differences, dobutamine stress and exercise stress have been considered interchangeable for clinical stress testing [56]. Several studies have been performed on small patient cohorts to compare the accuracy of each test to ground-truth invasive measurements. These tests found that sensitivity and specificity for dobutamine echo were 85% and 80%, respectively, [45], [53] and were lower, at 55% and 65%, respectively, for exercise stress testing. A further complication to their interchangeability is that the modalities used to evaluate ischemia in each stress type are different, i.e., exercise uses 12-lead ECG monitoring, and dobutamine uses echo ultrasound monitoring. The choice of different biomarkers (ultrasound imaging and ECG) for either stress type suggests the ischemia also develops differently. Only a handful of studies have compared the ischemic signatures of dobutamine and exercise stress on the same monitoring modality [57]–[59]. Of those studies, exercise was significantly more sensitive and specific to the 12-lead ECG, whereas dobutamine was more sensitive and specific to ultrasound [57]–[60]. Furthermore, some studies have shown no additional diagnostic benefit from ECG recordings when combined with dobutamine stress with ultrasound [61]. Combining the findings of these studies highlights the need for a careful examination of the ischemia that develops with each cardiac stress type. Improving our understanding of ischemia development will drive better detection modalities and test selection based on suspected underlying cardiac pathologies. Addressing these current difficulties will be the target of aim 2 of this dissertation research.

Clinical questions, reevaluations, and shared assumptions associated with ischemic biomarkers under various cardiac pathologies have also experienced a recent resurgence [62]–[64]. Several recent publications have questioned the diagnosis, risk stratification, and treatment of patients based on these long-held assumptions [62]. Other studies have shown that clinical criteria for correctly identifying patients with acute myocardial ischemia measured on the 12-lead ECG

are outdated [64]. Specifically, the threshold cutoffs of ST-segment elevation and mandatory evidence across several contiguous leads are too strict for ischemia detection criteria [64]. Several groups have proposed significant modifications that accommodate different pathologies other than coronary artery disease [63]. Furthermore, recent controlled trials have suggested that the typical treatment for coronary artery disease, coronary stent placement, may not provide any substantial benefit for patients suffering from stable angina [65]. These clinical implications drive important scientific reexaminations of partial flow ischemia development and the ideal biomarkers to use for detection.

The temporal evolution of partial occlusion acute myocardial ischemia during cardiac stress tests or other acute events has not been adequately explored. The temporal evolution of ischemia from full occlusion, i.e., myocardial infarction scenarios, has been well defined both experimentally and clinically [?], [16], [18]–[22]. However, similar biomarkers, spatial progression, and ischemic development have not been examined for acute, partial occlusions. Furthermore, an improved understanding of the temporal evolution of acute ischemia could contribute to better detection, risk stratification, and targeted treatments with a wide variety of pathologies that cause ischemia. The third aim of this dissertation research was to assess the transient recovery of ST-segment deviations on remote recording electrodes during a partial occlusion cardiac stress test.

2.5 References

- [1] R. MacLeod and M. Buist, “The forward problem of electrocardiography,” in *Comprehensive Electrocardiology*, P. Macfarlane, A. van Oosterom, O. Pahlm, P. Kligfield, M. Janse, and J. Camm, Eds. London, UK: Springer Verlag, 2010, pp. 247–298.
- [2] A. Pullan, L.K.Cheng, M. Nash, D. Brooks, A. Ghodrati, and R. MacLeod, “The inverse problem of electrocardiography,” in *Comprehensive Electrocardiology*, P. Macfarlane, A. van Oosterom, O. Pahlm, P. Kligfield, M. Janse, and J. Camm, Eds. London, UK: Springer Verlag, 2010, pp. 299–344.
- [3] R. MacLeod, R. Miller, M. Gardner, and B. Horáček, “Application of an electrocardiographic inverse solution to localize myocardial ischemia during percutaneous transluminal coronary angioplasty,” *J. Cardiovasc. Electrophysiol.*, vol. 6, pp. 2–18, 1995.

- [4] Bin He, Guanglin Li, and Xin Zhang, "Noninvasive imaging of cardiac transmembrane potentials within three-dimensional myocardium by means of a realistic geometry anisotropic heart model," *IEEE Trans. on Biomed. Eng.*, vol. 50, no. 10, pp. 1190–1202, Oct. 2003.
- [5] D. Wang, R. Kirby, R. MacLeod, and C. Johnson, "Inverse electrocardiographic source localization of ischemia: An optimization framework and finite element solution," *J. Comp. Phy.*, vol. 250, pp. 403–424, October 2013.
- [6] B. F. Nielsen, M. Lysaker, and A. Tveito, "On the use of the resting potential and level set methods for identifying ischemic heart disease: An inverse problem," vol. 220, no. 2, pp. 772 – 790, Jan. 2007. doi: <https://doi.org/10.1016/j.jcp.2006.05.040>. . [Online]. Available: <http://www.sciencedirect.com/science/article/pii/S0021999106002592>
- [7] B. Nielsen, X. Cai, and M. Lysaker, "On the possibility for computing the transmembrane potential in the heart with a one shot method: An inverse problem," *Math. Biosci.*, vol. 210, no. 2, pp. 523–553, Dec. 2007. doi: 10.1016/j.mbs.2007.06.003.
- [8] A. M. Katz, *Physiology of the Heart*. Lippincott Williams & Wilkins, 2010.
- [9] G. Ling and R. Gerard, "The normal membrane potential of frog sartorius fibers." *J. Cell Physiol.*, vol. 34, pp. 383–396, Dec. 1949.
- [10] B. Koidl, G. Zernig, and H. Tritthart, "Simultaneous measurements of action potentials and contractions in single cultured adult and embryonic heart muscle cells," *Basic Res. Cardiol.*, vol. 80, pp. 111–116, Jan. 1985.
- [11] W. Einthoven, "Le telecardiogramme," *Arch. Int. de Physiol.*, vol. 4, pp. 132–164, Jan. 1906.
- [12] E. Downar, M. J. Janse, and D. Durrer, "The effect of acute coronary artery occlusion on subepicardial transmembrane potentials in the intact porcine heart." *Circ.*, vol. 56, no. 2, pp. 217–224, Aug. 1977.
- [13] M. J. Janse, F. J. Van Capelle, H. Morsink, A. G. Kleber, F. Wilms-Schopman, R. Cardinal, C. N. D'Alnoncourt, and D. Durrer, "Flow of "injury" current and patterns of excitation during early ventricular arrhythmias in acute regional myocardial ischemia in isolated porcine and canine hearts. Evidence for two different arrhythmogenic mechanisms." *Circ. Res.*, vol. 47, no. 2, pp. 151–165, 1980.
- [14] M. J. Janse and A. G. Kleber, "Electrophysiological changes and ventricular arrhythmias in the early phase of regional myocardial ischemia." *Circ. Res.*, vol. 49, no. 5, pp. 1069–1081, Nov. 1981.
- [15] A. G. Kleber, M. J. Janse, F. J. L. van Capelle, and D. Durrer, "Mechanism and time course of st- and tq-segment changes during acute regional myocardial ischemia in the pig heart determined by extracellular and intracellular recordings," *Circ. Res.*, vol. 42, pp. 603–613, May 1978.

- [16] A. Kléber, M. Janse, F. Wilms-Schopmann, A. Wilde, and R. Coronel, "Changes in conduction velocity during acute ischemia in ventricular myocardium of the isolated porcine heart," *Circ.*, vol. 73, pp. 189–198, Jan. 1986.
- [17] F. Kornreich, T. Montague, M. Kavadias, J. Segers, P. Rautaharju, B. Horacek, and B. Taccardi, "Qualitative and quantitative analysis of characteristic body surface potential map features in anterior and inferior myocardial infarction," *Am. J. Cardiol.*, vol. 60, pp. 1230–1238, Dec. 1987.
- [18] A. Kléber, C. Riegger, and M. Janse, "Electrical uncoupling and increase of extracellular resistance after induction of ischemia in isolated, arterially perfused rabbit papillary muscle," *Circ. Res.*, vol. 61, pp. 271–279, Aug. 1987.
- [19] J. Degroot and R. Coronel, "Acute ischemia-induced gap junctional uncoupling and arrhythmogenesis," *Circ. Res.*, vol. 62, no. 2, pp. 323–334, May 2004. doi: <http://dx.doi.org/10.1016/j.cardiores.2004.01.033>.
- [20] J. Cinca, M. J. Janse, H. Morena, J. Candell, V. Valle, and D. Durrer, "Mechanism and time course of the early electrical changes during acute coronary artery occlusion," *Chest*, vol. 77, no. 4, pp. 499–505, Apr. 1980. doi: <http://dx.doi.org/10.1378/chest.77.4.499>.
- [21] D. C. Russell, J. S. Lawrie, R. A. Riemersma, and M. F. Oliver, "Mechanisms of phase 1a and 1b early ventricular arrhythmias during acute myocardial ischemia in the dog," *Am. J. Cardiol.*, vol. 53, no. 2, pp. 307–312, Jan. 1984. doi: [http://dx.doi.org/10.1016/0002-9149\(84\)90444-2](http://dx.doi.org/10.1016/0002-9149(84)90444-2).
- [22] W. T. Smith, W. F. Fleet, T. A. Johnson, C. L. Engle, and W. E. Cascio, "The Ib phase of ventricular arrhythmias in ischemic in situ porcine heart is related to changes in cell-to-cell electrical coupling," *Circ.*, vol. 92, pp. 3051–3060, Nov. 1995.
- [23] Q. Ni, "Assessment of spatial and temporal information in electric activity of the heart," Ph.D. dissertation, University of Utah, 2000.
- [24] B. Zenger, W. W. Good, J. A. Bergquist, B. M. Burton, J. D. Tate, L. Berkenbile, V. Sharma, and R. S. MacLeod, "Novel experimental model for studying the spatiotemporal electrical signature of acute myocardial ischemia: A translational platform," vol. 41, no. 1, p. 15002, Dec. 2020. doi: <http://dx.doi.org/10.1088/1361-6579/ab64b9>.
- [25] D. Brooks and R. MacLeod, "Electrical imaging of the heart: Electrophysical underpinnings and signal processing opportunities," *IEEE Sig. Proc. Mag.*, vol. 14, no. 1, pp. 24–42, May 1997.
- [26] Y. Rudy and B. Lindsay, "Electrocardiographic imaging of heart rhythm disorders: From bench to bedside," *Card. Electrophysiol. Clin.*, vol. 7, no. 1, pp. 17–35, Mar. 2015.
- [27] D. Wang, R. Kirby, and C. Johnson, "Finite-element-based discretization and regularization strategies for 3-D inverse electrocardiography," *IEEE Trans. Biomed. Eng.*, vol. 58, no. 6, pp. 1827–1838, Jun. 2011.

- [28] R. Holland and H. Brooks, "Spatial and nonspatial influences on the tq-st segment deflection of ischemia," *J. Clin. Invest.*, vol. 60, no. 1, pp. 197–214, Jul. 1977.
- [29] —, "TQ-ST segment mapping: Critical review and analysis of current concepts," *Am. J. Cardiol.*, vol. 40, no. 1, pp. 110–129, Jul. 1977.
- [30] W. Chang, T. Akitama, J. Richeson, R. Faillace, and P. Serrino, "Origin of the giant R wave in acute transmural myocardial infarctions in the pig." *Jap. Heart J.*, vol. 30, no. 6, pp. 863–883, Nov. 1989.
- [31] R. MacLeod, B. Taccardi, and R. Lux, "Mapping of cardiac ischemia in a realistic torso tank preparation," in *Building Bridges: International Congress on Electrocardiology Meeting*, Sep. 1995, pp. 76–77.
- [32] R. MacLeod, R. Lux, and B. Taccardi, "A possible mechanism for electrocardiographically silent changes in cardiac repolarization," *J. Electrocardiol.*, vol. 30, no. Suppl, pp. 114–121, Apr. 1997.
- [33] S. Sicouri, S. Moro, S. Litovsky, M. Elizari, and C. Antzelevitch, "Chronic amiodarone reduces transmural dispersion of repolarization in the canine heart." *J. Cardiovasc. Electrophysiol.*, vol. 8, no. 11, pp. 1269–79, Nov. 1997.
- [34] P. Ershler, R. Lux, and B. Steadman, "A 128 lead online intraoperative mapping system," in *Proceedings of the IEEE Engineering in Medicine and Biology Society 8th Annual International Conference*. IEEE Press, Jan. 1986, pp. 1289–1291.
- [35] W. J. Penny, "The deleterious effects of myocardial catecholamines on cellular electrophysiology and arrhythmias during ischaemia and reperfusion," *Europ. Heart J.*, vol. 5, no. 12, pp. 960–973, Dec. 1984. doi: <http://dx.doi.org/10.1093/oxfordjournals.eurheartj.a061616>.
- [36] S. Shome, R. Lux, B. Punske, and R. MacLeod, "Ischemic preconditioning protects against arrhythmogenesis through maintenance of both active as well as passive electrical properties in ischemic canine hearts," *J. Electrocardiol.*, vol. 40, no. 4, pp. S5–S6, Nov. 2007.
- [37] K. Aras, S. Shome, D. Swenson, J. Stinstra, and R. MacLeod, "Electrocardiographic response of the heart to myocardial ischemia," in *Computers in Cardiology 2009*, Sep. 2009, pp. 105–108.
- [38] K. Aras, "Bioelectric source characterization of acute myocardial ischemia," Ph.D. dissertation, University of Utah, 2015.
- [39] K. Aras, B. Burton, D. Swenson, and R. MacLeod, "Spatial organization of acute myocardial ischemia," *J. Electrocardiol.*, vol. 49, no. 3, pp. 689–692, May 2016.

- [40] B. Zenger, J. A. Bergquist, W. W. Good, L. C. Rupp, and R. S. MacLeod, "High-capacity cardiac signal acquisition system for flexible, simultaneous, multidomain acquisition," in *2020 Computing in Cardiol.*, Sep. 2020. doi: <http://dx.doi.org/10.22489/CinC.2020.190>. pp. 1–4.
- [41] A. Rodenhauser, W. Good, B. Zenger, J. Tate, K. Aras, B. Burton, and R. MacLeod, "PFEIFER: Preprocessing framework for electrograms intermittently fiducialized from experimental recordings," *J. Open Source Software*, vol. 3, no. 21, p. 472, 2018.
- [42] B. Burton, K. Aras, W. Good, J. Tate, B. Zenger, and R. MacLeod, "A framework for image-based modeling of acute myocardial ischemia using intramurally recorded extracellular potential," *Annal. Biomed. Eng.*, vol. 46, no. 9, pp. 1325–1336, 2018.
- [43] K. Reimer and R. Jennings, "Myocardial ischemia, hypoxia and infarction," in *The Heart and Cardiovascular System*, H. Fozzard *et al.*, Eds. New York: Raven Press, 1986, pp. 1133–2101.
- [44] B. Burton, K. Aras, W. Good, J. Tate, B. Zenger, and R. MacLeod, "Image-based modeling of acute myocardial ischemia using experimentally derived ischemic zone source representations," *J. Electrocardiol.*, vol. 51, no. 4, pp. 725–733, 2018.
- [45] B. Safdar, P. Ong, and P. G. Camici, "Identifying myocardial ischemia due to coronary microvascular dysfunction in the emergency department: introducing a new paradigm in acute chest pain evaluation," *Clin. Therapeutics*, pp. 1–11, Nov. 2018. doi: <http://dx.doi.org/10.1016/j.clinthera.2018.09.010>.
- [46] F. A. Bhuiya, S. R. Pitts, and L. F. McCaig, "Emergency department visits for chest pain and abdominal pain: United States, 1999–2008," *NCHS Data Brief*, no. 43, pp. 1–8, Sep. 2010.
- [47] B. Surawicz, "Ventricular repolarization in myocardial ischemia and myocardial infarction: Theory and practice," in *Comprehensive Electrocardiology*, 2nd ed., P. Macfarlane, A. van Oosterom, O. Pahlm, P. Kligfield, M. Janse, and J. Camm, Eds. London, England: Springer-Verlag, 2011, ch. 18, pp. 803–831.
- [48] L. Jespersen, S. Z. Abildstrøm, A. Hvelplund, and E. Prescott, "Persistent angina: highly prevalent and associated with long-term anxiety, depression, low physical functioning, and quality of life in stable angina pectoris," *Clin. Res. in Cardiol.*, vol. 102, no. 8, pp. 571–581, Aug. 2013. doi: <http://dx.doi.org/10.1007/s00392-013-0568-z>.
- [49] B. M. C. Noel, P. C. J., W. M. Norine, F. J. L., C. P. G., C. W. M., C. J. Austin, C. L. S., C. Filippo, D. C. Marcelo, D. P. S., G. Z. S., G. Paul, H. E. M., H. Ahmed, H. J. A., H. J. S., I. Erin, K. Ruth, L. G. N., L. Peter, L. Joao, M. Puja, D.-N. Patrice, O. Michelle, P. G. D., Q. A. A., R. Harmony, R. British, S. George, T. Viviany, W. Janet, and W. Nanette, "Ischemia and no obstructive coronary artery disease (INOCA)," *Circ.*, vol. 135, no. 11, pp. 1075–1092, Mar. 2017. doi: <http://dx.doi.org/10.1161/CIRCULATIONAHA.116.024534>.

- [50] L. Jespersen, A. Hvelplund, S. Z. Abildstrøm, F. Pedersen, S. Galatius, J. K. Madsen, E. Jørgensen, H. Kelbæk, and E. Prescott, "Stable angina pectoris with no obstructive coronary artery disease is associated with increased risks of major adverse cardiovascular events," *Europ. Heart J.*, vol. 33, no. 6, pp. 734–744, Mar. 2012.
- [51] A. H. Association, "Heart diseases and stroke statistics-2016 update," American Heart Association, Dallas, Texas, Tech. Rep., Dec. 2016.
- [52] S. Stern, "State of the art in stress testing and ischaemia monitoring." *Card. Electrophysiol. Rev.*, vol. 6, no. 3, pp. 204–208, Sep. 2002.
- [53] J. Knuuti, H. Ballo, L. E. Juarez-Orozco, A. Saraste, P. Kolh, A. W. S. Rutjes, P. Jüni, S. Windecker, J. J. Bax, and W. Wijns, "The performance of non-invasive tests to rule-in and rule-out significant coronary artery stenosis in patients with stable angina: A meta-analysis focused on post-test disease probability," *Europ. Heart J.*, vol. 39, no. 35, pp. 3322–3330, Sep. 2018. doi: <http://dx.doi.org/10.1093/eurheartj/ehy267>.
- [54] P. M. Okin, O. Ameisen, and P. Kligfield, "A modified treadmill exercise protocol for computer-assisted analysis of the ST segment/heart rate slope: Methods and reproducibility," *J. Electrocardiol.*, vol. 19, no. 4, pp. 311–318, Oct. 1986. doi: [http://dx.doi.org/10.1016/S0022-0736\(86\)81058-5](http://dx.doi.org/10.1016/S0022-0736(86)81058-5).
- [55] J. Bartunek, W. Wijns, G. R. Heyndrickx, and B. de Bruyne, "Effects of dobutamine on coronary stenosis physiology and morphology," *Circ.*, vol. 100, no. 3, pp. 243–249, Jul. 1999. doi: <http://dx.doi.org/10.1161/01.CIR.100.3.243>.
- [56] D. Mannering, T. Cripps, G. Leech, N. Mehta, H. Valentine, S. Gilmour, and E. D. Bennett, "The dobutamine stress test as an alternative to exercise testing after acute myocardial infarction." *Br. Heart J.*, vol. 59, no. 5, pp. 521–526, May 1988. doi: <http://dx.doi.org/10.1136/HRT.59.5.521>.
- [57] J. Shadeen, "Diagnostic value of 12-lead electrocardiogram during dobutamine echocardiographic studies," *Am. Heart J.*, vol. 136, no. 6, pp. 1061–1064, Dec. 1998. doi: [http://dx.doi.org/10.1016/S0002-8703\(98\)70163-2](http://dx.doi.org/10.1016/S0002-8703(98)70163-2).
- [58] M. R. Dhond, T. Nguyen, T. B. Whitley, K. Donnell, and W. J. Bommer, "Prognostic value of 12-Lead electrocardiogram during dobutamine stress echocardiography," *Echocardiography*, vol. 17, no. 5, pp. 429–432, Jul. 2000. doi: <http://dx.doi.org/10.1111/j.1540-8175.2000.tb01158.x>.
- [59] G. H. Mairesse, T. H. Marwick, J. L. J. Vanoverschelde, T. Baudhuin, W. Wijns, J. A. Melin, and J. M. R. Detry, "How accurate is dobutamine stress electrocardiography for detection of coronary artery disease? Comparison with two-dimensional echocardiography and technetium-99m methoxyyl isobutyl isonitrile (mibi) perfusion scintigraphy," *J. Am. Coll. Cardiol.*, vol. 24, no. 4, pp. 920–927, Oct. 1994. doi: [http://dx.doi.org/10.1016/0735-1097\(94\)90850-8](http://dx.doi.org/10.1016/0735-1097(94)90850-8).

- [60] B. D. Beleslin, M. Ostojic, J. Stepanovic, A. Djordjevic-Dikic, S. Stojkovic, M. Nedeljkovic, G. Stankovic, Z. Petrasinovic, L. Gojkovic, and Z. Vasiljevic-Pokrajcic, "Stress echocardiography in the detection of myocardial ischemia. Head-to-head comparison of exercise, dobutamine, and dipyridamole tests." *Circ.*, vol. 90, no. 3, pp. 1168–76, Sep. 1994. doi: <http://dx.doi.org/10.1161/01.cir.90.3.1168>.
- [61] E. G. Daoud, A. Pitt, and W. F. Armstrong, "Electrocardiographic response during dobutamine stress echocardiography," *Am. Heart J.*, vol. 129, no. 4, pp. 672–676, Apr. 1995. doi: [http://dx.doi.org/10.1016/0002-8703\(95\)90314-3](http://dx.doi.org/10.1016/0002-8703(95)90314-3).
- [62] S. A. Di Fusco, R. Rossini, F. Zilio, L. Pollarolo, F. S. di Uccio, A. Iorio, F. Lucà, M. M. Gulizia, D. Gabrielli, and F. Colivicchi, "Spontaneous coronary artery dissection: Overview of pathophysiology," *Trends in Cardiovas. Med.*, Jan. 2021. doi: <http://dx.doi.org/10.1016/j.tcm.2021.01.002>.
- [63] R. J. Myerburg, "Non-atherosclerotic causes of myocardial ischemia: With emphasis on spontaneous dissection of coronary arteries," *Trends in Cardiovas. Med.*, Feb. 2021. doi: <http://dx.doi.org/10.1016/j.tcm.2021.02.003>.
- [64] E. K. Aslanger, P. H. Meyers, and S. W. Smith, "STEMI: A transitional fossil in MI classification?" *J. Electrocardiol.*, vol. 65, pp. 163–169, Mar. 2021. doi: <http://dx.doi.org/10.1016/j.jelectrocard.2021.02.001>.
- [65] R. Al-Lamee, D. Thompson, H.-M. Dehbi, S. Sen, K. Tang, J. Davies, T. Keeble, M. Mielewczik, R. Kaprielian, I. S. Malik, S. S. Nijjer, R. Petraco, C. Cook, Y. Ahmad, J. Howard, C. Baker, A. Sharp, R. Gerber, S. Talwar, R. Assomull, J. Mayet, R. Wensel, D. Collier, M. Shun-Shin, S. A. Thom, J. E. Davies, D. P. Francis, R. Al-Lamee, D. Thompson, S. Sen, K. Tang, J. Davies, T. Keeble, R. Kaprielian, I. S. Malik, S. S. Nijjer, R. Petraco, C. Cook, Y. Ahmad, J. Howard, M. Shun-Shin, A. Sethi, C. Baker, A. Sharp, P. Ramrakha, R. Gerber, S. Talwar, R. Assomull, R. Foale, J. Mayet, R. Wensel, S. A. Thom, J. E. Davies, D. P. Francis, R. Khamis, N. Hadjiloizou, M. Khan, J. Kooner, M. Bellamy, G. Mikhail, P. Clifford, P. O'Kane, T. Levy, and R. Swallow, "Percutaneous coronary intervention in stable angina (ORBITA): A double-blind, randomised controlled trial," *Lancet*, vol. 391, no. 10115, pp. 31–40, Jan. 2018. doi: [http://dx.doi.org/10.1016/S0140-6736\(17\)32714-9](http://dx.doi.org/10.1016/S0140-6736(17)32714-9).

CHAPTER 3


NOVEL EXPERIMENTAL MODEL FOR STUDYING THE SPATIOTEMPORAL ELECTRICAL SIGNATURE OF ACUTE MYOCARDIAL ISCHEMIA: A TRANSLATIONAL PLATFORM

©Institute of Physics and Engineering in Medicine. Reproduced with permission. All rights reserved

PAPER**Novel experimental model for studying the spatiotemporal electrical signature of acute myocardial ischemia: a translational platform**

To cite this article: Brian Zenger *et al* 2020 *Physiol. Meas.* **41** 015002

View the [article online](#) for updates and enhancements.



AAS | **IOP Astronomy** ebooks

Part of your publishing universe and your first choice for astronomy, astrophysics, solar physics and planetary science ebooks.

iopscience.org/books/aas



PAPER

Novel experimental model for studying the spatiotemporal electrical signature of acute myocardial ischemia: a translational platform

RECEIVED
15 October 2019REVISED
18 December 2019ACCEPTED FOR PUBLICATION
20 December 2019PUBLISHED
5 February 2020

Brian Zenger^{1,2,3,4,5}, Wilson W Good^{1,2,4}, Jake A Bergquist^{1,2,4}, Brett M Burton¹, Jess D Tate¹,
Leo Berkenbile¹, Vikas Sharma¹ and Rob S MacLeod^{1,2,3,4}

¹ Scientific Computing and Imaging Institute, SLC, UT, United States of America² Nora Eccles Cardiovascular Research and Training Institute, SLC, UT, United States of America³ School of Medicine, University of Utah, SLC, UT, United States of America⁴ Department of Biomedical Engineering, University of Utah, SLC, UT, United States of America⁵ Author to whom any correspondence should be addressed.E-mail: zenger@sci.utah.edu**Keywords:** electrocardiography, electrophysiology, electrocardiographic imaging, myocardial ischemia, cardiac stress test**Abstract**

Myocardial ischemia is one of the most common cardiovascular pathologies and can indicate many severe and life threatening diseases. Despite these risks, current electrocardiographic detection techniques for ischemia are mediocre at best, with reported sensitivity and specificity ranging from 50%–70% and 70%–90%, respectively. *Objective:* To improve this performance, we set out to develop an experimental preparation to induce, detect, and analyze bioelectric sources of myocardial ischemia and determine how these sources reflect changes in body-surface potential measurements. *Approach:* We designed the experimental preparation with three important characteristics: (1) enable comprehensive and simultaneous high-resolution electrical recordings within the myocardial wall, on the heart surface, and on the torso surface; (2) develop techniques to visualize these recorded electrical signals in time and space; and (3) accurately and controllably simulate ischemic stress within the heart by modulating the supply of blood, the demand for perfusion, or a combination of both. *Main results:* To achieve these goals we designed comprehensive system that includes (1) custom electrode arrays (2) signal acquisition and multiplexing units, (3) a surgical technique to place electrical recording and myocardial ischemic control equipment, and (4) an image based modeling pipeline to acquire, process, and visualize the results. With this setup, we are uniquely able to capture simultaneously and continuously the electrical signatures of acute myocardial ischemia within the heart, on the heart surface, and on the body surface. *Significance:* This novel experimental preparation enables investigation of the complex and dynamic nature of acute myocardial ischemia that should lead to new, clinically translatable results.

1. Introduction

Despite several decades of research progress, ischemic heart disease remains one of the most common heart pathologies, affecting over 8 million people globally (Safdar *et al* 2018). Myocardial ischemia occurs when there is inadequate perfusion to a specific region of the heart, leading to mechanical, electrical, and functional abnormalities. A surprising range of pathologies can cause acute transient ischemia, including coronary artery disease, coronary microvascular dysfunction, Takotsubo cardiomyopathy, and coronary artery dissection (Jespersen *et al* 2012, 2013, Noel *et al* 2017, Safdar *et al* 2018). Each pathology carries a significant risk of short- and long-term mortality that can be reduced substantially by early detection. Therefore, detecting myocardial ischemia early is paramount to preventing long-term negative consequences (Kontos *et al* 1999, Noel *et al* 2017, Knuuti *et al* 2018, Safdar *et al* 2018). For decades, the electrocardiogram (ECG) has been the primary acute detection method for myocardial ischemia (McCarthy *et al* 1990), however, current performance using these methods is mediocre at best, with reported sensitivity and specificity ranging from 50%–70% and

70%–90%, respectively (Stern 2002, Knuuti *et al* 2018). This poor performance indicates that many patients may be discharged from clinical care unaware of their potentially life-threatening condition, and others may receive care they do not need. Improvements in the electrical detection of myocardial ischemia must be made to ensure confident and accurate diagnoses of myocardial ischemia to prevent fatal long-term consequences.

This poor ECG-based performance may stem from our limited understanding of the ischemic bioelectric sources within the myocardium and how they manifest as electrical signals on the body surface. Past studies based on limited measurement capabilities have suggested that myocardial ischemia originates on the endocardial surface of the heart and progresses radially outward to the epicardium (Savage *et al* 1977, Janse *et al* 1979). However, our recent experimental studies have shown that these assumptions are not supported, at least in large mammal models. Aras *et al* showed acute ischemia originating throughout the myocardial wall (Shome *et al* 2007, Aras *et al* 2011b). These findings and the poor clinical performance of ECG ischemia detection have spurred discussion about other assumptions and re-evaluations of the conventional description of ischemic sources within the heart, but conclusions have been limited in their understanding of physiology and clinical application because experimental models have lacked some key components. Currently, no experimental model has been reported that can control the ischemic load and simultaneously record the electrical potentials within the heart, on the heart surface, and on the body surface. Without these data from an experimental model, improved methods of detection cannot be verified, which in turn inhibits the testing and implementation of new methods for detecting myocardial ischemia.

To maximize its translational potential, an experimental model of acute myocardial ischemia must (1) have comprehensive and simultaneous high-resolution electrical recordings within the myocardial wall, on the heart surface, and on the torso surface; (2) be supported by techniques to visualize these recorded electrical signals in time and space; and (3) accurately and controllably simulate ischemic stress within the heart by modulating the supply of blood, the demand for perfusion, or a combination of both. Previous experimental models that have included some of these criteria have been applied to other targets: high-resolution recordings on some surfaces, controlled ischemic load, and other unique recording or interventional techniques (Spach and Barr 1975, Bear *et al* 2015a, Cluitmans *et al* 2017, Zenger *et al* 2018). However, all previously reported models have lacked at least one of the three necessary criteria for a comprehensive examination of acute myocardial ischemia.

Here we report on the development and validation of an experimental preparation to detect and analyze bioelectric sources of myocardial ischemia and determine how these sources reflect changes in body-surface potential measurements. We have achieved all the requirements listed above and created an experimental preparation that will enable significant progress in the understanding and detection of acute myocardial ischemia.

2. Methods

We developed techniques to achieve the three major goals for this study. To simultaneously record within the heart, on the epicardial surface, and on the body surface, we used custom arrays of recording electrodes based on silver and silver chloride substrate and a custom multiplexing system that could record up to 1024 channels at 1 kHz. To process the recorded signals and create three-dimensional models, we used a combination of open-source and custom software applications produced at the Scientific Computing and Imaging Institute (www.sci.utah.edu). This processing pipeline was used to create three-dimensional geometric models that provide a framework for interactive visualization and for simulations of bioelectric fields, such as electrocardiographic imaging (ECGI) (Cluitmans *et al* 2017, Tate *et al* 2018). Finally, we controlled ischemic load by increasing cardiac demand through pacing or pharmacological stimulation and by decreasing cardiac supply with a hydraulic vascular occluder placed around the left anterior descending coronary (LAD).

2.1. Animal model

Swines and canines were selected for this experimental preparation because their cardiac anatomy, electrical system, and vascular structure are similar to those of humans. The animals were 25–35 kg in weight and 8 months to several years of age. They were purpose bred for use in experimental research and all studies were approved by the Institutional Animal Care and Use Committee at the University of Utah and conformed to the Guide for Care and Use of Laboratory Animals. After 12 h of fasting, canines were sedated using an intravenous propofol bolus of 5–8 mg kg⁻¹, and swine were sedated using a mixture of telazol (4.4 mg kg⁻¹), ketamine (2.2 mg kg⁻¹), and xylazine (2.2 mg kg⁻¹). Once intubated, isoflurane gas (1%–5%) was used for anesthesia. At the end of the experiment, the animals were euthanized while under general anesthesia, with intravenous Beuthanasia 1 ml/10 kg. The heart was then removed for further evaluation.

2.2. Surgical procedure

Following sedation, a sternotomy was performed to expose the thoracic cavity. The pericardium was opened and the heart was suspended in a pericardial cradle. Following exposure, a portion of the left anterior descending

coronary artery (LAD) was dissected, and a calibrated hydraulic occluder (Access Technologies, Skokie, IL, USA) was placed around the dissected LAD. An atrial pacing clip was then placed on the appendage of the right atrium. Following placement of the electrical recording equipment (described below), the pericardium was sutured closed, and the sternum was wired and sutured together. To limit air within the volume conductor, chest tubes were tunneled into the mediastinal, pleural, and pericardial cavities and held under constant suction (5–20 mmHg). The outer layers of dermis were sutured closed and checked for separations. Standard laboratory markers, including blood pH, PaCO₂, oxygen saturation, temperature, and blood pressure, were measured and recorded throughout the experiment.

2.3. Electrical recording equipment

2.3.1. Electrode arrays

All electrodes and recording equipment were custom-built at the Nora Eccles Treadwell Cardiovascular Research and Training Institute (CVRTI) and similar to our work described previously with several important modifications (Shome *et al* 2007, Aras *et al* 2009, 2011b, 2016b). The electrical signals within the myocardium were measured using the Utah intramural plunge needle arrays (UIPNAs). Each needle in the array had 10 electrodes on a 1.5 mm shaft spaced 1.8 or 1.1 mm apart for left and right ventricular needles, respectively (figures 1(A)–(C)). The needle electrodes were housed within of a hollow plastic tube with openings for each electrode that was custom fabricated using 3D printing (FormLabs, MA, USA). All ten electrode wires (0.0762 mm, high purity silver, California Fine Wire Company, CA, USA) terminated at an individual hole in the tube and passed through the tube, through strain relief built into the tube end, and then to 24-pin connectors. For these experiments, 12–25 needles were placed in the approximated perfusion bed of the LAD and concentrated on the anterior aspect of the heart.

The epicardial potentials were measured separately using the Utah high density epicardial sock (UHDES), an array of 247 silver wire electrodes tied into a nylon sock. The electrode wires were 0.127 mm insulated silver wires (California Fine Wire Company, CA, USA) spaced at approximately 10 mm; the end of each was stripped and then electroplated with silver chloride to reduce polarizing potentials. A subset of the electrodes also received color-coded beads that provided references for subsequent digitization of sock position (figure 1(D)).

The torso surface electrodes were grouped in strips of 12 electrodes evenly spaced 3 cm apart. Each electrode had an 11 mm diameter Ag–AgCl sensor embedded in an epoxy housing with a 2 mm deep gel cavity. The number of strips applied to the torso surface varied between 6–10 (72–120 total electrodes) depending on the body-surface area accessible for each animal.

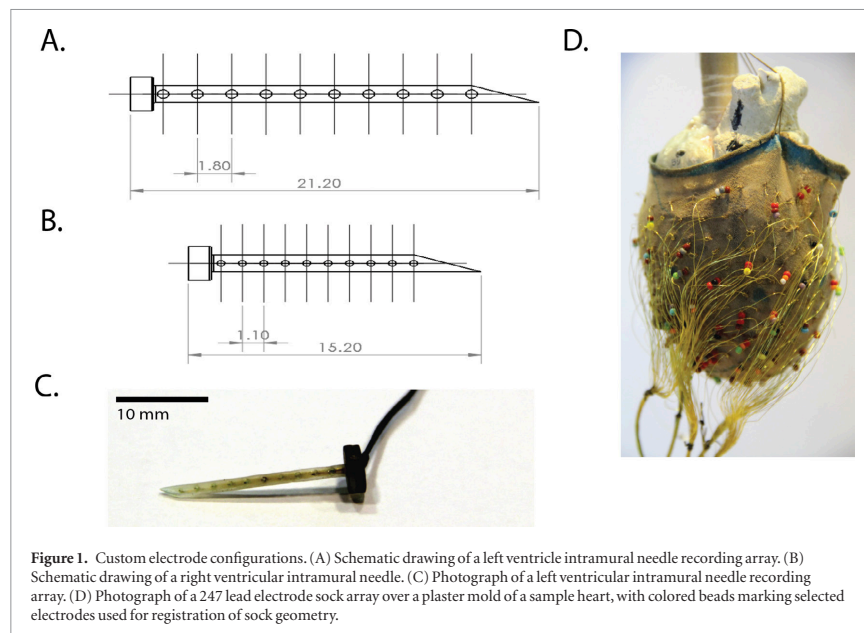
2.3.2. Signal acquisition

The electrical potentials from the needle, sock, and torso surface electrodes were captured using a custom acquisition system that could record simultaneously from 1024 channels at 1 kHz sampling rate and 12 bit resolution (Ershler *et al* 1986). The acquisition system consisted of variable gain input amplifiers, multiplexers, A/D converters, interface circuitry, and a personal computer (PC) hosting a custom program written in Labview (National Instruments, Austin, TX, USA) that managed the hardware and allowed continuous signal acquisition. A bandpass filter with cutoff frequencies at 0.03 and 500 Hz avoided both DC potentials and aliasing. Wilson's central terminal leads were used as the remote reference for all the unipolar signals recorded from the sock, needles, and torso surface electrodes. Prior to each experiment, calibration signals were recorded on each channel to allow subsequent gain adjustments to accommodate thermal variations (figure 2 right pathway).

2.4. Ischemia intervention protocols

Ischemia intervention protocols can be designed to test different clinical or scientific hypotheses by varying the time of ischemia, relative ischemic load, and other important variables. We induced several transient ischemic interventions, each lasting 8–15 min, during each experiment, followed by a 30 min recovery period, similar to our previous studies (Aras *et al* 2016b). One ischemic protocol mimicked the Bruce exercise stress test by first reducing the coronary diameter by 50%–70% and then pacing the heart at an increasing increment above resting heart rate every 3 min for a total of 15 min similar to protocols reported in the literature (Okin *et al* 1986). The intervention was terminated prematurely by the presence of a sequence of three or more premature ventricular contractions.

Another example of an ischemic protocol we applied was based on the clinical dobutamine stress test. Dobutamine is used as a pharmacological stress agent because of its direct stimulation of beta-1 sympathetic receptors on the heart, causing increased heart rate and contractility. In our dobutamine stress protocol, the animal was continuously infused at a sequence of increasing doses, each for 3 min, following routine clinical protocols (Mannerling *et al* 1988). As with the Bruce protocol, the intervention again lasted 15 min or until a sequence of three or more premature ventricular contractions occurred. The LAD occlusion level was again fixed throughout the 15 min episode.



Each of these protocols utilized changes in the ST segment voltage as a surrogate for ischemia within the myocardial wall. Cellular and mechanistic studies have shown that changes in the ST segment correspond to ischemia forming in the underlying myocardial substrate (Kubota *et al* 1993, Li *et al* 1998).

2.5. Image acquisition and processing

2.5.1. Image acquisition and segmentation

A major goal of studies using this model is to construct accurate, subject-specific geometric models that include the anatomy and electrode locations. To this end, after the animal was euthanized, the intact torso was imaged with a clinical 3 T MRI scanner (Siemens Medical, Erlangen, Germany) for gross anatomy and electrode positions. Following the torso scan, the heart was excised, filled with dental alginate to preserve heart chamber shape, fixed in formalin, and scanned with a 7 T MRI scanner (Bruker BIOSPEC 70/30, Billerica, MA) using FISP (fast imaging with steady-state precession) and FLASH (fast low angle shot) imaging sequences. To visualize fiber orientation in each heart, a diffusion-weighted MRI sequence was also performed. Capitalizing on the combined advantages of both FISP (consistent volume boundaries) and FLASH sequences (high internal contrast), we produced geometric segmentations of cardiac tissue, blood, and intramural plunge needle geometries using the Seg3D open-source software package⁶. To visualize the perfusion bed and vasculature, the coronaries were injected with BriteVue contrast agent (Scarlet Imaging, SLC, UT, USA), and the heart was scanned using an Inveon microCT Scanner (Siemens, Munich, Germany) (figure 2 center pathway).

From the segmented cardiac volumes we then created three-dimensional, tetrahedral meshes of the heart and torso using the the Cleaver open-source software package⁷ for use in subsequent visualization and simulation (figure 2 central pathway).

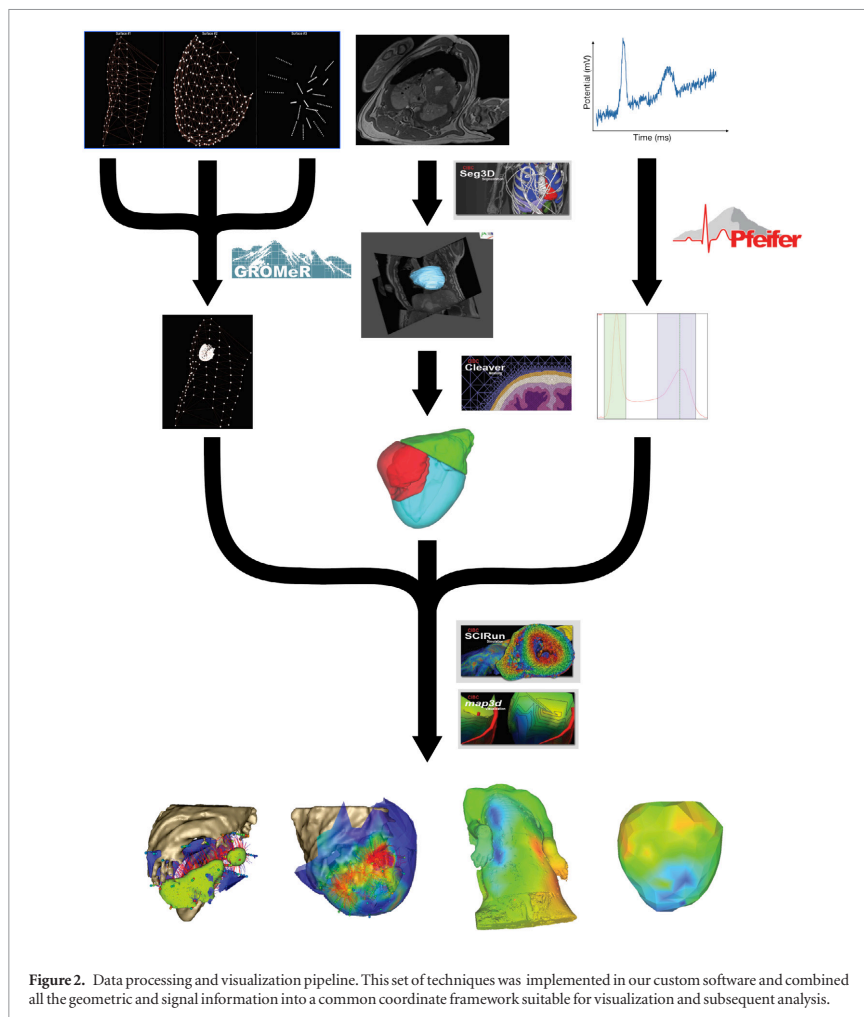
2.6. Geometric registration

2.6.1. Landmark point recordings

At the conclusion of each experiment, the locations of the torso surface electrode strips, the reference sock electrodes, and plunge needle insertion sites on the cardiac surface were measured manually using a microscribe three-dimensional digitizer (Solution Technologies, Oella, MD, USA). In addition, anatomical landmark sites, including the location of the occlusion site, major epicardial coronary arteries, and the outline of the myocardial shape were also captured using the digitizer. Once the locations of the plunge needles were recorded, they were replaced with plastic spacers that preserved the intramural needle array tracts and could be visualized in subsequent imaging (described above) (figure 2 left pathway).

⁶ www.sci.utah.edu/software/seg3d.

⁷ www.sci.utah.edu/software/cleaver.



2.6.2. Registration pipeline

We have developed and implemented a sequence of registration techniques to identify and register electrode locations relative to cardiac and gross anatomical structures (Bergquist *et al* 2019). First, the high-resolution *ex vivo* FISP and FLASH MRIs of the explanted heart were registered to the full torso MRI scan via an affine transformation using the needle electrode locations in each geometric space. Next, the 247 electrode sock array was registered to the high-resolution heart mesh generated from the images. This step involved an affine transformation that moved the digitized subset of sock array electrodes to the torso MRI space. The transformed, digitized sock points were then snapped (by nearest neighbor) to the myocardial surface. To register the rest of the sock electrodes, we used a nominal sock mesh generated previously by stretching the sock over a heart model and digitizing all electrodes. This nominal sock mesh was first roughly fitted to the high-resolution heart mesh by contracting the sock along its base-apex axis to adjust vertical electrode spacing. The sock was then aligned on the heart mesh using correspondence-driven iterative closest points registration and then snapped to the heart mesh. Finally, the sock correspondence points were used to register the remaining electrodes with a geodesically constrained radial basis deformation as described previously (Bergquist *et al* 2019) (figure 2 right pathway).

2.7. Signal processing

The electrical signals recorded during the study were processed in the preprocessing framework for electrograms intermittently fiducialized from experimental recordings (PFEIFER), an open-source MATLAB-based signal processing platform designed to process bioelectric signals acquired from experiments, as outlined schematically in the upper right panel of figure 2 (Rodenhauser *et al* 2018). Using PFEIFER, the recorded signals were calibrated, baseline corrected, filtered, and marked at specific time instances within each beat for further analysis. The filter was an amplitude normalized 11th order rational transfer function. Gain correction for the amplifiers was performed on each individual channel by acquiring a reference sine wave of known amplitude(s) at the start of each experiment. A linear baseline drift correction was applied by selecting two assumed isoelectric points at the beginning and end of each beat. Signals of obviously poor quality from any electrode were discarded and Laplacian interpolated from the nearest neighboring electrodes (Oostendorp *et al* 1989). We also identified and discarded electrograms recorded from needle electrodes within the blood cavities from their morphology; electrograms without an initial positive deflection were assumed to be from within the blood pool (Taccardi *et al* 2008).

A separate global root mean squared (RMS) signal was computed from each of the sock, intramural, and torso surface signals and then used to mark temporal fiducials around the QRS complex and the T wave. PFEIFER can then utilize intermittent, manually annotated beats to automatically identify and annotate the remaining beats within the recorded signals. From these markings, we extracted the ST40%, QT-interval, and QRS amplitude for further analysis. ST40% is the measured voltage at 40% of the ST segment duration, selected because of previous studies that showed changes in the ST segment relating to ischemia (Janse *et al* 1980). Algorithms also automatically extracted the activation and recovery times from the each electrogram using methods described previously (Millar *et al* 1985, Lux and Ershler 1987). PFEIFER greatly accelerated these processing steps by propagating and adjusting fiducial markers set by the user from one beat to all subsequent beats in an continuously acquired run.

2.8. Electrical potential mapping and data visualization

Finally, the processed electrograms and extracted parameters (ST40%, QT-interval, etc) were mapped to the associated electrode locations within the heart and on the epicardial and torso surfaces. Experimental model datasets were then visualized interactively using *map3d* (www.sci.utah.edu/software/map3d) or SCIRun (www.sci.utah.edu/software/scirun), open-source software packages that provided for extensive spatio-temporal exploration, an example of which is shown in the lower panel of figure 2.

2.9. Model validation

2.9.1. Canine and porcine comparison metrics

We implemented several standard electrocardiographic metrics to verify our signal processing techniques and compare baseline and ischemic electrophysiological parameters in canine and porcine subjects. Time intervals were determined from the root-mean-square of all recorded signals, voltages were calculated from each individual electrode within a recording surface. The QRS amplitude was defined as the absolute difference between the minimum and maximum voltage measured during the QRS interval independent of morphology. The corrected QT interval was calculated using Bazett's formula. Each metric is reported as an average plus or minus standard deviation. Student's t-tests were performed on a subset of experimental data as described in results where p-values less than 0.05 were considered significant.

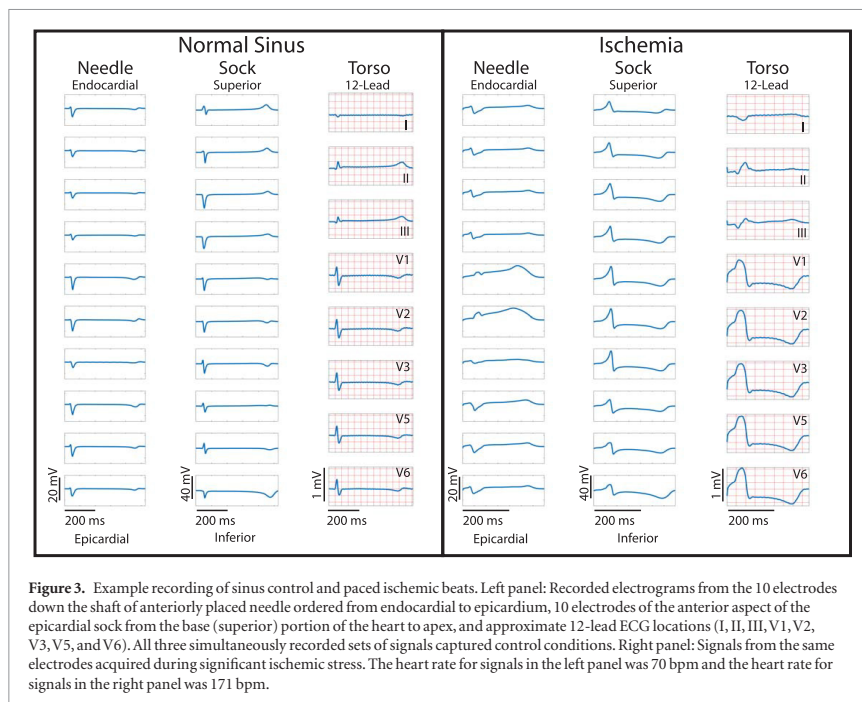
2.9.2. Changes induced by electrical recording equipment

A natural concern in such a preparation is that signals recorded after the surgery do not resemble those beforehand. To examine such questions, prior to sternotomy, we placed torso surface electrodes and recorded normal sinus rhythm. We then opened the chest, placed the sock and needle electrode arrays and ischemic control equipment, and then closed the chest and recorded normal sinus rhythm from the same torso surface electrodes. We then compared the pre- and post-surgical values of QRS duration, QRS amplitude, and ST40%. To evaluate the changes specifically induced by placement of the needle electrodes, we applied the epicardial sock array and recorded before and 90 min after the insertion of the needle arrays and then compared values of QRS duration, QRS amplitude, and ST40% values. Student's t-tests were performed on a subset of experimental data as described in results, where p-values less than 0.05 were considered significant.

3. Results

3.1. Multiregion detection of ischemia

Figure 3 shows sample measurements of electrograms and ECGs across all measured regions during normal sinus and induced ischemia. The left main panel shows measured potentials along a single transmural needle ordered (from top to bottom as endocardium to the epicardium); a strip of sock electrodes ordered from base to



apex, and an approximate 12-lead ECG signal including leads I, II, and III and unipolar precordial leads V1, V2, V3, V5, and V6 during a normal sinus control recording. The right panel shows signals from the same electrodes recorded during significant ischemic stress.

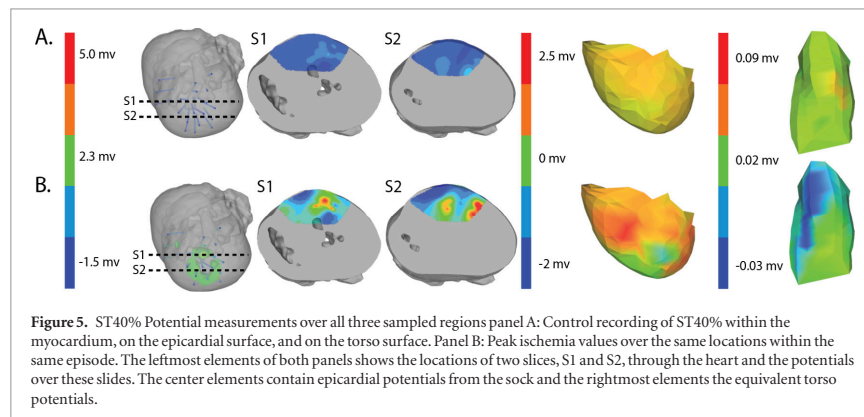
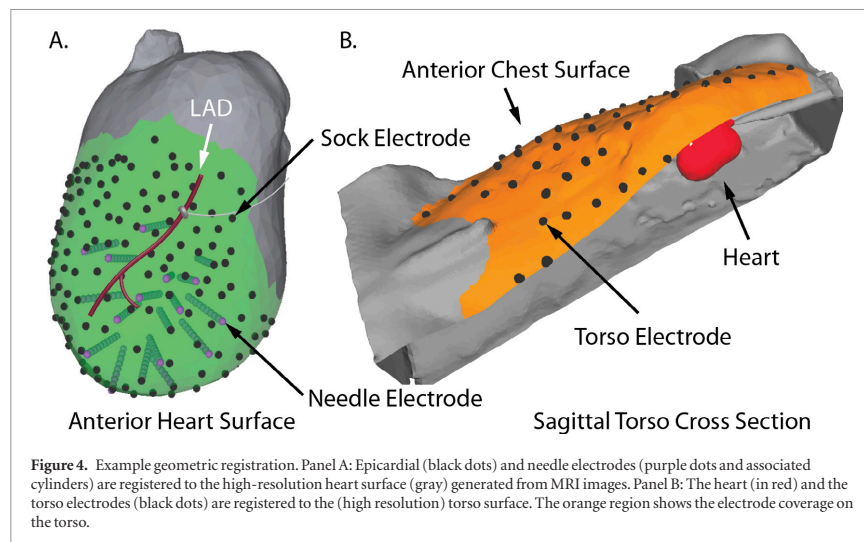
All signals across the different recording domains were automatically time aligned because they were all recorded simultaneously and all signals in the figure show typically high quality and with low noise following standard filtering. The differences in signal morphologies between control and peak ischemia in the figure are dramatic with ST-segment deviations and T-wave changes through the myocardium (needles) and the superior leads of both the epicardial and precordial torso leads. The QRS complexes also showed Q waves and prolonged activation duration throughout most of the regions.

3.2. Processing and visualization pipeline

To register all elements of the anatomy and electrode locations and visualize these signals, we used a novel processing and visualization pipeline that leveraged tools from a combination of open-source projects. Figure 4 shows one example of the electrode locations and thoracic anatomy after registration into the same coordinate space. Panel (A) in the figure shows the epicardial sock and measurement electrodes (black dots) and the plunge needles (purple points at the ends of cylinders), and the gray occluder placed over the red LAD. The sock electrodes were evenly distributed around the entire ventricles, from the apex to the base. Panel (B) shows a subset of the torso surface electrodes (black dots) and the overall electrode coverage (orange surface) in a cutaway view of the torso with the heart partially visible (in red). The distance between intramural plunge needles was typically 9–11 mm, the distances between epicardial recording electrodes in the range of 6–8 mm, and the spacing between torso surface electrodes was 4–5 cm.

3.3. Ischemic load control

Figure 5 shows an example of the results from the same episode of induced ischemia, in which we rapidly stimulated the heart under reduced coronary flow. Panel (A) shows the control values of ST40% potentials in all three regions and panel (B) shows the this same parameter during peak ischemic load. The range of measured ST40% values during peak ischemia was -1 mV to $+11$ mV in the intramural plunge needles, -2 mV to $+7$ mV on the epicardial sock, and -0.2 mV to $+0.2$ mV on the torso surface. Typical clinical indications for acute myocardial ischemia are ST segment deviations of more negative than -0.1 mV or more positive than $+0.2$ mV



3.4. Model validation

3.4.1. Effects of surgery and electrode placement

Table 1 shows recorded torso potentials before and after surgery and the placement of the epicardial sock and needle electrode arrays during one experiment. Using a paired Student's t-test, the QRS interval and QRS amplitude showed no significant difference on the torso surface recordings before and after placement of the electrode recording equipment.

Changes caused by the placement of needle electrode arrays were also observed on the epicardial sock in figure 6 and table 2. Figure 6 shows ST40% potentials measured on an example sock array before, immediately after, and 90 min after placement of the transmural plunge needles. Immediately following needle placement there is an increase in ST40% potentials which recover to below baseline recordings within 90 min of final needle placement. Table 2 shows little changes to relevant ECG parameters before and after 90 min rest following needle placement. There was no significant difference in QRS amplitude before and after placement of the plunge needles ($p > 0.05$). There was, however, a significant difference in QRS interval before and after placement of transmural plunge needles ($p < 0.05$).

3.4.2. Canine versus porcine species

Tables 3 and 4 show a statistical comparison of signals recorded for both canine and porcine subjects during sinus rhythm and atrially paced beats at control rates. Canine subjects showed larger voltages across all surfaces

Table 1. Recorded torso potentials prior to sternotomy, with no sock or needle electrodes placed, compared to those acquired after placement of the cardiac electrodes and closure of the chest. Values were the mean and standard deviations across all torso electrodes.

Metric	Prior to sternotomy	After chest closure
QRS Interval (ms)	52.11 ± 2.10	51.86 ± 1.09
QRS Peak to peak amplitude (mV)	0.45 ± 0.33	0.53 ± 0.13
ST40% (mV)	0.009 ± 0.01	-0.001 ± 0.011

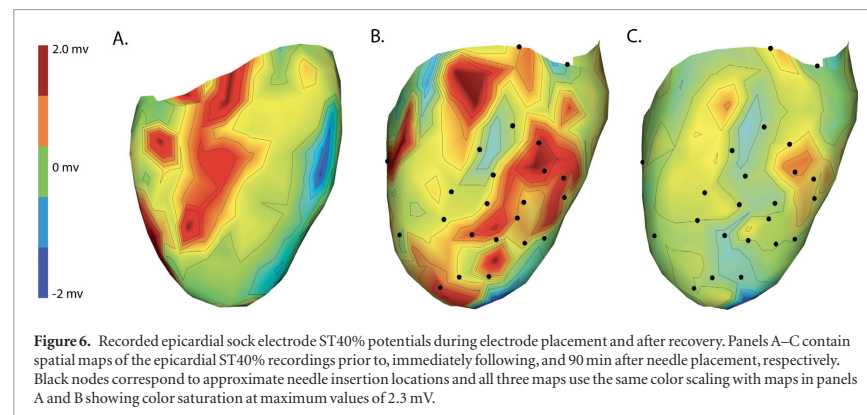


Table 2. Recorded epicardial sock potentials before, 30 min after, and 90 min after placement of needle electrodes. Values were the mean and standard deviations across all sock electrodes.

Metric	Prior	30 min	90 min
QRS interval (ms)	49.74 ± 1.86	54.78 ± 1.72	52.88 ± 2.46
QRS Peak to peak amplitude (mV)	11.34 ± 3.72	10.89 ± 3.31	10.05 ± 3.33
ST40% (mV)	0.29 ± 0.70	0.32 ± 0.42	0.07 ± 0.34

Table 3. Table showing the recorded voltages separated by canine, porcine, and different recording surfaces. S and AP stand for Sinus and Atrial Paced recordings, respectively, QRS Amp and VRange stand for QRS peak to peak amplitude and voltage range across all electrodes, respectively. Each metric was derived from each individual electrode.

Metric	Canine (<i>n</i> = 2)			Porcine (<i>n</i> = 3)		
	Needles (mV)	Sock (mV)	Torso (mV)	Needles (mV)	Sock (mV)	Torso (mV)
S QRS Amp	16.77 ± 8.37	18.62 ± 5.21	1.58 ± 0.61	8.09 ± 4.04	7.87 ± 3.11	0.37 ± 0.13
AP QRS Amp	17.61 ± 8.95	19.07 ± 5.57	1.50 ± 0.58	9.11 ± 4.29	8.45 ± 3.18	0.37 ± 0.14
S VRange	(0.01–47.30)	(0.002–40.73)	(0.007–3.20)	(0.006–29.00)	(0.005–29.31)	(0.0002–1.10)
AP VRange	(0.01–47.59)	(0.002–41.41)	(0.007–3.14)	(0.002–27.42)	(0.006–28.90)	(0.005–1.48)
Peak ST40%	6.77 ± 4.94	-0.10 ± 3.28	-0.09 ± 0.13	0.93 ± 2.36	-1.28 ± 1.70	-0.12 ± 0.20

compared to porcine. Results in table 4 show no significant difference between QRS intervals ($p > 0.05$), however, QTc intervals were significantly different between species ($p < 0.05$).

4. Discussion

In this study we developed a novel experimental approach that supports comprehensive, high-resolution, three-dimensional exploration of the development and electrical manifestations of myocardial ischemia. We have shown that it is possible to create controllable, transient myocardial ischemia documented by measurements of bioelectric time signals from the heart and torso and associated anatomical images. We have shown that it is also feasible using open source software tools to process these recordings and visualize the spatial and temporal development of ischemia. Specific improvements over other reported models include simultaneously measuring bioelectric signals within the myocardium, on the heart surface, and on the torso surface in a physiologically and anatomically realistic setting of a closed chest under cardiovascular and respiratory control. Our previous studies

Table 4. Table showing the recorded time intervals in canine versus porcine subjects. Each metric was derived from the from a manual marking of the root-mean-squared (RMS) signal.

Metric	Canine ($n = 2$)	Porcine ($n = 3$)
Sinus QRS interval (ms)	50.94 \pm 5.28	56.77 \pm 7.40
Atrial paced QRS interval (ms)	51.63 \pm 4.75	53.94 \pm 10.27
Sinus QTc interval (ms)	346.65 \pm 16.54	483.56 \pm 39.75
Atrial paced QTc interval (ms)	365.53 \pm 9.33	459.65 \pm 26.71

reported on progress in controlling ischemic load via hydraulic occlusion of coronary vasculature combined with rapid pacing or pharmacological stress (Shome *et al* 2007, Aras *et al* 2009, 2011b, Aras *et al* 2011a, 2014). We have also created a signal processing pipeline and registration system to generate the associated geometric model and to visualize the electrical signals in three-dimensional space, across geometries, throughout an ischemic intervention (Rodenhauser *et al* 2018, Berguist *et al* 2019).

Previous studies have reported similar, closed chest animal models (Spach *et al* 1977, Bear *et al* 2015a, Cluitmans *et al* 2017), but none have achieved the extent and resolution of coverage of this study, nor were they designed to explicitly study myocardial ischemia. The first such reports by Spach *et al* showed that a re-closed torso preparation was surgically feasible. They achieved simultaneous recordings from 200 sites within the myocardium, 20–30 sites on the epicardium, and 50 sites on the torso surface (Spach *et al* 1977). While a masterful achievement, the limits of technology at that time restricted the scope and resolution of the measurements and also the reconstructions and visualization of the results. Bear *et al* again achieved the closed-chest preparation in the early 2000s, but they did not record electrical signals from within the myocardium, but rather the ventricular and torso surfaces (Bear *et al* 2015b). Finally, Cluitmans *et al* succeeded in placing epicardial and torso surface electrodes, but they, too, had no recordings from within the myocardium and focused their approach on activation sequence recovery in order to validate their electrocardiographic imaging (ECGI) approaches (Cluitmans *et al* 2017). Another important element missing from these preparations was the ability to control ischemic load on the heart. None of these preparations had an efficient and standardized way to induce this pathology, which further limited their application to the study of myocardial ischemia.

Our early findings using a somewhat simpler experimental model of myocardial ischemia have motivated both the reported advances and additional interventions and analyses. Results from those studies suggested a mechanism of variable, distributed ischemia development, in sharp contrast to conventional assumptions. For example, we have showed that distributed ischemia was more likely to form in the midmyocardium rather than at the endocardial borders. Results from studies that capture the three-dimensional extent of intramyocardial ischemia by means of the needle electrodes have also motivated simulation studies and allowed us to compare measured and simulated epicardial potentials (Burton *et al* 2016, 2018, 2018b), studies that allowed us to refine the understanding of the fundamental nature of intramyocardial bioelectric sources (Burton *et al* 2018b).

The data collected from the experiments conducted by Aras *et al* also supported studies of ECGI and simulation of ischemia, which have shown that representing ischemia with realistic source models produces more accurate potentials on the heart surface than those based on simplified source models or those anchored to the subendocardium (Burton *et al* 2011, 2018, 2018b). However, these studies all lacked measured body-surface potentials, limiting their translational impact. The combination of these findings and other similar preliminary results has motivated our novel experimental preparation. Following analysis, these experimental datasets will be made publicly available on the experimental data and geometric analysis repository (EDGAR) that hosts datasets for such applications (Aras *et al* 2015).

Both canines and porcines were used in this experimental preparation, providing an opportunity to compare their responses to acute ischemia and at least speculate on the relevance of these responses to humans. There are relevant anatomical and physiological differences between the two species and humans that may contribute to the differences seen in the measured bioelectric fields. First, canines have an extensive coronary collateral vascular network which decreases the amount of ischemia induced during an ischemic intervention, unlike humans and swine, who have comparatively limited coronary collateral circulation (White *et al* 1992). Second, the swine conduction system is located in the midmyocardial region, unlike humans and canines, which have conduction systems anchored on the endocardial border (Verdouw *et al* 1983). While both species showed very similar QRS duration, the canine subjects show shorter QT intervals and substantially larger amplitudes of QRS complexes, T waves, and ST-segment shifts than the porcine subjects. The explanations for the amplitude findings could be two-fold as the canines had larger heart sizes (measured as nearly double the tissue volume) and also closer distances from the heart to the torso surface, which were reflected by relatively larger increases in torso potentials than cardiac potentials. The slightly reduced QRS duration in canines may be due to the differences in conduction system between the species. The increased QTc duration between species could explain the increased susceptibility of porcine subjects to ventricular fibrillation during procedures and interventions on the heart.

We also carried out careful evaluations of the impact of both instrumenting the heart and closing the chest on torso potentials and inserting the needle on the epicardial potentials. On the torso surface, we found relatively small and insignificant changes in the QRS duration and QRS amplitude values before and after surgery indicating no significant insulative effects from the needles or epicardial sock. However, there was a change in the measured ST40% potentials before and after surgery, as measured on the torso surface. These changes remained a small fraction of those observed during acute episodes of myocardial ischemia and may arise due to the effects of anesthesia and general injury from the procedure.

Immediately following needle insertion, there was a substantial and expected increase in ST40% epicardial potentials in the regions explored by the needles. However, 30 min after the needles were in place, the ST40% values had returned to levels obtained prior to needle placement and at 90 min, ST40% values had fallen below the original baseline levels. We suspect that the levels fall below baseline values because the recordings at baseline were immediately after the midline sternotomy and severing the pericardium, which could already insult the heart and increase epicardial potentials. To create context for these injury potentials, ST40% changes immediate following insertion varied between -2 and $+2$ mV, while the changes during peak ischemic stress were tenfold larger, from -10 to $+20$ mV. Changes in QRS duration following needle insertion were also minimal and recovered to near normal levels after 90 min. These results suggest that our recording and occlusion equipment did not substantially change the overall electrical function of the heart.

Creating and standardizing this experimental preparation presented several challenges and retains several limitations. We had to manufacture very high capacity (1024 channel) signal-acquisition equipment to record simultaneously from the different high-density electrode arrays. Such equipment is becoming available on the market, albeit at either high cost or only with substantial customization. Interfacing so many signals from individual electrodes designed for different locations and capturing signals at a range of amplitudes spanning two orders of magnitude also presents instrumentation challenges that result in some compromises in the achievable dynamic range and signal quality. Another challenge was maintaining the stability of the animal model in the face of surgical insult. Specific challenges included the invasiveness of the procedure, puncturing the heart wall with intramural plunge needles, and the resulting increased likelihood of cardiac arrhythmia, which was mitigated in swine with constant low-dose lidocaine infusions. There was inevitable variability in ischemic responses across different animals and experiments because of difference in cardiac and coronary anatomy and physiology. To reduce such inconsistencies, we placed the hydraulic occluder at approximately the same segment of the LAD for each experiment and also developed 'stress protocols' at the start of each experiment to capture individualized values for parameters such as maximal heart rate and level flow reduction that the subject could tolerate. Despite this approach, inconsistencies are typical in most large-animal preparations and require that the resulting measurements be considered somewhat independently. Finally, because of difference in human and animal anatomy, human 12-lead ECGs are impossible to completely recreate. Therefore, we approximated the location of each lead based on replicating the spatial relationships between each electrode location and the heart.

Our experimental model has several important applications in acute myocardial ischemia detection and the potential to contribute to the knowledge of acute ischemia. First, the addition of torso-surface recordings makes this the most clinically translational animal model of electrocardiography to date. Even with interspecies differences, this model still accurately detects and controllably induces episodes of transient myocardial ischemia that generate realistic electrical changes on the torso-surface ECGs.

While this experimental model was developed to detect and examine acute ischemia, it could also be used to study other cardiac pathologies. For example, it would be very straightforward to induce complete acute infarction to simulate STEMI or NSTEMI similar to clinical studies in humans using percutaneous coronary intervention balloon angioplasty. We could also induce premature ventricular contractions over a wide range of intramyocardial locations via bipolar stimulation with the needles and record the resulting three-dimensional activation patterns throughout at least a portion of the heart as well as over the epicardium and body surface. Because of the control of pacing location and rate, the model could also be used to study general arrhythmia formation and development. Even though intramural coverage is restricted to a region of the heart, the epicardial sock provides 360-degree, high-resolution coverage of the ventricles that could be used to examine complex wavefront development.

Such data sets have clear value for developing and validating bioelectric field models, specifically for electrocardiographic imaging (ECGI). ECGI requires an anatomical model of the heart and torso surface and high-density recordings of potentials on the body surface (Brooks and MacLeod 1997, Pullan *et al* 2010, Rudy and Lindsay 2015). Validation of ECGI requires measurements from the heart against which to compare computed values (Oster *et al* 1997, MacLeod and Brooks 1998, Brooks *et al* 1999, Potyagaylo *et al* 2014, Cluitmans *et al* 2015, Dubois *et al* 2015, Shah *et al* 2015, Wang *et al* 2016, Wann *et al* 2018, Cluitmans *et al* 2018). The inclusion of both epicardial and intramyocardial source measurements will provide unique opportunities for ECGI approaches that can be specific to ischemia or focus on general detection of localized cardiac activity.

In summary, we have significantly improved an experimental model of electrocardiographic evaluation of myocardial ischemia to be used as a novel standard for studies of mechanisms, bioelectric source computations, and cardiac simulation and modeling studies. With these data now achievable and available, significant strides can be made to improve the accuracy of noninvasive clinical tests to detect and localize myocardial ischemia. Future goals of this model includes improving its stability and further perfecting our experimental preparation. We will use it to assess and validate several key modeling and physiological parameters such as three-dimensional conduction velocity, bioelectric field and source models, different approaches to clinical stress testing, and ECG Imaging.

Acknowledgments

We would like to acknowledge the support from the Nora Eccles Treadwell Cardiovascular Research and Training Institute staff including Jayne Davis, Ala Booth, Wilson Lobaina, and Bruce Steadman for preparing and maintaining equipment and coordinating logistics of the experiments.

Author contributions

Brian Zenger:

- Scientific need and development
- Data analysis
- Manuscript preparation
- Experimental model design
- Experimentation setup and execution

Wilson W Good:

- Scientific need and development
- Data analysis
- Manuscript preparation
- Experimental model design
- Experimentation setup and execution

Jake A Bergquist:

- Scientific need and development
- Data analysis
- Manuscript preparation
- Experimental model design
- Experimentation setup and execution

Brett M Burton:

- Scientific need and development
- Experimentation setup and execution

Jess D Tate:

- Scientific need and development
- Experimentation setup and execution

Leo Berkenbile:

- Scientific need and development
- Experimentation setup and execution
- Recording equipment design and manufacturing

Vikas Sharma:

- Scientific need and development
- Experimental expertise
- Experimentation execution

Rob S MacLeod:

- Scientific need and development
- Data analysis
- Manuscript preparation


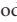






Novel translational experimental ischemia model

In this manuscript we have created the first experimental preparation to record intramural, epicardial surface, and torso surface electrical potentials from the heart during controlled episodes of acute myocardial ischemia. We have also created a data processing and visualization pipeline for investigation and analysis.

Grant support

Support for this research came from the NIH NIGMS Center for Integrative Biomedical Computing (www.sci.utah.edu/cibc), NIH NIGMS Grant No. P41GM103545 and the Nora Eccles Treadwell Foundation for Cardiovascular Research.

ORCID iDs

Brian Zenger  <https://orcid.org/0000-0002-0039-9184>
 Wilson W Good  <https://orcid.org/0000-0002-0111-9076>
 Jake A Bergquist  <https://orcid.org/0000-0002-4586-6911>
 Brett M Burton  <https://orcid.org/0000-0002-3971-4225>
 Jess D Tate  <https://orcid.org/0000-0002-2934-1453>
 Leo Berkenbile  <https://orcid.org/0000-0002-4720-8816>
 Vikas Sharma  <https://orcid.org/0000-0001-7939-5209>
 Rob S MacLeod  <https://orcid.org/0000-0002-0000-0356>

References

- Aras K, Burton B, Swenson D and MacLeod R 2014 Sensitivity of epicardial electrical markers to acute ischemia detection *J. Electrocardiol.* **47** 836–41
- Aras K, Burton B, Swenson D and MacLeod R 2016b Spatial organization of acute myocardial ischemia *J. Electrocardiol.* **49** 323–36
- Aras K et al 2015 Experimental data and geometric analysis repository: EDGAR *J. Electrocardiol.* **48** 975–81
- Aras K, Shome S, Swenson D, Stinstra J and MacLeod R 2009 Electrocardiographic response of the heart to myocardial ischemia *Computers in Cardiology* pp 105–8
- Aras K, Swenson D and MacLeod R 2011a Heterogeneous electrographic myocardial response during ischemia *J. Electrocardiol.* **44** 748
- Aras K, Swenson D and MacLeod R 2011b The origin of myocardial ischemia is not limited to the sub-endocardium *Int. Society for Computerized Electrocardiology*
- Bear L, Cheng L, LeGrice I, Sands G, Lever N, Paterson D and Smail B 2015a Forward problem of electrocardiography: is it solved? *Circ. Arrhythmia Electrophysiol.* **8** 677–84
- Bear L, Cuculich P, Bernus O, Efimov I and Dubois R 2015b Introduction to noninvasive cardiac mapping *Cardiac Electrophysiol. Clin.* **7** 1–16
- Bergquist J A, Good W W, Zenger B, Tate J D and MacLeod R S 2019 GRÖMeR: a pipeline for geodesic refinement of mesh registration *Funct. Imaging Model. Heart* **11** 504 37–45
- Brooks D, Ahmad G, MacLeod R and Maratos G 1999 Inverse electrocardiography by simultaneous imposition of multiple constraints *IEEE Trans. Biomed. Eng.* **46** 3–18
- Brooks D and MacLeod R 1997 Electrical imaging of the heart: electrophysical underpinnings and signal processing opportunities *IEEE Signal Proc. Mag.* **14** 24–42
- Burton B, Aras K, Good W, Tate J, Zenger B and MacLeod R 2018a A framework for image-based modeling of acute myocardial ischemia using intramurally recorded extracellular potential *Ann. Biomed. Eng.* **46** 1325–36
- Burton B, Aras K, Good W, Tate J, Zenger B and MacLeod R 2018b Image-based modeling of acute myocardial ischemia using experimentally derived ischemic zone source representations *J. Electrocardiol.* **51** 725–33
- Burton B, Aras K, Tate J, Good W and MacLeod R 2016 The role of reduced left ventricular, systolic blood volumes in ST segment potentials overlying diseased tissue of the ischemic heart *IEEE Computers in Cardiology* vol **43** pp 1–4

- Burton B, Tate J, Erem B, Swenson D, Wang D, Brooks D, van Dam P and MacLeod R 2011 A toolkit for forward/inverse problems in electrocardiography within the scirun problem solving environment *Proc. IEEE Engineering in Medicine and Biology Society 33rd Annual Int. Conf. (IEEE)* pp 1–4
- Cluitmans M *et al* 2018 Consensus on validation and opportunities of electrocardiographic imaging: from technical achievements to clinical applications *Frontiers Physiol.* **9** 1–19
- Cluitmans M J M *et al* 2017 *In vivo* validation of electrocardiographic imaging *JACC: Clin. Electrophys.* **3** 232–42
- Cluitmans M, Peeters R, Westra R and Volders P 2015 Noninvasive reconstruction of cardiac electrical activity: update on current methods, applications and challenges *Neth. Heart J.* **23** 301–11
- Dubois R *et al* 2015 Non-invasive cardiac mapping in clinical practice: application to the ablation of cardiac arrhythmias *J. Electrocardiol.* **48** 966–74
- Ershler P, Lux R and Steadman B 1986 A 128 lead online intraoperative mapping system *Proc. IEEE Engineering in Medicine and Biology Society 8th Annual Int. Conf. (IEEE)* pp 1289–91
- Janse M, Cinca J, Morena H, Fiolet J, Kleber A, de Vries G, Becker A and Durrer D 1979 The border zone in myocardial ischemia: an electrophysiological, metabolic and histochemical correlation in the pig heart *Circ. Res.* **44** 576–88
- Janse M, van Capelle F, Morsink H, Kleber A, Wilms-Schopman F, Cardinal R, d'Alnoncourt C and Durrer D 1980 Flow of 'injury' current and patterns of excitation during early ventricular arrhythmias in acute regional myocardial ischemia in isolated porcine and canine hearts *Circ. Res.* **47** 151–65
- Jespersen L, Abildstrom S Z, Hvelplund A and Prescott E 2013 Persistent angina: highly prevalent and associated with long-term anxiety, depression, low physical functioning, and quality of life in stable angina pectoris *Clin. Res. Cardiol.* **102** 571–81
- Jespersen L, Hvelplund A, Abildstrom S Z, Pedersen F, Galatius S, Madsen J K, Jørgensen E, Kelbæk H and Prescott E 2012 Stable angina pectoris with no obstructive coronary artery disease is associated with increased risks of major adverse cardiovascular events *Eur. Heart J.* **33** 734–44
- Knuuti J, Ballo H, Juarez-Orozco L E, Saraste A, Kolh P, Rutjes A W S, Jüni P, Windecker S, Bax J J and Wijns W 2018 The performance of non-invasive tests to rule-in and rule-out significant coronary artery stenosis in patients with stable angina: a meta-analysis focused on post-test disease probability *Eur. Heart J.* **39** 3322–30
- Kontos M, Anderson F, Schmidt K, Ornato J, Tatum J and Jesse R 1999 Early diagnosis of acute myocardial infarction in patients without ST-segment elevation *Am. J. Cardiol.* **83** 155–8
- Kubota I, Yamaki M, Shibata T, Ikano E, Hosoya Y and Tomoike H 1993 Role of ATP-sensitive K channel on ECG ST segment elevation during a bout of myocardial ischemia *Circulation* **88** 1845–51
- Li D, Li C, Yong A and Kilpatrick D 1998 Source of electrocardiographic ST changes in subendocardial ischemia *Circ. Res.* **82** 957–70
- Lux P and Ershler P 1987 Reducing uncertainty in the measures of cardiac activation and recovery *Proc. IEEE Engineering in Medicine and Biology Society 9th Annual Int. Conf. (IEEE)*
- MacLeod R and Brooks D 1998 Recent progress in inverse problems in electrocardiology *IEEE Eng. Med. Biol. Soc. Mag.* **17** 73–83
- Mannering D, Cripps T, Leech G, Mehta N, Valentine H, Gilmour S and Bennett E D 1988 The dobutamine stress test as an alternative to exercise testing after acute myocardial infarction *Br. Heart J.* **59** 521–6
- McCarthy B, Wong J and Selker H 1990 Detecting acute cardiac ischemia in the emergency department: a review of the literature *J. Gen. Intern. Med.* **5** 365–73
- Millar C, Kralios F and Lux R 1985 Correlation between refractory periods and activation-recovery intervals from electrograms: effect of rate and adrenergic interventions *Circulation* **72** 1372–9
- Noel B M C *et al* 2017 Ischemia and no obstructive coronary artery disease (INOCA) *Circulation* **135** 1075–92
- Okin P M, Ameisen O and Kligfield P 1986 A modified treadmill exercise protocol for computer-assisted analysis of the ST segment/heart rate slope: methods and reproducibility *J. Electrocardiol.* **19** 311–8
- Oostendorp T, van Oosterom A and Huiskamp G 1989 Interpolation on a triangulated 3D surface *J. Comput. Phys.* **80** 331–43
- Oster H, Taccardi B, Lux R, Ershler P and Rudy Y 1997 Noninvasive electrocardiographic imaging: reconstruction of epicardial potentials, electrograms, and isochrones and localization of single and multiple electrocardiac events *Circulation* **96** 1012–24
- Potyagaylo D, Schulze W H W and Doessel O 2014 Local regularization of endocardial and epicardial surfaces for better localization of ectopic beats in the inverse problem of ECG *Computers in Cardiology* pp 837–40
- Pullan A, Cheng L K, Nash M, Brooks D, Ghodrati A and MacLeod R 2010 The inverse problem of electrocardiography *Comprehensive Electrocardiology* ed P Macfarlane *et al* (London: Springer) pp 299–344
- Rodenhauser A, Good W, Zenger B, Tate J, Aras K, Burton B and MacLeod R 2018 PFEIFER: preprocessing framework for electrograms intermittently fiducialized from experimental recordings *J. Open Source Softw.* **3** 472
- Rudy Y and Lindsay B 2015 Electrocardiographic imaging of heart rhythm disorders: from bench to bedside *Cardiac Electrophysiol. Clin.* **7** 17–35
- Safdar B, Ong P and Camici P G 2018 Identifying myocardial ischemia due to coronary microvascular dysfunction in the emergency department: introducing a new paradigm in acute chest pain evaluation *Clin. Ther.* **40** 1920–30
- Savage R, Wagner G, Ideker R, Podolsky S and Hackel D 1977 Correlation of postmortem anatomic findings with electrocardiographic changes in patients with myocardial infarction *Circulation* **5** 279–85
- Shah A *et al* 2015 Noninvasive mapping of ventricular arrhythmias *Cardiac Electrophys. Clin.* **7** 99–107
- Shome S, Lux R, Punske B and MacLeod R 2007 Ischemic preconditioning protects against arrhythmogenesis through maintenance of both active as well as passive electrical properties in ischemic canine hearts *J. Electrocardiol.* **40** S5–6
- Spach M, Barr R, Lanning C and Tucek P 1977 Origin of body surface QRS and T-wave potentials from epicardial potential distributions in the intact chimpanzee *Circulation* **55** 268–78
- Spach M S and Barr R C 1975 Ventricular intramural and epicardial potential distributions during ventricular activation and repolarization in the intact dog *Circ. Res.* **37** 243–57
- Stern S 2002 State of the art in stress testing and ischaemia monitoring *Card Electrophys. Rev.* **6** 204–8
- Taccardi B, Punske B, Macchi E, MacLeod R and Ershler P 2008 Epicardial and intramural excitation during ventricular pacing: effect of myocardial structure *Am. J. Physiol.* **294** H1753–66
- Tate J, Stinstra J, Pilcher T, Poursaid A, Jolley M, Saarel E, Triedman J and MacLeod R 2018 Measuring defibrillator surface potentials: the validation of a predictive defibrillation computer model *Comput. Biol. Med.* **102** 402–10

- Verdouw P, Wolffebuttel B and Giessen J 1983 Domestic pigs in the study of myocardial ischemia *Eur. Heart J.* **4** 61–7
- Wang L, Gharbia O A, Horáček B M and Sapp J L 2016 Noninvasive epicardial and endocardial electrocardiographic imaging of scar-related ventricular tachycardia *J. Electrocardiol.* **49** 887–93
- Wann D, Waks J W and Kramer D B 2018 Clinical and regulatory considerations for novel electrophysiology mapping systems: lessons from FIRM *Pacing Clin. Electrophysiol.* **41** 617–32
- White F, Carroll S, Magnet A and Bloor C 1992 Coronary collateral development in swine after coronary artery occlusion *Circ. Res.* **71** 1490–500
- Zenger B, Good W W, Bergquist J A, Tate J D, Sharma V and Macleod R S 2018 Electrocardiographic comparison of dobutamine and BRUCE cardiac stress testing with high resolution mapping in experimental models *Comput. Cardiol.* **45** 1–5

CHAPTER 4

PHARMACOLOGICAL AND SIMULATED EXERCISE CARDIAC STRESS TESTS PRODUCE DIFFERENT ISCHEMIC SIGNATURES IN HIGH- RESOLUTION EXPERIMENTAL MAPPING STUDIES

4.1 Abstract

4.1.1 Objective

Test the hypothesis that exercise and pharmacological cardiac stressors create different electrical ischemic signatures.

4.1.2 Introduction

Current clinical stress tests for detecting ischemia lack sensitivity and specificity. One unexplored source of the poor detection is whether pharmacological stimulation and regulated exercise produce identical cardiac stress.

4.1.3 Methods

We used a porcine model of acute myocardial ischemia in which animals were instrumented with transmural plunge-needle electrodes, an epicardial sock array, and torso arrays to simultaneously measure within the heart wall, the epicardial surface, and the torso surface, respectively. Ischemic stress via simulated exercise and pharmacological stimulation were created with rapid electrical pacing and dobutamine infusion, respectively, and mimicked clinical stress tests of five three-minute stages. Perfusion to the myocardium was regulated by a hydraulic occluder around the left anterior descending coronary artery. Ischemia was measured as deflections to the ST-segment on ECGs and electrograms.

4.1.4 Results

Across eight experiments with 30 (14 simulated exercise and 16 dobutamine) ischemic interventions, the spatial correlations between exercise and pharmacological stress diverged at stage three or four during interventions ($p < 0.05$). We found more detectable ST-segment changes on the epicardial surface during simulated exercise than with dobutamine ($p < 0.05$). The intramyocardial ischemia formed during simulated exercise had larger ST40 potential gradient magnitudes ($p < 0.05$).

4.1.5 Conclusion

We found significant differences on the epicardium between cardiac stress types using our experimental model, which became more pronounced at the end stages of each test. A possible mechanism for these differences was the larger ST40 potential gradient magnitudes within the myocardium during exercise. The presence of microvascular dysfunction during exercise and its absence during dobutamine stress may explain these differences.

4.2 Introduction

Acute myocardial ischemia is the most common cause of chest pain and indicates many different pathologies, including Takotsubo cardiomyopathy, myocardial infarction, coronary artery disease, or coronary artery spasm [1], [2]. Acute myocardial ischemia occurs in regions with inadequate perfusion, and is routinely identified noninvasively with a cardiac stress test. Cardiac stress tests monitor heart function through a 12-lead electrocardiogram (ECG) or imaging modality (i.e., MRI or ultrasound) during increasing cardiovascular effort [1], [3], [4]. Clinically, the effort consists of a graded cardiac stressor, such as pharmacological stimulants or regulated exercise. Despite their ubiquity, the sensitivity and specificity of cardiac stress tests to acute myocardial ischemia are persistently poor, with the exercise stress tests using ECG monitoring around 55% and 65% and dobutamine stress test using ultrasound imaging (echocardiography) around 85% and 80%, respectively [1], [3], [4]. The poor detection or misdiagnosis of ischemia can lead to several adverse consequences, including accelerated cardiac decompensation or

unnecessary procedural interventions.

One possible and unexplored source of this inadequate detection is differences between cardiac stress types. Cardiac stress is induced clinically using regulated exercise via treadmill walking or pharmacological stimulation via dobutamine infusion [4]. Dobutamine infusion stimulates the heart through beta-1 receptors to increase heart contractility and heart rate [5]. Regulated exercise stimulates the heart by decreasing vagal tone, increasing sympathetic stimulation, and increasing cardiac preload. Both stress methods follow explicitly defined clinical protocols. Despite the obvious mechanistic differences between pharmacological stimulation and exercise, few studies have directly compared the different stress types directly at high spatial resolution and in three dimensions. Most previous studies have compared the sensitivity and specificity of detecting ischemia using exercise with ECG and dobutamine with ultrasound echocardiography (echo) [4], [6]–[8]. These studies report variable ranges of sensitivity and specificity, with the majority showing dobutamine with echo outperforming exercise with ECG. Some studies have examined 12-lead ECG measurements during both exercise and dobutamine stress. These studies found exercise to be significantly more sensitive and specific than dobutamine [9]. However, the authors were unable to offer a clear explanation for these differences because of the limited resolution of the 12-lead ECG. Most of these previous studies found differences in the diagnostic performance between the two cardiac stressors. However, the nature and possible mechanisms for this difference have not been well characterized in an experimental or clinical setting.

Recent advancements in large-animal experimental models of acute myocardial ischemia have made it possible to examine electrical changes during a controlled ischemic episode with high-resolution recording arrays. The biophysical basis for detecting myocardial ischemia electrically is well characterized. Remote recording electrodes measure potentials created by current flowing within the myocardium. Increased current drives increased potential measurements. In a healthy heart, no current should be flowing during the ST-segment. However, ischemic changes to cardiomyocyte action potentials create potential differences between ischemic and healthy tissue [10]–[12]. Under these conditions, passive current, also called injury

current, flows from the relatively positive healthy tissue to the relatively negative ischemic tissue during the ST segment. [13]. Injury current appears as positive or negative deflections to the ST segment from remote recording electrodes. Injury current increases with larger potential gradients between healthy and ischemic tissue.

The goal of this study was to characterize the differences in the electrical signatures of ischemia induced via dobutamine and simulated exercise from high-resolution electrocardiographic mapping in a controlled experimental model. We chose to assess electrical changes because of their ubiquity in clinical practice and, at least at the cellular level, there is a precise biophysical mechanism for ischemic changes. Based on previous clinical studies, we hypothesized a significant difference in the ischemia developed between dobutamine and simulated exercise. We tested this hypothesis using a novel large-animal experimental preparation of acute myocardial ischemia to simulate repeated clinical cardiac stress tests under controlled conditions. We recorded the electrical signals of ischemia at high resolution (over 600 electrodes) within the heart wall (intramural), on the heart surface (epicardial), and on the torso surface. We identified ischemic signatures based on changes to the ST-segment potentials (ST40%) of electrograms (measured within the heart or on the heart surface) or electrocardiograms (measured on the torso surface).

4.3 Methods

4.3.1 Experimental Preparation

4.3.1.1 Animal Model Selection and Surgical Procedure

The experimental preparation used in this study has been described previously in Zenger et al. [14]. Briefly, we used 30 Kg male and female Yucatan minipigs because of their similar cardiovascular structure to humans and validated use in previous acute myocardial ischemia studies [14]. A midline sternotomy was performed to expose the anterior surface of the heart. The heart was suspended in a pericardial cradle and the left anterior descending coronary artery was exposed and a hydraulic occluder was placed around the vessel. Recording arrays

described below were then placed. The pericardium and chest wall were then sutured closed and checked for residual air. The animals were purpose-bred for use in experimental research. All studies were approved by the Institutional Animal Care and Use Committee at the University of Utah and conformed to the Guide for Care and Use of Laboratory Animals (protocol number 17-04016 approved on 05/17/2017).

4.3.1.2 Recording Arrays

Recording arrays sampled electrical signatures within the heart wall (intramural), on the heart surface (epicardial), and on the torso surface. Each intramural plunge needle array recorded extracellular potentials at 10 depths, 1.6 mm apart. For each experiment, 20–30 needles were placed in the anterior ventricular myocardium. The epicardial sock recorded at 247 sites around both ventricles with approximately 6.6 mm² resolution. Finally, vertical torso strips were aligned cranial to caudal on the torso surface. Each strip had 12 electrodes, spaced 3 cm apart, and eight vertical strips were placed on the anterior torso for each experiment (Figure 4.1). All signals were recorded with a custom signal acquisition system, which low-pass filtered, gain adjusted, and recorded up to 1024 channels at 1 kHz [15].

4.3.2 Cardiac Stress Test Protocols

We simulated cardiac stress tests by mimicking clinical protocols. Each simulated cardiac stress test, or intervention, lasted up to 15 minutes, broken into 5, 3-minute stages. Interventions were terminated if mean arterial blood pressure dropped more than 30 mmHg from baseline or a series of three or more PVCs occurred. We performed two simulated exercise and two dobutamine stress tests per animal. Both cardiac stressors were used in each animal to compare under identical physiological circumstances while controlling for animal-to-animal variability. The order of interventions (i.e., dobutamine or simulated exercise occurring first) varied between experiments. A 30-minute rest period preceded each ischemic intervention, which has been previously shown as adequate time for the heart to return to baseline [14]. Figure 4.2 shows an example of signals acquired from an intramural recording electrode throughout an ischemic intervention. To reduce

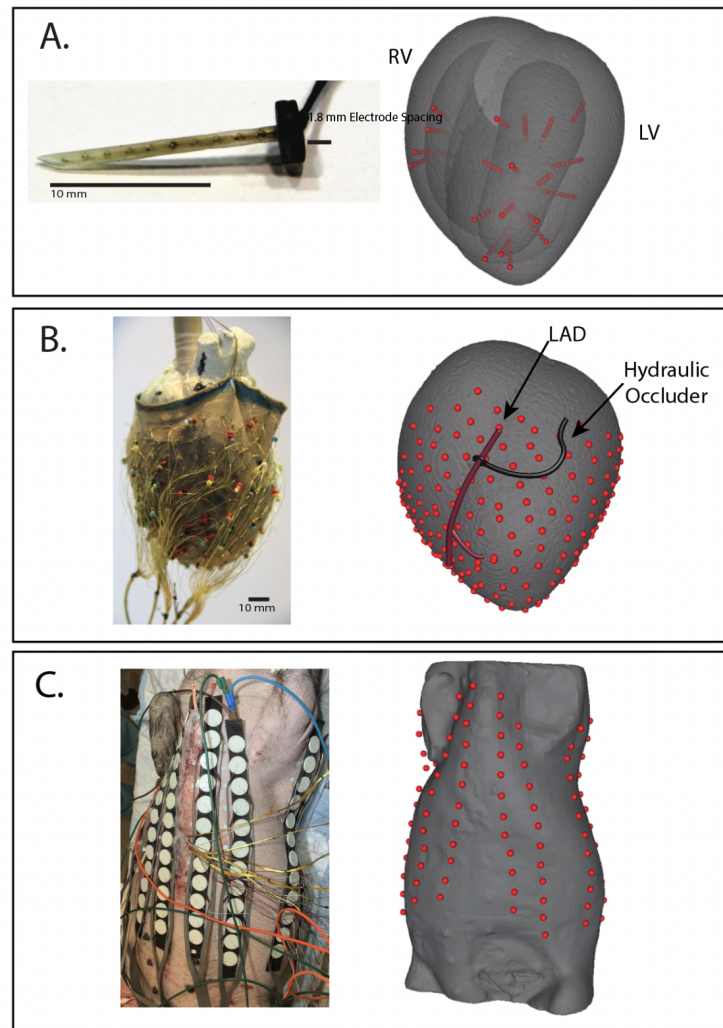


Figure 4.1: Measurement domains and electrode configurations. A. Intramural plunge needle arrays in both physical form (left) and rendered (red) within the three-dimensional geometric model of the heart (right) B. Epicardial sock electrode array in both physical form (left) and registered to geometric model of the heart (right) C. Torso surface potential electrode strips in both physical form (left) and registered to the geometric model of the torso surface (right).

the effects of ischemic preconditioning, two normalization ischemia protocols were induced prior to recorded ischemic episodes. Each normalization episode lasted 10 minutes with occlusion and pacing.

4.3.2.1 Simulated Cardiac Stress

To simulate exercise stress on the heart, we paced from the right atrium at set levels above resting heart rate. The levels were based on clinical Bruce exercise stress tests shown in Table 4.1 and were held constant throughout each stage [16]. Pacing has been shown to produce similar ECG responses compared to exercise and is the most similar analog to exercise considering the experimental preparation [17]–[19]. No studies to our knowledge have performed high resolution comparisons of pacing and exercise cardiac stress. To replicate clinical pharmacological stimulation, we used the dobutamine infusion protocols shown in Table 4.1. The infusion rate was held constant throughout each stage [20].

4.3.2.2 Hydraulic Vessel Occlusion

Perfusion deficits were created by placing a hydraulic occluder around the left anterior descending (LAD) coronary artery. The occluder controllably reduced the cross-sectional area of the LAD by 50–90%. For each experiment, the tolerated occlusion amount was determined based on cardiovascular stability (i.e., maintaining sinus rhythm without trains of three or more premature ventricular contractions) and held constant throughout each ischemic intervention. Occlusion was relaxed completely during rest periods.

4.3.3 Signal Processing

4.3.3.1 Quantification of Ischemia

Signals (electrograms and electrocardiograms) were referenced to Wilson’s central terminal, digitally processed, and fiducialized using the open-source PFEIFER platform [21]. Signals with unacceptable noise were manually identified and removed in the intramural case or reconstructed via Laplacian interpolation from the surrounding electrode neighborhood in the epicardial and torso surface cases. ST segment changes were used as local indicators for acute myocardial ischemia and

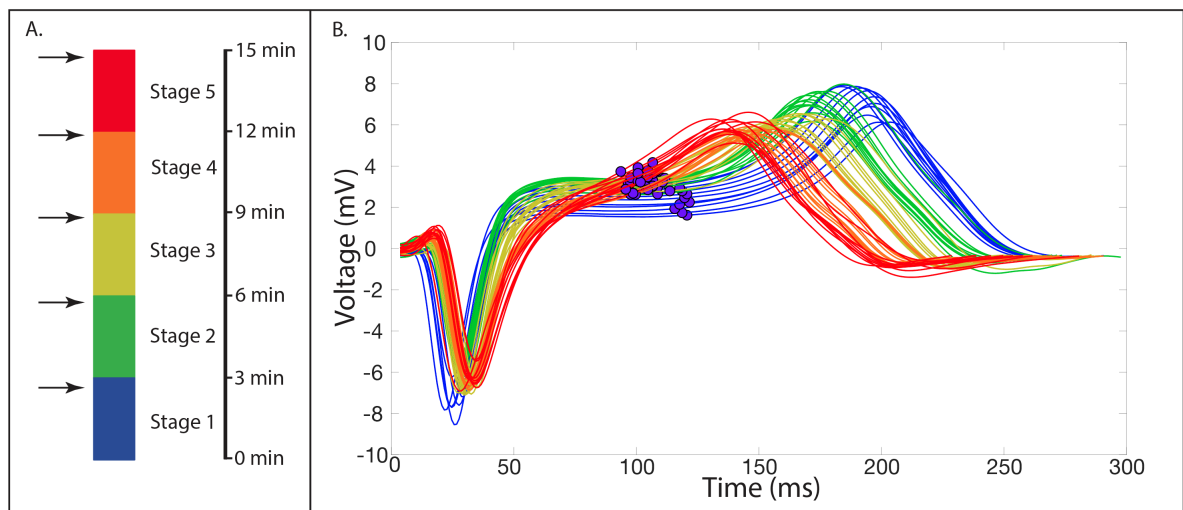


Figure 4.2: Sample electrograms during a single episode of ischemia. A. The colormap applied to the electrograms, showing the stages within a single episode of ischemia with arrows indicating the ends of each stage, when we captured signals representative of the stage. B. Example electrograms from an intramural electrode during a dobutamine ischemic intervention. Purple markers indicate the ST40% potential values extracted from each of the electrograms captured at the end of the five stages.

Table 4.1: Dobutamine infusion rates and heart rate increase by stage within an intervention

Stage	Dobutamine Infusion Rate ($\mu\text{g}/(\text{kg} * \text{min})$)	Heart Rate Above Resting (bpm)
1	5	37
2	10	55
3	20	76
4	30	91
5	40	102

chosen because of the regular clinical use and strong biophysical mechanism for indicating ischemia [12], [22]. Specifically, for each beat, we identified the potential value at 40% of the ST segment duration (ST40%) and averaged the values over a ± 5 ms window to reduce noise or signal artifacts. The ST40% potentials for each stage were determined from recordings at the end of each stage (i.e., each 3-minute interval) to allow for the ischemia to reach a steady-state with consistent cardiac stress. Figure 4.2 shows an example of the ST40% values on intramural electrograms as well as the sampling time points during an ischemic intervention. For torso surface recordings, we found that signals from the inferior end of each strip extended significantly into the abdomen across all animals and showed very little cardiac signal. Therefore, we removed the bottom two electrodes from each strip used in the analysis.

4.3.3.2 Geometric Model Generation

Following each experiment, animals were imaged postmortem in a 3-Tesla MRI scanner (Siemens Medical, Erlangen, Germany) from which the thorax as well as the needle, sock, and torso electrodes could be imaged. Following the full-thorax scan, the heart was removed, fixed, and scanned at submillimeter resolution using a 7-Tesla MRI scanner (Bruker BIOSPEC 70/30, Billerica, MA). By first segmenting (using the Seg3D software, <https://www.sci.utah.edu/cibc-software/seg3d>) and then merging the elements from the two MRI scans, we could construct geometric tetrahedral models using our Cleaver meshing software (<https://www.sci.utah.edu/software/cleaver>). Further aligning and electrode location refinement were implemented using the GRÖMER registration pipeline [23]. For intramural volumetric analyses, ST40 potentials were interpolated from intramural measurement nodes throughout the high-resolution mesh using thin-plate spline radial basis functions. Visualizations were performed using the *map3d* (<https://www.sci.utah.edu/software/map3d>) and SCIRun open-source software packages and MATLAB (Mathworks, MA, USA).

4.3.4 Comparisons of Ischemic Electrical Responses

ST40 potential values were extracted and compared at the end of each stage throughout an ischemic intervention as shown in Figure 4.2. Pairwise correlation metrics were calculated between all dobutamine and pacing interventions within the same animal experiment. In a typical scenario, two simulated exercise and two dobutamine interventions were performed during an experiment. Four correlation coefficients were then calculated at each time point (dobutamine one vs. simulated exercise one, dobutamine one vs. simulated exercise two, dobutamine two vs. simulated exercise one, dobutamine two vs. simulated exercise two). Pairwise correlation values were not calculated between interventions from other experiments. We also calculated general intervention characteristic variables and compared them across interventions and experiments.

4.3.4.1 Spatial Correlation of Ischemic Signatures

We compared ischemic signatures of simulated exercise to dobutamine stress tests using spatial correlation, which captures similarities of patterns within a recording domain (i.e., intramural, epicardial, and torso surface) between two intervention types.

4.3.4.2 Clinically Detectable ST40 Changes on Remote Recording Arrays:

We also assessed the presence of clinically detectable ST40 changes, which we defined as ST40 potential shifts above or below set threshold values. Epicardial sock thresholds were set to potentials above 1 mV or below -0.5 mV based on the ratio between the QRS amplitude and ST-elevation thresholds used clinically. Torso-surface signal amplitude varied drastically; therefore, we thresholded the clinical signal to be two standard deviations above or below the mean ST40 potentials acquired during control recordings (no ischemia). We then compared the number of electrodes above and below threshold in dobutamine and simulated exercise interventions.

4.3.4.3 Intramural Volume Analysis

Interpolated ST40 potentials within the tissue volume provided a means to identify ischemic zones, which were defined as ST40 potentials above 1 mV. We then computed the volume of these ischemic zone and compared differences in absolute ischemic-zone volume between dobutamine and simulated exercise interventions.

4.3.4.4 Ischemic Zone Dice Overlap

Using the ischemic zones, we calculated the Dice overlap coefficient, which provides a normalized measure, between 0 and 1, of overlap between two volumes [24]. In this case, we computed the Dice overlaps between ischemic zones created from different intervention types. Excellent overlap is above 0.8, moderate above 0.6, and poor below 0.6 [24].

4.3.4.5 Intramural ST40-Potential Gradient Magnitude Analysis

Again using the interpolated ST40 potentials, we computed the gradient of electrical potential throughout the myocardial region sampled by the intramural plunge needles. To compare dobutamine and simulated exercise interventions, we averaged the top quartile of gradient magnitudes for each intervention type. We then compared differences in top quartile gradient magnitude between stress types throughout the experiments.

4.3.4.6 Statistical Variability Analysis of All Calculated Metrics

To compare intervention characteristic variables (i.e., ischemic volume, gradient magnitudes, and clinical signal detection) for statistical differences, we performed a random effects multilevel regression analysis, which compensated for repeated measures within one animal experiment. We also statistically compared the correlation metrics that inherently computed differences between dobutamine and simulated exercise interventions (i.e., spatial correlation and Dice overlap correlation). For correlation metrics, we determined if the computed correlation values between different intervention types were within the variability of computed cor-

relations for identical intervention types. This analysis determines if the changes in the correlation metrics were significantly different compared to the intrinsic variability of interventions. Again, we performed a random effects multilevel regression to compensate for repeated measures within subjects. Statistical significance was defined as $p < 0.05$. The plots generated show the mean with the standard error unless otherwise noted. Statistical analysis was performed using STATA 16.1 stats software package (StatCorp, Texas, USA).

4.4 Results

For this study, we used eight animals and performed 30 ischemic interventions (14 simulated exercise and 16 dobutamine). Two simulated exercise interventions were not performed because animals died from arrhythmic events prior to the final intervention. Figure 4.3 shows example ST40 potentials mapped within the myocardium, on the epicardial surface, and on the torso surface during stage five (peak ischemia) of each cardiac stress type. The locations of elevated ischemic potentials were similar at multiple myocardial cross sections between dobutamine and simulated exercise interventions. The spatial correlation value comparing these intramural signals was 0.64, and the Dice overlap coefficient was 0.72. In this example figure, the positive amplitudes in the simulated exercise were markedly increased compared to dobutamine interventions (15 mV vs. 5 mV, respectively). Ischemic signatures were also larger in amplitude on the epicardial surface during simulated exercise, with higher and lower extrema than during dobutamine stress (-3.5 mV to 3.5 mV vs. -1 mV to 2 mV, respectively). The epicardial spatial correlation between these two interventions was low at 0.02. Finally, the torso-surface potentials showed marked elevations during simulated exercise, which were not present during dobutamine, and the spatial correlation was 0.79.

4.4.1 Spatial Correlation of Ischemic Signatures

We assessed aggregated spatial correlations to compare the two cardiac stress types based on the ST40 values from the intramural, epicardial, and torso-surface signals. As shown in Figure 4.4 in red, the spatial correlation dropped substan-

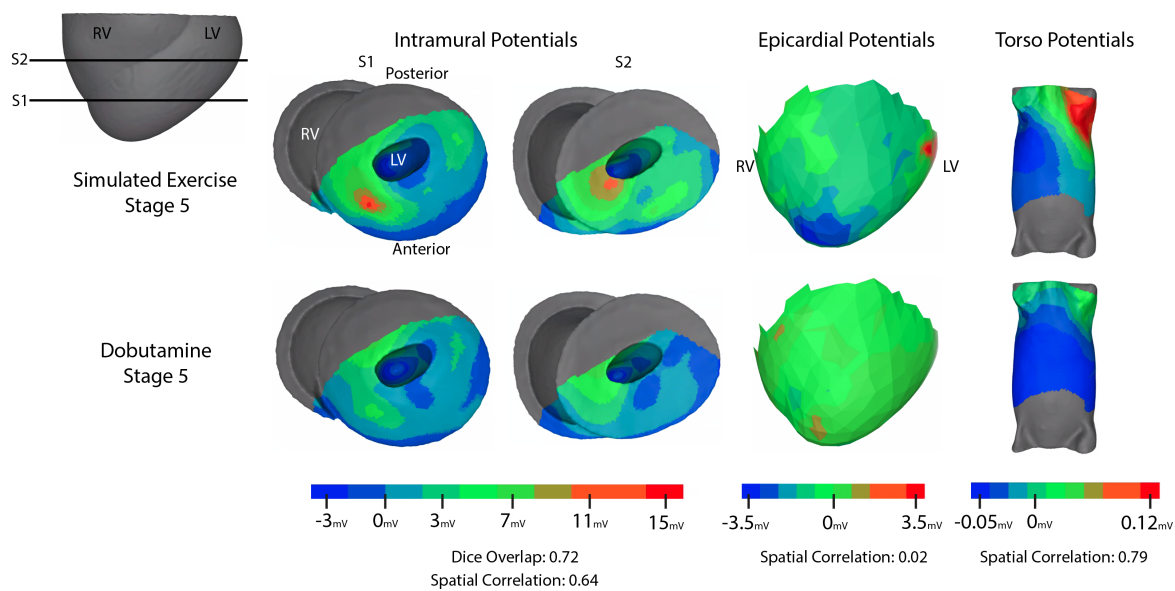


Figure 4.3: Sample measured ST40 potentials. Row 1: Simulated exercise intervention stage 5. Row 2: Dobutamine intervention stage 5. Columns 1 and 2: Interpolated ST40 potentials from intramyocardial recording arrays at different basal/apical levels. Column 3: Epicardial sock potentials. Column 4: Torso surface potentials.

tially between different intervention types across all recording domains through all stages of the ischemic interventions. Specifically, at the end of stage one, the spatial correlation remained high (above 0.75) across all experiments. At stages two to three, the spatial correlation dropped in the intramural (0.75 to 0.6), epicardial (0.85 to 0.6), and torso surface (from 0.8 to 0.6) recordings. At the end of stage five, the mean spatial correlation was below 0.6 across all surfaces, with the epicardial surface spatial correlation at 0.2. These results show a decreased similarity of the ischemic signature patterns for different cardiac stressors across the intramural, epicardial, and torso domains as the intervention progress (i.e., from stage 1 to 5).

We also performed a statistical variability analysis to determine if the spatial correlations comparing different cardiac stress types were similar to the spatial correlations comparing identical cardiac stress types. As shown in Figure 4.4, the identical comparisons had spatial correlations that remained above 0.7 throughout the interventions (blue). The spatial correlations between different intervention types were significantly lower than spatial correlations between identical intervention types. Statistical significance was identified in all stages for the needle measurements, all stages for the sock measurement, and stages one, four, and five for the torso measurements ($p < 0.05$ for all). These results show that spatial correlations between different cardiac stress types were significantly lower than spatial correlations of identical stress types throughout ischemic interventions.

4.4.2 Detectable Signal on the Epicardial and Torso Surfaces

We also examined a 'clinically detectable signal' on the epicardial and torso surfaces. The detectable signals used threshold cutoffs described in section 4.3.4, from which we counted the numbers of electrodes that exceeded these thresholds. We observed no significant difference among the numbers of electrodes with detectable clinical signals during stages one through three on the epicardial surface (Figure 4.5, $p > 0.05$). We found significantly more detectable electrodes during stage four and five during simulated exercise compared to dobutamine on the epicardium (Stage 4 Simulated Exercise = 60 electrodes and Stage 4 Dobutamine = 15 electrodes $p < 0.05$, Stage 5 Simulated Exercise = 80 electrodes and Stage 5

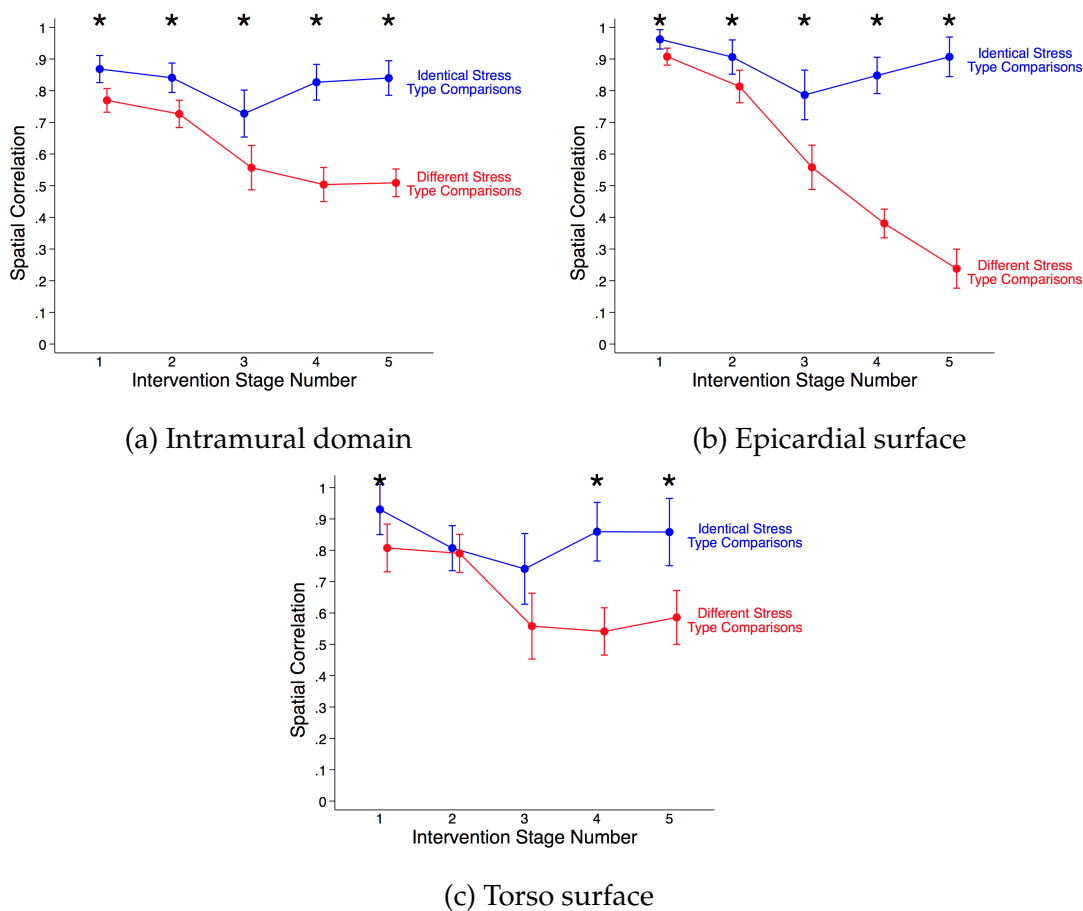


Figure 4.4: Summary of spatial correlation values across all experiments comparing different cardiac stress types (dobutamine and simulated exercise). Red lines are average spatial correlation values comparing different intervention types. Blue lines are average spatial correlation values of identical intervention types. Black stars indicate statistically significant differences between identical and different spatial correlation calculations. Error bars are derived from standard error calculations.

dobutamine =18 electrodes $p < 0.05$).

On the torso surface, there were no differences found between the number of electrodes throughout the entire intervention ($p > 0.05$ for all). On average, dobutamine and simulated exercise interventions induced clinical signals in 20 to 30 torso electrodes. The number of clinically identifiable electrodes did not vary markedly between stages two through five. The standard error was large (approximately 10 electrodes) throughout stages two through five for both intervention types.

4.4.3 Intramural Signal Analysis

To determine the underlying mechanisms for the differences noted between ischemic signatures, we assessed the differences of ischemic potentials within the myocardium.

4.4.3.1 Ischemic Zone Volume

Using interpolated intramyocardial ST40 potentials, we assessed the changes in ischemic zone volume throughout the ischemic interventions (Figure 4.6). The volume increased in stage three of the ischemic interventions (mean up to 20,000 mm³), then for dobutamine dropped in stage 4 to amounts similar to stage one (mean 18,000 mm³) and then rose again to slightly elevated levels (19,000 mm³). For simulated exercise, the values rose gradually to peak at stage 4 and then return to slightly elevated values (18,000 mm³ vs. 16,000 mm³). We did not identify any significant differences between the dobutamine or simulated exercise ischemic volume throughout an intervention ($p > 0.05$). From these results we concluded there was no difference between ischemic zone volume induced via dobutamine or simulated exercise throughout the interventions.

4.4.3.2 Dice Overlap

Dice overlap coefficients, which compare the spatial distribution of ischemic volumes within the myocardium (Figure 4.7), showed a decreasing trend of both identical and different comparisons throughout the interventions. Specifically, Dice coefficients calculated comparing identical intervention types decreased from

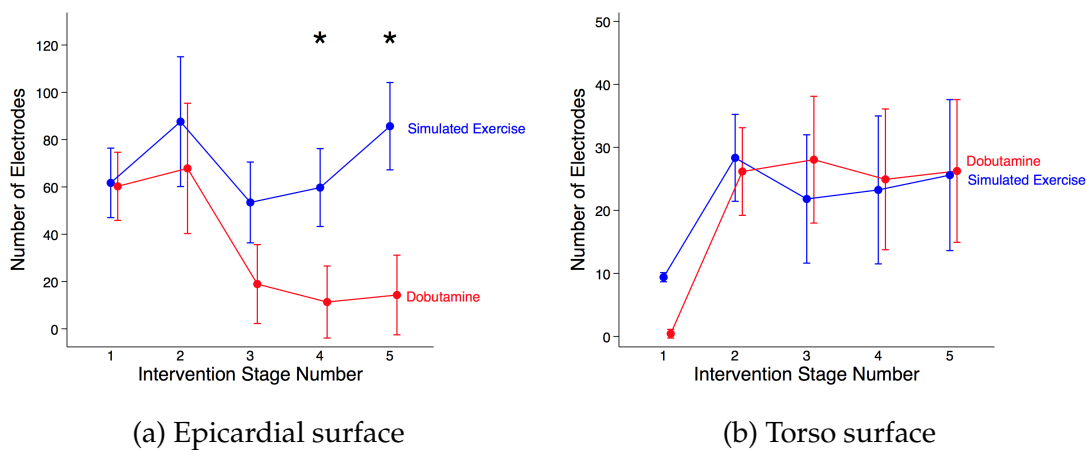


Figure 4.5: Mean number of electrodes with detectable clinical signal on the epicardial (A) and torso surfaces (B). Blue lines indicate simulated exercise interventions and red lines indicate dobutamine intervention. Error bars are standard error calculations. Black stars indicate significant differences between intervention types ($p < 0.05$).

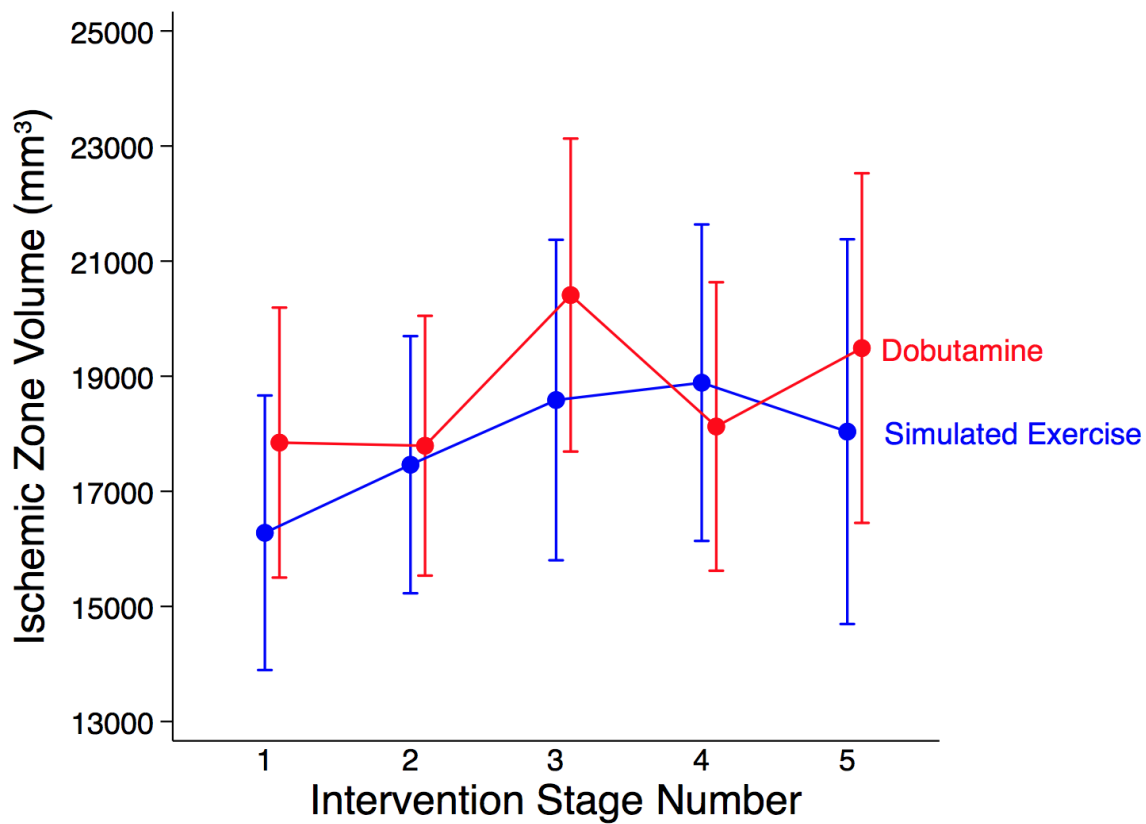


Figure 4.6: Average ischemic zone volumes measured from intramyocardial electrodes throughout an ischemic intervention. Blue lines represent simulated exercise interventions and red lines represent dobutamine interventions. No statistical significance was identified.

0.85 and 0.75, and different comparisons decreased from 0.75 to 0.58. Statistical differences between different and identical Dice coefficient comparisons were noted at every stage throughout an intervention ($p < 0.05$ for all).

4.4.3.3 Intramural Gradient Magnitudes

Figure 4.8 shows results of the magnitude of ischemic gradients (in mV/mm) calculated from intramyocardial ST40 values. Gradient magnitudes in both dobutamine and simulated exercise interventions varied over time (between 0.65 mV/mm and 0.93 mV/mm), however, the temporal patterns differed for the two stress types. Dobutamine gradient magnitudes initially increased to 0.85 mV/mm, but then dropped to 0.7 mV/mm, which contrasted with the results from simulated exercise. Gradients for exercise increased initially as well, but then remained constant at approx. 0.9 mV/mm for stages two through five. Simulated exercise interventions produced significantly larger gradient magnitudes than dobutamine interventions during stages four and five ($p < 0.05$).

4.5 Discussion

The goal of this study was to test the hypothesis that there are significant differences between ischemia induced by dobutamine and simulated exercise cardiac stress. Our experimental model simulated partial blockage, demand-based ischemia and with the goal of simulating clinical stress tests by matching Bruce-protocol target heart rates and dobutamine infusion rates used in humans. We identified significant differences in at least some of the electrical metrics of ischemia between dobutamine and simulated exercise interventions within the heart, on the epicardium, and the torso surface, the three recording domains we captured. These differences became larger near the end of the interventions (stages 3–5), for example, as spatial correlations decreased and differences in the clinical signals increased, where clinical signal is defined as number of electrodes above or below ST40 threshold cutoffs. Focusing on the intramyocardial signals allowed us to explore possible mechanisms to explain the differences in ischemia generated by both stress mechanisms. We found no significant differences in the ischemic zone

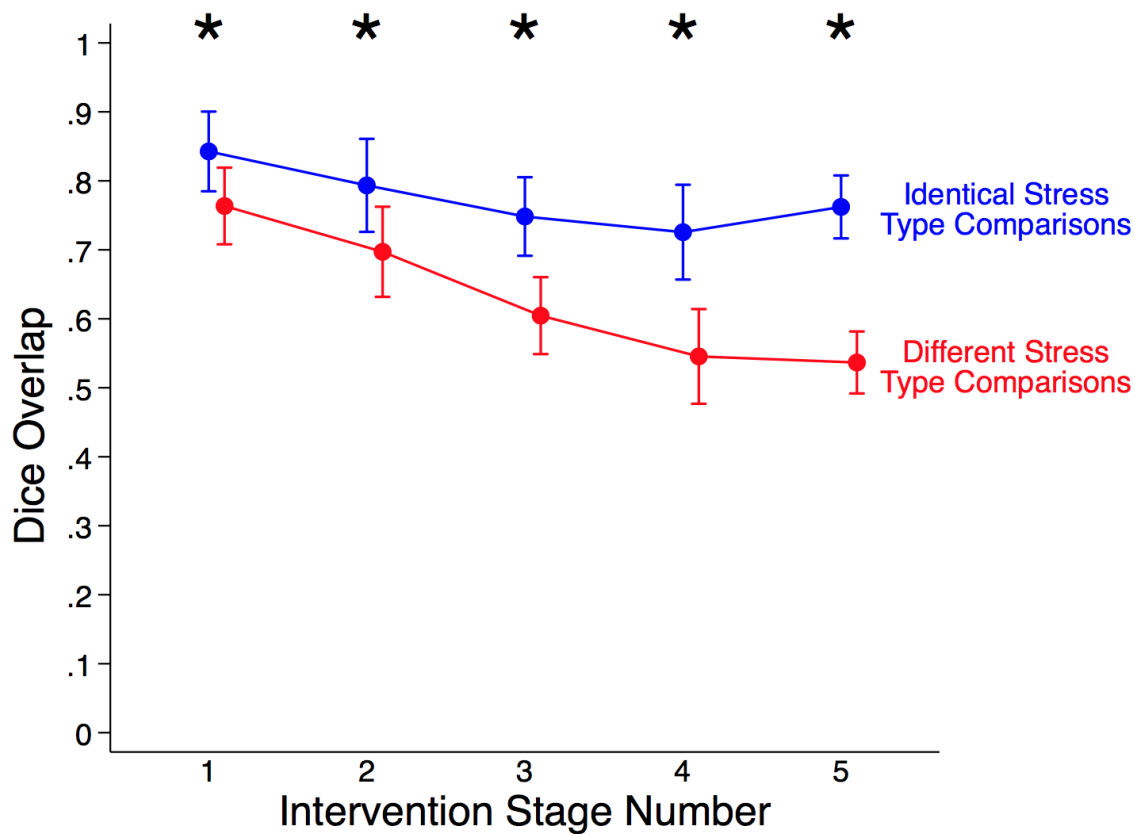


Figure 4.7: Average ischemic zone volumetric Dice overlap coefficients from intramyocardial electrodes recordings. Blue lines represent dice coefficients calculated between identical intervention types, and red lines represent dice coefficients calculated between different intervention types. Black stars indicate significant differences between identical and different dice coefficient distributions ($p < 0.05$).

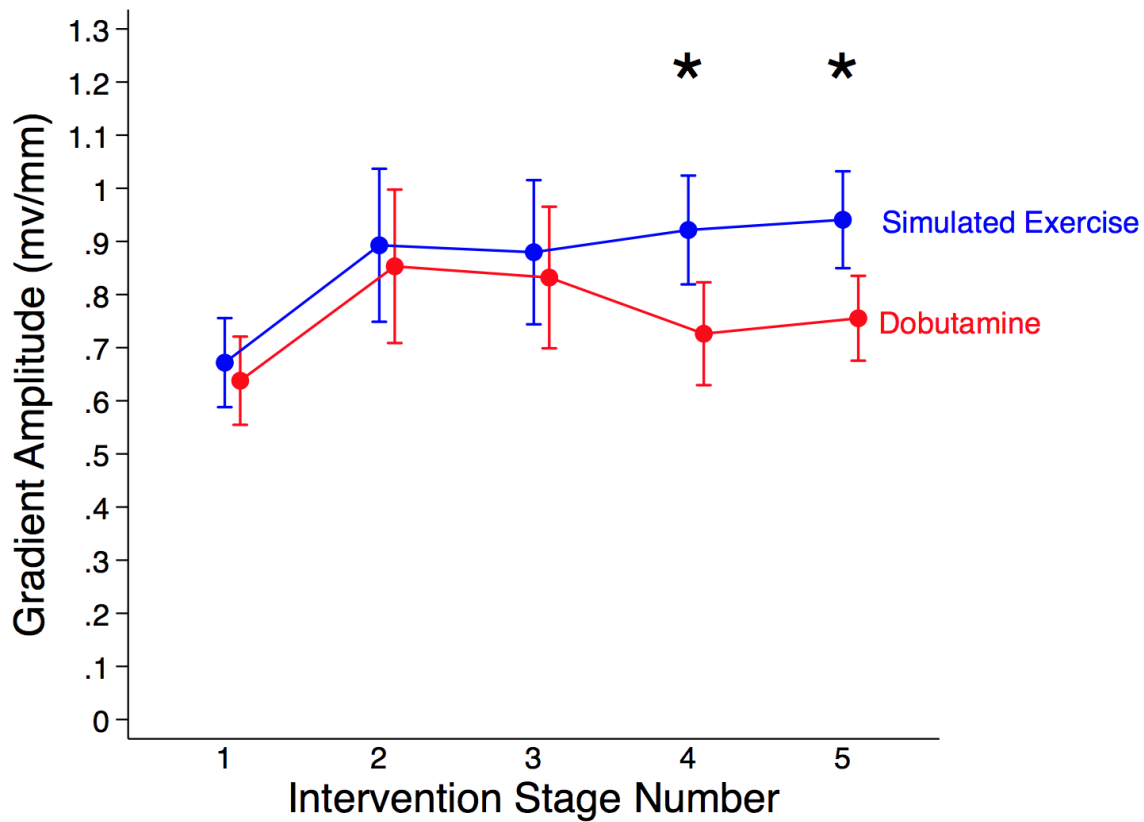


Figure 4.8: Mean of the top quartile of ischemic potential gradient magnitudes throughout the recorded area of intramural plunge needles. Blue lines represent simulated exercise interventions and red lines represent dobutamine interventions. Black stars indicate significant differences between intervention types ($p < 0.05$).

volumes; however, we did measure differences in the Dice overlap coefficients and ischemic potential gradient magnitudes. We propose that these two variables, spatial distribution of ischemic potentials and ischemic potential gradients, drive the differences observed on the epicardial sock and torso surface potentials.

4.5.1 Differences in Electrical Signatures of Ischemia Between Dobutamine and Simulated Exercise

Our findings suggest that significant differences exist between dobutamine and simulated exercise stress types, differences that appear most predominantly at the end of the ischemic interventions. Spatial correlations of ST40 potentials were significantly different throughout the interventions, however, these differences grew in the middle and later stages (3–5) (Figure 4.4) across all domains. Similar patterns were visible in several other metrics, such as the ST40 shifts on the epicardium (Figure 4.5), overlap of ischemic zones (Figure 4.7), and gradient magnitudes of ST40 potentials (Figure 4.8).

The torso surface recordings were less sensitive to these findings than cardiac signals (Figure 4.5) likely for reasons shared by many ECG-based metrics. Torso signals are a spatial average of a large myocardial region and are blurred as they project to the torso surface. Epicardial potentials are much closer to the ischemic sources and capture more of their features than the torso surface, as indicated by results in Figure 4.5. A further source of ambiguity is the finding that ischemic volumes were not significantly different between stressors (Figure 4.6), although they had different locations, amplitudes, potential gradients, and shapes (Figures 4.3, 4.4, 4.7, and 4.8). The ECG lacks the intrinsic resolution and sensitivity to differentiate these features. Another possible source of diminished ECG sensitivity are the experimental and natural variability between subjects. In our experiments, signal amplitude on the torso surface varied from animal to animal, likely due to difference in skin preparation and impedance as well as the closure and subsequent image-based reconstruction of the chest cavity. We applied vacuum suction to ensure minimal air remained in the chest cavity; however, a perfect seal was unlikely. Finally, the noise within the torso recordings was substantial and may have concealed electrical markers of ischemia.

4.5.2 Microvascular Dysfunction as a Possible Mechanism for Differences Between Cardiac Stress Types

A possible mechanistic explanation for the differences in intramural ischemic potentials is the development of microvascular dysfunction during only one of the cardiac stressors. Microvascular dysfunction is a paradoxical increase in small vessel resistance seen within ischemic tissue. During exercise or simulated exercise with pacing, clinical and experimental studies have shown the development of considerable microvascular dysfunction [25]–[29]. By contrast, other studies have shown that dobutamine stress decreases microvascular resistance through off-target beta-2 vasodilation [5], [30]. Although our experiments lacked explicit measurements of microvascular resistance, the consistent findings in previous studies reasonably suggest microvascular dysfunction as a possible mechanism for different levels of intramyocardial perfusion and hence electrical signatures.

Our observations support the presence of microvascular dysfunction during simulated exercise because we observed more intense ischemia within underperfused regions during simulated exercise than dobutamine stress. Potential (ST40) gradients we computed within the tissue supported these findings. There were significantly larger (approximately 30%) gradient magnitudes within the myocardium during the latter stages of exercise vs. dobutamine interventions (Figure 4.8). The larger gradient magnitudes indicate more severe ischemia flanked by healthy tissue even though the volume of ischemic tissue remained similar between stressors (Figure 4.6). The enhanced intramyocardial potential gradient magnitudes in simulated exercise drive an increase in injury current throughout the myocardium, which increases ST40 amplitudes on remote recording electrodes. We hypothesize that dobutamine with ECG analysis performs poorly because microvascular dysfunction is diminished during dobutamine infusion, resulting in decreased ST40 amplitudes on the epicardium and torso surface. To our knowledge, this is the first reported study to suggest microvascular dysfunction as a possible mechanistic driver for differences in ECG-based detection of ischemia.

4.5.3 Implications for Selection of Clinical Stress Type

These results provide novel clinical insights into how to select the best stress mechanism to diagnose specific clinical pathologies. The pathology of microvascular dysfunction is becoming more recognized as a crucial component of myocardial ischemia formation and patient-reported symptoms. Patient burden is likely a complex mixture of many conditions such as CAD, coronary spasm, and myocardial infarction with nonobstructive coronary arteries (MINOCA), all of which can be linked to microvascular dysfunction [31]–[34]. Therefore, testing strategies to detect microvascular dysfunction have become more defined and include invasive testing, advanced imaging, and local drug challenges [33], [35]. However, few studies exist that describe routine non-invasive tests for microvascular dysfunction, tests which could enhance early detection. Our findings suggest a possible means for such tests as they revealed large ischemic potential gradient magnitudes within the intramural myocardium that resulted in increases in ST40 potentials on the epicardial surface during simulated exercise stress (Figures 4.8 and 4.5). By contrast, dobutamine stress produced smaller ischemic electrical signals, which in the clinical setting may mask patient burden by eliminating microvascular dysfunction. In pathologies with major microvascular dysfunction components, dobutamine stress testing may under-diagnose patients. Our findings suggest both a possible mechanistic basis for this insensitivity as well as an indication to rely on exercise stress when microvascular dysfunction is suspected.

4.5.4 Limitations

The main limitations of any study based on animals models is how well the response matches those expected in humans. We simulated exercise in anesthetized pigs through rapid pacing and simulated pre-existing coronary artery disease or vascular spasm with mechanically induced partial occlusions, which only approximate real exercise. However, this model showed similar responses to those observed during a clinical cardiac stress test and, therefore, can serve as a useful model to explore mechanisms of hyperacute ischemia [17]–[19]. Furthermore, each animal had both dobutamine and simulated exercise stress tests performed, which

controlled for baseline differences in function. Another valuable measurement that was not recorded is blood pressure. This would provide insights to the hemodynamic differences between dobutamine and simulated exercise and further clarify the differences between exercise and electrical pacing. Hydraulic occlusion may not adequately represent naturally occurring decreased perfusion to myocardial tissue and our preparation omitted explicit measurement of the blood flow through the coronary vasculature. Additionally, we did not measure microvascular resistance changes to confirm microvascular dysfunction; however, previous experimental and clinical studies have indicted the regular presence of this dysfunction under the conditions we emulated. We also limited the measurements to electrical markers of ischemia rather than perform additional echocardiography to determine if wall motion abnormalities were present; the extreme electrical instrumentation of the heart precluded clear ultrasound imaging. We omitted baseline or control recordings in the results presented here because there was little ischemia present at the beginning of either intervention type. There are drawbacks to using spatial correlation coefficients to capture differences between body surface electrical potentials, especially with the substantial signal blurring and smoothing that occurs through the torso volume. However, these metrics were still sensitive enough to reveal significant differences between responses to the two intervention types. Additionally, we could have compared intervention types across animal studies or conducted entire studies with only one intervention type. However, the goal of this study was to examine differences between intervention types within the same individual subject. Finally, the number of animals and experiments could always be increased, although we did achieve statistical significance and measured consistent responses.

4.5.5 Data Sharing and Availability

Another contribution of this study is the geometric and electrical data collected, which will serve as material for future hypothesis testing and validation of computer simulations. The Consortium for ECG imaging (CEI) will manage the data from this study, making it available for analysis and collaborations. The goal of

the CEI is to achieve progress in ECGI through open, international collaboration and the sharing of ideas, software, and data. The CEI uses a combination of open-source software and a data-sharing platform <http://edgar.sci.utah.edu/> to collaborate across multiple labs and disciplines, which enables substantial growth and discovery [36]. The datasets described in this study will be available on the CEI data-sharing platform, EDGAR. All software used in this study is also available with open-source licensing on the <https://github.com/SCIIInstitute>. Further, the explicit data used in this study is available through the figshare online repository at <https://doi.org/10.6084/m9.figshare.14150057> and <https://doi.org/10.6084/m9.figshare.14150069>

The application of ECG Imaging in the measurement of ischemia is especially relevant as our findings showed clear improvements in diagnostic performance of epicardial electrograms over torso-surface ECGs. A specific goal of ECGI is to provide noninvasive access to cardiac signals by removing the blurring effects of the torso. By making available to the ECGI community geometric models and measured potentials from experiments of controlled ischemia, we will enable optimization of ECGI for this common condition that remains poorly diagnosed.

4.6 Conclusion

In conclusion, we found significant differences in the electrical signatures of ischemia induced by dobutamine and simulated exercise cardiac stressors through comprehensive measurements within the heart, on the epicardium, and on the torso surface of a porcine animal model. We have reported for the first time that exercise stress created significantly larger gradient magnitudes of ischemic potentials throughout the myocardium, which resulted in larger ST-segment potentials on the epicardium. We suggest that differences in microvascular dysfunction between the two stressor types drive these findings. The clinical implications of this study suggest dobutamine and exercise stress methods should not be considered interchangeable. Furthermore, if the suspected pathologies have substantial components of microvascular dysfunction, exercise or pacing should be used rather than dobutamine stress.

4.7 References

- [1] B. Safdar, P. Ong, and P. G. Camici, "Identifying myocardial ischemia due to coronary microvascular dysfunction in the emergency department: introducing a new paradigm in acute chest pain evaluation," *Clin. Therapeutics*, pp. 1–11, Nov. 2018. doi: <http://dx.doi.org/10.1016/j.clinthera.2018.09.010>.
- [2] F. A. Bhuiya, S. R. Pitts, and L. F. McCaig, "Emergency department visits for chest pain and abdominal pain: United States, 1999-2008," *NCHS Data Brief*, no. 43, pp. 1–8, Sep. 2010.
- [3] S. Stern, "State of the art in stress testing and ischaemia monitoring." *Card. Electrophysiol. Rev.*, vol. 6, no. 3, pp. 204–208, Sep. 2002.
- [4] J. Knuuti, H. Ballo, L. E. Juarez-Orozco, A. Saraste, P. Kolh, A. W. S. Rutjes, P. Jüni, S. Windecker, J. J. Bax, and W. Wijns, "The performance of non-invasive tests to rule-in and rule-out significant coronary artery stenosis in patients with stable angina: A meta-analysis focused on post-test disease probability," *Europ. Heart J.*, vol. 39, no. 35, pp. 3322–3330, Sep. 2018. doi: <http://dx.doi.org/10.1093/eurheartj/ehy267>.
- [5] J. Bartunek, W. Wijns, G. R. Heyndrickx, and B. de Bruyne, "Effects of dobutamine on coronary stenosis physiology and morphology," *Circ.*, vol. 100, no. 3, pp. 243–249, Jul. 1999. doi: <http://dx.doi.org/10.1161/01.CIR.100.3.243>.
- [6] J. Shadeen, "Diagnostic value of 12-lead electrocardiogram during dobutamine echocardiographic studies," *Am. Heart J.*, vol. 136, no. 6, pp. 1061–1064, Dec. 1998. doi: [http://dx.doi.org/10.1016/S0002-8703\(98\)70163-2](http://dx.doi.org/10.1016/S0002-8703(98)70163-2).
- [7] M. R. Dhond, T. Nguyen, T. B. Whitley, K. Donnell, and W. J. Bommer, "Prognostic value of 12-Lead electrocardiogram during dobutamine stress echocardiography," *Echocardiography*, vol. 17, no. 5, pp. 429–432, Jul. 2000. doi: <http://dx.doi.org/10.1111/j.1540-8175.2000.tb01158.x>.
- [8] G. H. Mairesse, T. H. Marwick, J. L. J. Vanoverschelde, T. Baudhuin, W. Wijns, J. A. Melin, and J. M. R. Detry, "How accurate is dobutamine stress electrocardiography for detection of coronary artery disease? Comparison with two-dimensional echocardiography and technetium-99m methoxyl isobutyl isonitrile (mibi) perfusion scintigraphy," *J. Am. Coll. Cardiol.*, vol. 24, no. 4, pp. 920–927, Oct. 1994. doi: [http://dx.doi.org/10.1016/0735-1097\(94\)90850-8](http://dx.doi.org/10.1016/0735-1097(94)90850-8).
- [9] B. D. Beleslin, M. Ostojic, J. Stepanovic, A. Djordjevic-Dikic, S. Stojkovic, M. Nedeljkovic, G. Stankovic, Z. Petrasinovic, L. Gojkovic, and Z. Vasiljevic-Pokrajcic, "Stress echocardiography in the detection of myocardial ischemia. Head-to-head comparison of exercise, dobutamine, and dipyridamole tests." *Circ.*, vol. 90, no. 3, pp. 1168–76, Sep. 1994. doi: <http://dx.doi.org/10.1161/01.cir.90.3.1168>.
- [10] M. J. Janse and A. G. Kleber, "Electrophysiological changes and ventricular arrhythmias in the early phase of regional myocardial ischemia." *Circ. Res.*, vol. 49, no. 5, pp. 1069–1081, Nov. 1981.

- [11] A. G. Kléber, M. J. Janse, F. J. Van Capelle, and D. Durrer, "Mechanism and time course of st and tq segment changes during acute regional myocardial ischemia in the pig heart determined by extracellular and intracellular recordings." *Circ. Res.*, vol. 42, no. 5.
- [12] F. Kornreich, T. Montague, M. Kavadias, J. Segers, P. Rautaharju, B. Horacek, and B. Taccardi, "Qualitative and quantitative analysis of characteristic body surface potential map features in anterior and inferior myocardial infarction," *Am. J. Cardiol.*, vol. 60, pp. 1230–1238, Dec. 1987.
- [13] M. Janse, F. van Capelle, H. Morsink, A. Kleber, F. Wilms-Schopman, R. Cardinal, C. d Alnoncourt, and D. Durrer, "Flow of "injury" current and patterns of excitation during early ventricular arrhythmias in acute regional myocardial ischemia in isolated porcine and canine hearts," *Circ. Res.*, vol. 47, no. 2, pp. 151–165, Aug. 1980.
- [14] B. Zenger, W. Good, J. Bergquist, B. Burton, J. Tate, L. Berkenbile, V. Sharma, and R. MacLeod, "Novel experimental model for studying the spatiotemporal electrical signature of acute myocardial ischemia: a translational platform." *J. Physiol. Meas.*, vol. 41, no. 1, p. 015002, Feb 2020.
- [15] B. Zenger, J. A. Bergquist, W. W. Good, L. C. Rupp, and R. S. MacLeod, "High-capacity cardiac signal acquisition system for flexible, simultaneous, multidomain acquisition," in *2020 Computing in Cardiol.*, Sep. 2020. doi: <http://dx.doi.org/10.22489/CinC.2020.190>. pp. 1–4.
- [16] P. M. Okin, O. Ameisen, and P. Kligfield, "A modified treadmill exercise protocol for computer-assisted analysis of the ST segment/heart rate slope: Methods and reproducibility," *J. Electrocardiol.*, vol. 19, no. 4, pp. 311–318, Oct. 1986. doi: [http://dx.doi.org/10.1016/S0022-0736\(86\)81058-5](http://dx.doi.org/10.1016/S0022-0736(86)81058-5).
- [17] G. V. Heller, J. M. Aroesty, R. G. McKay, J. A. Parker, K. J. Silverman, P. C. Come, and W. Grossman, "The pacing stress test: A reexamination of the relation between coronary artery disease and pacing-induced electrocardiographic changes," *Am. J. Cardiol.*, vol. 54, no. 1, pp. 50–55, Jul. 1984.
- [18] V. Marangelli, S. Iliceto, G. Piccinni, G. De Martino, L. Sorgente, and P. Rizzon, "Detection of coronary artery disease by digital stress echocardiography: Comparison of exercise, transesophageal atrial pacing and dipyridamole echocardiography," *J. Am. Coll. Cardiol.*, vol. 24, no. 1, pp. 117–124, Jul. 1994.
- [19] K. Schröder, H. Völler, H. Dingerkus, H. Münzberg, R. Dissmann, T. Linderer, and H.-P. Schultheiss, "Comparison of the diagnostic potential of four echocardiographic stress tests shortly after acute myocardial infarction: Submaximal exercise, transesophageal atrial pacing, dipyridamole, and dobutamine-atropine," *Am. J. Cardiol.*, vol. 77, no. 11, pp. 909–914, May 1996.
- [20] D. Mannering, T. Cripps, G. Leech, N. Mehta, H. Valentine, S. Gilmour, and E. D. Bennett, "The dobutamine stress test as an alternative to exercise testing after acute myocardial infarction." *Br. Heart J.*, vol. 59, no. 5, pp. 521–526, May 1988. doi: <http://dx.doi.org/10.1136/HRT.59.5.521>.

- [21] A. Rodenhauer, W. Good, B. Zenger, J. Tate, K. Aras, B. Burton, and R. MacLeod, "PFEIFER: Preprocessing framework for electrograms intermittently fiducialized from experimental recordings," *J. Open Source Software*, vol. 3, no. 21, p. 472, 2018.
- [22] K. Aras, B. Burton, D. Swenson, and R. MacLeod, "Sensitivity of epicardial electrical markers to acute ischemia detection." *J. Electrocardiol.*, vol. 47, no. 6, pp. 836–841, 2014.
- [23] J. A. Bergquist, W. W. Good, B. Zenger, J. D. Tate, and R. S. MacLeod., "GRÖMeR: A pipeline for geodesic refinement of mesh registration," in *Lecture Notes in Computer Science*, vol. 11504, Functional Imaging and Model of the Heart (FIMH). Springer Verlag, Jun. 2019, pp. 37–45.
- [24] L. R. . Dice, "Measures of the amount of ecologic association between species," *Ecology*, vol. 26, no. 3, pp. 297–302, Jul. 1945. doi: <http://dx.doi.org/10.2307/1932409>.
- [25] D. Duncker, "Regulation of coronary vasomotor tone under normal conditions and during acute myocardial hypoperfusion," *Pharmacol. & Therapeut.*, vol. 86, no. 1, pp. 87–110, Apr. 2000. doi: [http://dx.doi.org/10.1016/S0163-7258\(99\)00074-1](http://dx.doi.org/10.1016/S0163-7258(99)00074-1).
- [26] S. A. J. Chamuleau, M. Siebes, M. Meuwissen, K. T. Koch, J. A. E. Spaan, and J. J. Piek, "Association between coronary lesion severity and distal microvascular resistance in patients with coronary artery disease," *Am. J. Physiol.*, vol. 285, no. 5, pp. H2194–H2200, Nov. 2003. doi: <http://dx.doi.org/10.1152/ajpheart.01021.2002>.
- [27] S. Gianmario, M. Mario, M. Paolo, S.-E. Jan, G. Enri, P. Oberdan, and L. Antonio, "Coronary vasoconstriction during myocardial ischemia induced by rises in metabolic demand in patients with coronary artery disease," *Circ.*, vol. 95, no. 12, pp. 2652–2659, Jun. 1997. doi: <http://dx.doi.org/10.1161/01.CIR.95.12.2652>.
- [28] D. J. Duncker and R. J. Bache, "Regulation of coronary blood flow during exercise," *Physiol. Rev.*, vol. 88, no. 3, pp. 1009–1086, Jul. 2008. doi: <http://dx.doi.org/10.1152/physrev.00045.2006>.
- [29] G. Sambuceti, M. Marzilli, S. Fedele, C. Marini, and A. L'Abbate, "Paradoxical increase in microvascular resistance during tachycardia downstream from a severe stenosis in patients with coronary artery disease: Reversal by angioplasty," *Circ.*, vol. 103, no. 19, pp. 2352–2360, May 2001. doi: <http://dx.doi.org/10.1161/01.CIR.103.19.2352>.
- [30] J. Bartunek, W. Wijns, G. R. Heyndrickx, and B. de Bruyne, "Effects of dobutamine on coronary stenosis physiology and morphology," *Circ.*, vol. 100, no. 3, pp. 243–249, Jul. 1999. doi: <http://dx.doi.org/10.1161/01.CIR.100.3.243>.

- [31] S. Pasupathy, R. Tavella, and J. F. Beltrame, "Myocardial infarction with nonobstructive coronary arteries (MINOCA)," *Circ.*, vol. 135, no. 16, pp. 1490–1493, Apr. 2017. doi: <http://dx.doi.org/10.1161/CIRCULATIONAHA.117.027666>.
- [32] P. Ong, A. Athanasiadis, S. Hill, T. Schäufele, H. Mahrholdt, and U. Sechtem, "Coronary microvascular dysfunction assessed by intracoronary acetylcholine provocation testing is a frequent cause of ischemia and angina in patients with exercise-induced electrocardiographic changes and unobstructed coronary arteries," *Clin. Cardiol.*, vol. 37, no. 8, pp. 462–467, Aug. 2014. doi: <http://dx.doi.org/10.1002/clc.22282>.
- [33] G. A. Lanza and F. Crea, "Primary coronary microvascular dysfunction," *Circ.*, vol. 121, no. 21, pp. 2317–2325, Jun. 2010. doi: <http://dx.doi.org/10.1161/CIRCULATIONAHA.109.900191>.
- [34] J. C. Kaski, F. Crea, B. J. Gersh, and P. G. Camici, "Reappraisal of ischemic heart disease: Fundamental role of coronary microvascular dysfunction in the pathogenesis of angina pectoris," *Circ.*, vol. 138, no. 14, pp. 1463–1480, Oct. 2018. doi: <http://dx.doi.org/10.1161/CIRCULATIONAHA.118.031373>.
- [35] P. Ong, B. Safdar, A. Seitz, A. Hubert, J. F. Beltrame, and E. Prescott, "Diagnosis of coronary microvascular dysfunction in the clinic," *Circ. Res.*, vol. 116, no. 4, pp. 841–855, Mar. 2020. doi: <http://dx.doi.org/10.1093/cvr/cvz339>.
- [36] K. Aras, W. Good, J. Tate, B. Burton, D. Brooks, J. Coll-Font, O. Doessel, W. Schulze, D. Patyogaylo, L. Wang, P. van Dam, and R. MacLeod, "Experimental data and geometric analysis repository: EDGAR," *J. Electrocardiol.*, vol. 48, no. 6, pp. 975–981, 2015.

CHAPTER 5

TRANSIENT RECOVERY OF EPICARDIAL AND TORSO ST-SEGMENT ISCHEMIC SIGNALS DURING CARDIAC STRESS TESTS: A POSSIBLE PHYSIOLOGICAL MECHANISM

5.1 Abstract

5.1.1 Background

Acute myocardial ischemia has several characteristic ECG findings, including clinically detectable ST-segment deviations. However, the sensitivity and specificity of ECG-based ST-segment changes are low. Furthermore, ST-segment deviations have been shown to be transient and spontaneously recover without any indication the ischemic event has subsided.

5.1.2 Objective

Assess the transient recovery of ST-segment deviations on remote recording electrodes during a partial occlusion cardiac stress test and compare them to intramyocardial ST-segment deviations.

5.1.3 Methods

We used a previously validated experimental model of acute myocardial ischemia with controllable ischemic load and measurement electrodes within the heart wall, on the epicardial surface, and on the torso surface. Simulated cardiac stress tests were induced by occluding a coronary artery while simultaneously pacing or infusing dobutamine to stimulate cardiac function. Postexperimental imaging created anatomical models for data visualization and quantification. Markers of ischemia were identified as deviations in the potentials measured at 40% of the ST-segment. Intramural cardiac conduction speed was also determined using the

inverse gradient method. Changes in intramyocardial ischemic volume proportion, conduction speed, clinical presence of ischemia on remote recording arrays, and regional changes to intramyocardial ischemia were assessed. Peak deviation response time was the time interval after onset of ischemia that maximum ST-segment deviation was achieved, and ST-recovery time was the interval when ST deviation returned to below 1mV of ST elevation.

5.1.4 Results

In both epicardial and torso recordings, the peak ST-segment deviation response time was 4.9 ± 1.1 min and the ST-recovery time was approximately 7.9 ± 2.5 min, both well before the termination of the ischemic stress. At peak response time, conduction speed was reduced by 50% and returned to near baseline at ST-recovery. The overall ischemic volume proportion initially increased to 37% at peak response time; however, it recovered only to 30% at the ST-recovery time. By contrast, the subepicardial region of the myocardial wall showed 40% ischemic volume at peak response time and recovered much more strongly to 25% as epicardial ST-segment deviations returned to baseline.

5.1.5 Conclusion

Our data show that remote ischemic signal recovery correlates with a recovery of the subepicardial myocardium, while subendocardial ischemic development persists.

5.2 Introduction

Chest pain is the most common chief complaint of a patient arriving at the emergency department, with acute myocardial ischemia being the most worrisome underlying cause [1], [2]. During the subsequent assessment, patients receive an electrocardiogram (ECG) to measure the electrical activity from the heart and identify deviations typical of ischemia. However, ECG signals indicating acute myocardial ischemia are transient and may not detect ischemia despite the occurrence of an event [3], [4]. Previously, the disappearance of these ischemic ECG signals was interpreted to mean the ischemic event had ended and the cardiac

tissue was recovering. However, detailed studies showed, despite the decreasing or absent ischemic ECG markers, the ischemia within the myocardium may persist [3], [4]. Without intervention, the myocardium will continue to degrade, leading to cell death and significant long-term risks of increased morbidity and mortality [5]. Therefore, it is crucial to understand the evolution and progression of remotely recorded ischemic signals related to underlying ischemic myocardial substrates and the possible mechanisms that lead to decreased ischemic ECG signals.

Many previous experimental and clinical studies have shown the transient disappearance of ischemic ECG signals during a controlled ischemic event [6]–[8]. During the ischemic episode, ischemic ECG signals initially increase, also known as ST-segment deviations, accompanied by a significant increase in arrhythmic events such as premature ventricular contractions or other re-entrant type arrhythmic patterns [6], [8]. Following this initial phase, which can last up to 15 minutes, there is a significant decrease in ST-segment deviations and arrhythmic events, indicating myocardial “recovery” even as the critically reduced myocardial perfusion persists [6], [8]. This persistence is apparent only under closer examination of the myocardial tissue (possible only in experiments), which can show persistent ischemia at the cellular level, including cell-to-cell uncoupling [9]. This uncoupling reduces passive current flow between cells and eliminates the ST-segment deflections recorded on remote electrodes [9]. Furthermore, cellular uncoupling leads to significant conduction velocity slowing, which can be monitored and characterized in an experimental preparation as a temporal spreading of the QRS complex and prolongation of activation times [10].

However, these studies showed this transient recovery only during complete occlusion ischemic events. They did not investigate changes during a partial occlusion event or added cardiac stress, such as a cardiac stress test. Partial occlusion ischemia has significantly different effects than complete occlusion ischemia, including the nontransmural formation of ischemic tissue [11]. Partial occlusion ischemia is induced and detected using cardiac stress tests, which stimulate the heart via regulated exercise or drug infusion to expose perfusion deficits to cardiac tissue regions [12], [13]. As ischemia develops, key biomarkers are monitored for

responses, including changes to the ST-segment of electrocardiograms [12], [13]. Previous partial occlusion myocardial ischemia studies lacked the high-resolution and multidomain recording arrays that would enable a comprehensive analysis of the transient changes in ischemic electrical signals throughout the myocardium, on the epicardial surface, and the torso surface.

This study aims to examine the transient recovery of ischemic signals during a simulated cardiac stress test with partial flow ischemia. We will use a previously validated experimental model of partial occlusion acute myocardial ischemia, instrumented with electrode arrays within the myocardium, on the epicardial surface, and the torso surface to examine this recovery phenomenon. We controlled ischemic stress using hydraulic occlusion with pacing or pharmacological stimulation. We will then assess several different ischemia metrics, including typical ST-segment deviations, changes in intramyocardial conduction speed, and regional recovery of ischemic electrical signals. Our results showed a significant recovery of epicardial and torso surface ischemic ST-segment potentials throughout a simulated cardiac stress test. Using conduction speed measurements, we found no evidence this recovery was related to cell-to-cell uncoupling. Furthermore, we identified preferential recovery of ischemic potentials in the subepicardial myocardial tissue.

5.3 Methods

5.3.1 Experimental Model

The experimental model used in this study has been described previously in Zenger et al. [14]. In short, midline sternotomies were performed on anesthetized 30 Kg male or female Yucatan minipigs to expose the anterior cardiac surface. Each animal was instrumented with intramural, epicardial, and torso surface electrode arrays. Intramural arrays were custom fabricated plunge needles with 10 individual recording electrodes spaced 1.6 mm down the needle shaft. For each experiment, 20–30 needles were placed in the approximate left anterior descending coronary artery (LAD) perfusion bed with an approximate inter-needle spacing of 5-10 mm at the epicardium. A 247-electrode epicardial sock array was placed

around the ventricular epicardium with approximately 6.6 mm² electrode resolution and approximately 10 mm spacing between electrodes. After instrumentation, the chest wall was closed with sutures, and residual air was evacuated. Torso electrode strips, each with 12 electrodes spaced 3 cm apart, were placed from superior to inferior across the animal torso with 8–12 strips spanning around the thorax. All signals were low-pass filtered, gain adjusted, and sampled simultaneously with a custom digital multiplexer at 1 kHz [15]. All animals were purpose-bred for use in experimental research. All studies were approved by the Institutional Animal Care and Use Committee at the University of Utah and conformed to the Guide for Care and Use of Laboratory Animals (protocol number 17-04016 approved on 05/17/2017).

5.3.2 Quantification of Ischemia

Signals were processed and filtered using the PFEIFER open-source ECG and electrogram annotation suite [16]. Signals with low signal-to-noise values were manually identified and removed from intramural recordings or reconstructed via Laplacian interpolation from the surrounding electrodes on the epicardial and torso surfaces. ST-segment changes were used as indicators for acute myocardial ischemia. From each beat, we extracted the potential value at 40% into the ST-segment duration and averaged the values over a ± 5 ms time frame. Representative ST40% potentials were extracted from continuous data every 15 seconds throughout the experiment.

5.3.3 Simulated Cardiac Stress Test

Controlled cardiac stress was induced by limiting coronary perfusion and increasing cardiac activity. A calibrated hydraulic occluder was placed around the left anterior descending coronary artery (LAD) to reduce perfusion. The occluder could then be adjusted from 0–100% of the original cross-sectional area. Cardiac stress was induced using right atrial pacing or pharmacological stimulation via dobutamine infusion. Typical clinical protocols were used for target pacing and drug infusion rates [12], [13]. Each intervention lasted 15 minutes with a fixed level

of occlusion, which was determined on an experiment by experiment basis by the animal stability. Each 15-minute intervention was broken into five 3-minute stages. After each stage, the pacing or pharmacological infusion rate was increased. A 30-minute rest period followed each ischemic intervention, which has been shown as adequate time for the heart to return to baseline potentials [14]. Up to four interventions were performed in each animal.

5.3.4 Image-Based Modeling Pipeline

The torso geometries and electrode locations were acquired via postmortem magnetic resonance imaging (MRI) (Siemens Medical, Erlangen, Germany). We then explanted the heart and acquired submillimeter high-resolution MRI imaging (Bruker BIOSPEC 70/30, Billerica, MA). Torso geometries, cardiac anatomy, and electrode locations were segmented using the Seg3D open-source software package (www.seg3d.org, SCI Institute, SLC, UT). The anatomical structures were meshed to create triangulated tetrahedral models using the Cleaver mesh tool (SCI Institute, SLC, UT). Geometries were registered and further refined using the GRÖMER registration pipeline [17]. Visualizations were performed using the *map3d* (www.sci.utah.edu/software/map3d) and SCIRun (www.sci.utah.edu/software/scirun) open-source software packages and MATLAB (Mathworks, MA, USA). Measured ST40% potentials were interpolated into the intramyocardial volume using thin-plate spline radial basis functions, which assigned an ST40% potential at every node within the high-resolution mesh.

Following the anatomical model creation, each high-resolution cardiac mesh was parameterized using the Universal Ventricular Coordinate (UVC) scheme from the Cardiac Arrhythmia and Research Package (CARP) [18]. These parameterizations assigned a unique four-parameter location to each node in the mesh according to values for z , ρ , ϕ , and left or right ventricle, as described previously [19]. These values could then be translated across experiments as relative positions. For this analysis, we used the ρ parameter to indicate the relative intramyocardial depth (from 0–1) of each node within the myocardial wall. We defined the subepicardial region and subendocardial/midmyocardial regions in terms of ρ

as $\rho > 0.66$ and $\rho \leq 0.66$, respectively.

5.3.5 Three-Dimensional Conduction Velocity Measurements

Three-dimensional conduction velocity was calculated using validated techniques described previously [20]. In short, activation times were first identified from intramural plunge needle electrodes and reconstructed within the sampled region of the high-resolution cardiac mesh using thin-plate spline radial basis functions [20]. We used the inverse gradient technique to calculate conduction velocity from the interpolated activation times, which inverts the activation time gradient throughout the myocardium and takes the partial derivative on an element-wise basis. Conduction velocity was further reduced to conduction speed per element by taking the conduction velocity vector magnitude.

5.3.6 Metrics of Ischemia and Statistical Analysis

For intramural recordings, ST40% potentials of 1 mV or larger were considered ischemic. For epicardial recordings, ST40% potentials above 2 mV or below -1 mV indicate ST-segment elevation or depression, respectively. On the torso surface, ST40% potentials above 0.05 mV or below -0.05 mV were indicative of ST-segment elevation or depression, respectively. These thresholds were used to determine the number of electrodes on the epicardial and torso surfaces considered “clinically detectable” as these thresholds mimic those used in evaluating ST segments in patients.

To quantify the transient changes in ischemic ST-segment potentials, we identified the time of peak ischemic ST-segment potentials and the time of recovery of ST-segment potentials during an ischemic intervention. To calculate peak and recovery ST40% response times, we identified epicardial electrodes, which became positively ischemic during each intervention. We then calculated the time point at each electrode was at its maximum and selected the median time as the time of peak ST40% for an intervention. We then determined the time when electrodes that developed positive ischemic potentials returned to below the ischemic threshold. The median time of these recovered electrograms was chosen to represent the recovery ST40% response time per intervention.

Statistical differences between metrics were compared using a random-effects multilevel regression to compensate for repeated measures within subjects. Statistical significance was defined as $p < 0.05$. The plots generated show the mean \pm standard error unless otherwise noted. Statistical analysis was performed using STATA 16.1 stats software package (StatCorp, Texas, USA).

5.4 Results

5.4.1 ST-Segment Changes Throughout a Simulated Cardiac Stress Test

An example of a typical progression in the transient changes in epicardial electrograms and torso surface ECGs throughout an ischemic intervention is shown in Figure 5.1. We observed an increase in ST40% potentials across a large proportion of electrodes, which peaked at approximately the 6-minute mark and returned to near baseline levels at the 12-minute mark despite increasing ischemic stress (pacing rate or dobutamine level). An example of the ST40% potentials at baseline, peak, recovery, and end of the intervention on each recording domain is shown in Figure 5.2. We noted the presence of high ST40% potentials at the peak ST-segment response time of the intervention, followed by a recovery in potentials across all surfaces.

We examined these trends across six animal experiments and 15 ischemic interventions (nine dobutamine stimulation and six right atrial pacing). A summary of peak and recovery ST40% response times across all interventions is shown in Figure 5.3. The average time to peak was 4.9 ± 1.1 minutes, and the average time to recovery was 7.9 ± 2.5 minutes. The separation between each time distribution was almost perfect, with the peak response times significantly lower than the recovery response times ($p < 0.05$).

The changes in clinically detectable signals on the epicardial and torso surfaces are shown in Figure 5.4. At peak ST-segment response time, the numbers of leads with clinically detectable ST40% shifts were 80 of 247 epicardial and 55 of 96 on the torso surface, indicating a significant amount of clinically detectable ischemia. At the recovery ST40% response time, the number of electrodes where the clin-

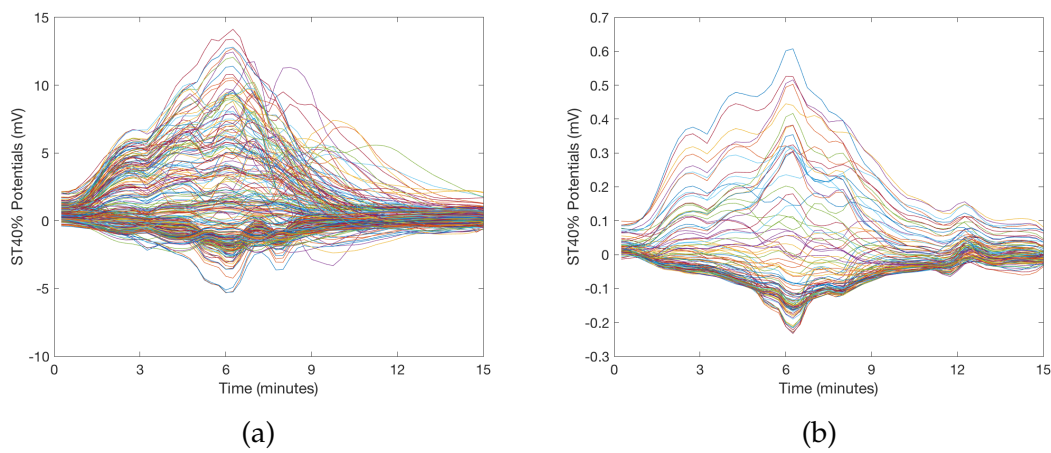


Figure 5.1: Example metric plot of ST40% potential changes throughout an ischemic intervention (15 minutes). Panel (a) shows epicardial sock ST40% potentials across all 247 electrodes. Panel (b) shows torso surface ST40% potentials across all 96 torso electrodes. Each line represents a sequence of the ST40% potential values from one electrode throughout an ischemic intervention.

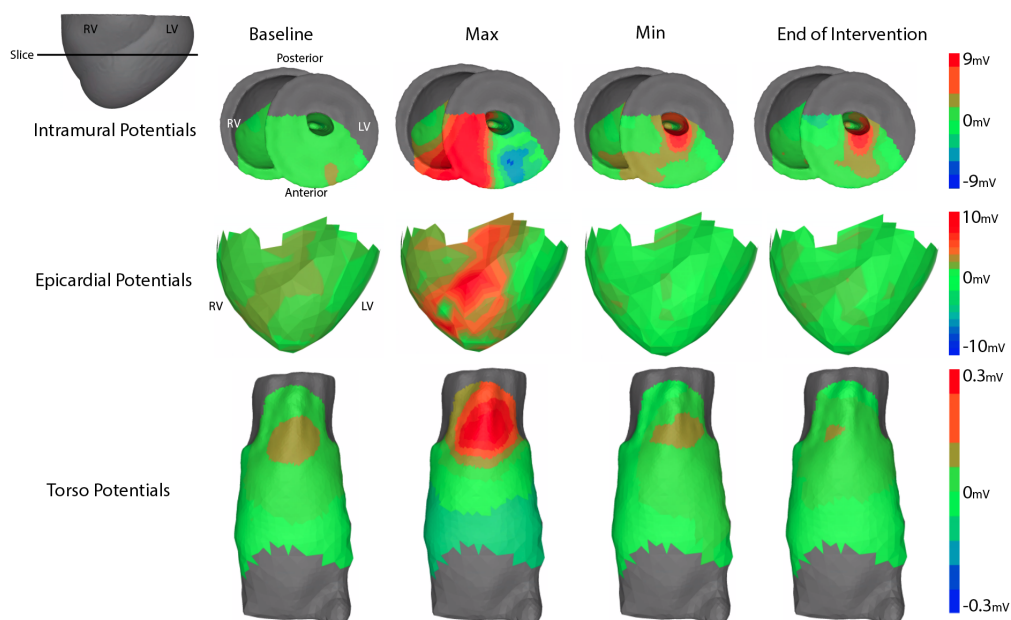


Figure 5.2: Example ST40% potential values measured within all recording domains at baseline, peak ST40% response time, recovery ST40% response time, and end of the intervention at max cardiac stress

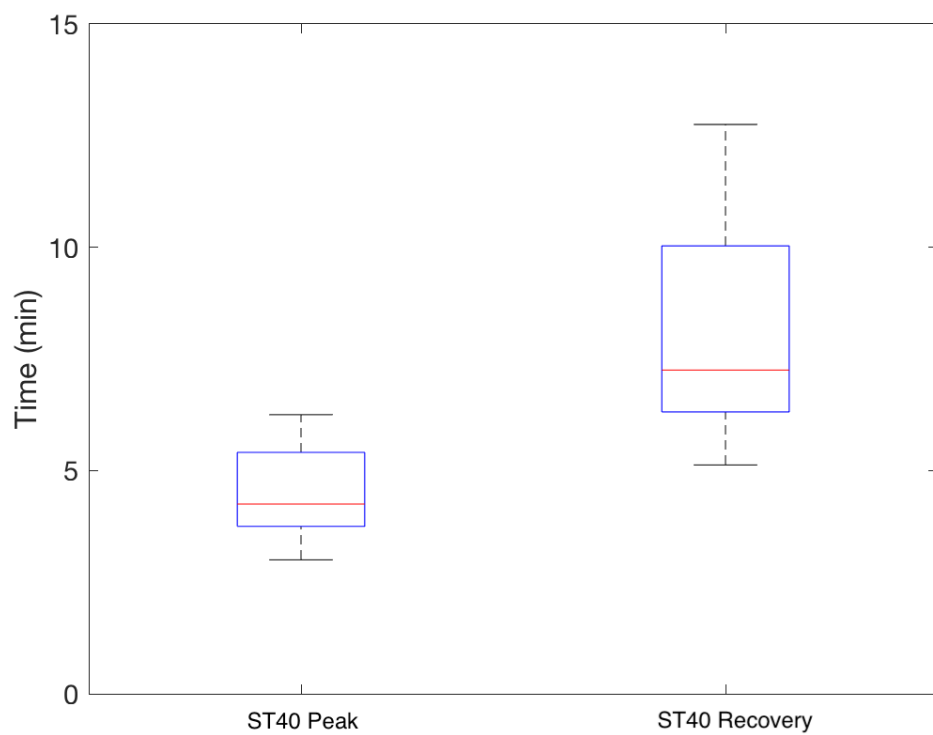


Figure 5.3: Average time to peak and recovery ST40% values as measured on the epicardial sock electrodes.

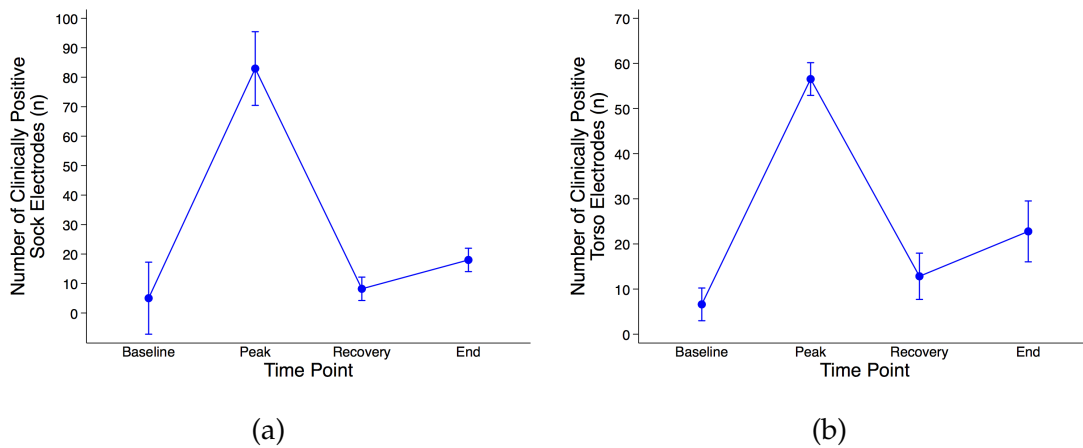


Figure 5.4: Changes in measured clinically detectable signal (as either depressions or elevations) as measured on the (a) epicardial and (b) torso surfaces at four time points, baseline, peak epicardial ST40% time, recovered epicardial ST40%, and the end of the ischemic intervention at max cardiac stress.

ically detectable signal could be identified returned to near baseline levels with approximately 10 epicardial electrodes and 10 torso electrodes with positive ST40% clinical signals, which indicates nearly all clinically detectable ST deviations had disappeared.

5.4.2 Changes in 3D Conduction Speed

At baseline, the average conduction speed through the sampled myocardium was approximately 1.5 ± 0.2 m/s. At peak ST-segment response time, average conduction speed dropped to approximately 0.7 ± 0.3 m/s, and at recovery ST40% response time, the conduction speed returned to approximately baseline values, 1.4 ± 0.3 m/s (Figure 5.5).

5.4.3 Changes in Ischemic Zone Volumes Within the Myocardium

At baseline, less than 5% of the sampled volume was considered ischemic. At peak ST40% response time, approximately 37% of the sampled myocardium had become ischemic, which dropped to 30% at the minimum point and stayed relatively stable through the end of the intervention (Figure 5.6).

We then separated the sampled region into two subregions: the subepicardial and the subendocardial/midmyocardial. The ischemic volume proportion in the subendocardial/midmyocardial regions followed similar trends to those of the whole myocardial region with a 35% ischemic at peak response time and 29% at recovery response time (Figure 5.7). The subepicardial region, however, showed a more profound recovery, peaking at approximately 40% and dropping to 25% at recovery ST40% response time, which further dropped to 23% at the end of interventions (Figure 5.7).

5.5 Discussion

This study aimed to examine the temporal changes of ischemic ST-segment potentials during partial flow cardiac stress tests. We identified transient recovery of ST-segment potentials on average 8 minutes into a 15-minute simulated cardiac stress test. We examined these transient recoveries from multiple domains,

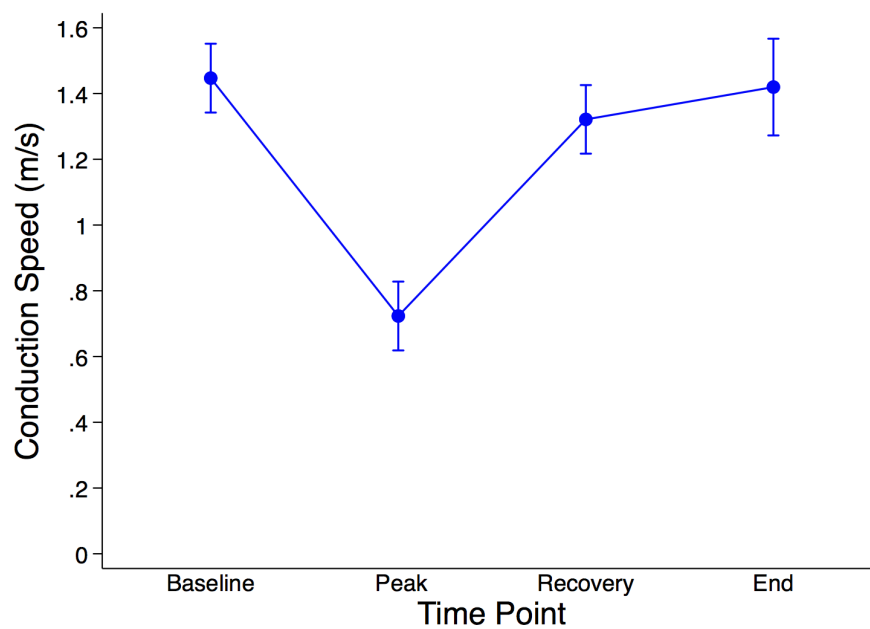


Figure 5.5: Average median cardiac conduction speed measured in the myocardium at four time points, baseline, peak epicardial ST40% time, recovered epicardial ST40%, and the end of the ischemic intervention.

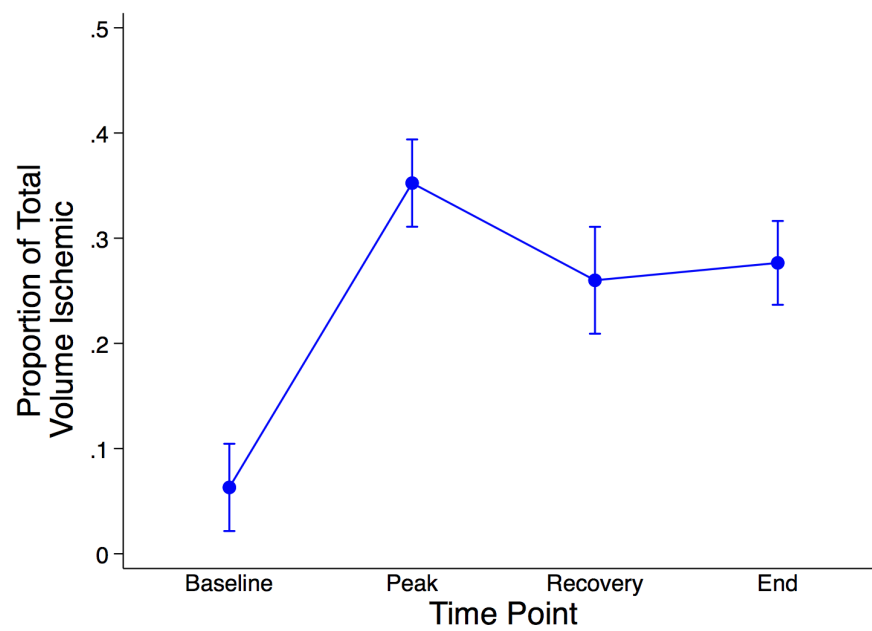
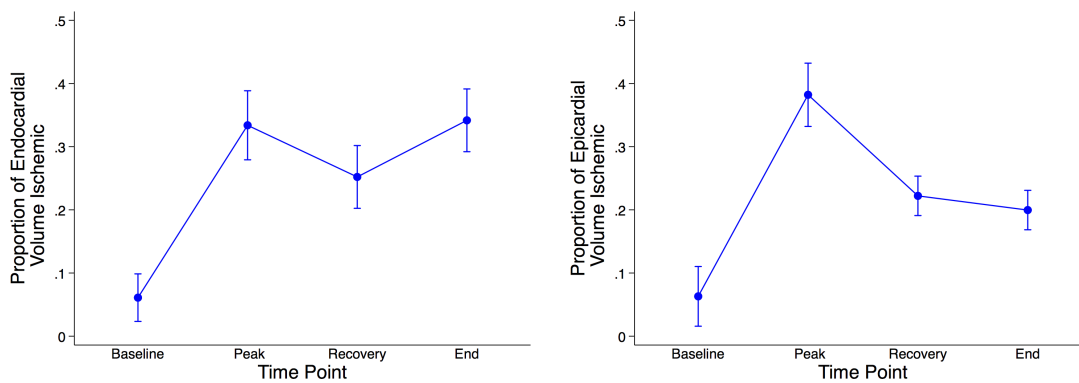


Figure 5.6: Total volume proportion that is ischemic at four time points, baseline, peak epicardial ST40% time, recovered epicardial ST40%, and the end of the ischemic intervention.



(a) Subendocardial volume proportion

(b) Subepicardial volume proportion

Figure 5.7: Subendocardial/midmyocardial and subepicardial ischemic volume proportions at four time points, baseline, peak epicardial ST40% time, recovered epicardial ST40%, and the end of the ischemic intervention.

including changes in intramyocardial conduction speed and regional changes in ischemic potentials within the myocardium. We found the complete recovery of cardiac conduction speed (a surrogate for cellular conductance changes) correlated with recovery of ischemic ST-segment potentials. We also found the recovery of remote ischemic ST-segment potentials was associated with a regional recovery in the subepicardial myocardial tissue, while significant ischemia persisted within the midmyocardial and subendocardial regions.

5.5.1 Transient Recovery of Intramyocardial Conduction Speed During Ischemic Interventions

To pinpoint a possible mechanism for the transient recovery of ischemic potentials, we examined the conduction speed throughout the myocardium during ischemic stress. We found a similar recovery trend in conduction speed as in ischemic potentials on the epicardial and torso surfaces. Specifically, we observed a 50% conduction speed decrease at the peak response time of epicardial ST40% potentials and a near-complete return to baseline conduction speeds at recovery response time. The initial decrease in conduction speed from ischemia is well documented [10], [21]. The subsequent recovery of conduction speed indicates that the electrical function of the cardiomyocyte remained intact, despite persistent ischemic stress.

The conduction speed recovery is a crucial finding to determine a possible recovery mechanism of transient ischemic potentials. Previous research in complete occlusion experimental models has shown a significant decrease in cell-to-cell coupling as the biophysical basis for the decrease in ST40% deviations [6], [8], [9]. Initial deviations of isoelectric ST40% potentials are created by passive injury currents that flow intracellularly from healthy to ischemic tissue through gap junctions [22]. Intracellular conductance decreases significantly during complete occlusion, which correlates with a decrease in the ST-segment ischemic potentials. It has been shown that decreased intracellular conductance decreases injury currents and results in decreased extracellular ST-segment potentials [22]. In our experimental model, conduction speed can be used as a surrogate for cell-to-cell coupling because the rapid propagation of current throughout myocardial tissue is

dependent on cellular coupling via gap junctions. It has been shown that without intact cell-to-cell coupling, conduction speed drops to near zero [6]. Our results, by contrast, show a significant recovery in conduction speed, corresponding to the recovery in ischemic potentials, which suggests cell-to-cell uncoupling is not the primary mechanism for transient recovery of ischemic signals during our simulated cardiac stress tests.

5.5.2 Differences in Recovery of Ischemic Signals Across Intramyocardial Depth

We also examined the changes in ischemic potentials throughout the myocardial volume. When examining the ST40% potential changes based on intramural depth, we found a near-complete recovery in the subepicardial regions with persistent ischemic zones within the midmyocardial and subendocardial regions. We found the subepicardial third displayed almost entirely recovered potentials, whereas the subendocardial two-thirds also recovered, but to a significantly lesser extent. We observed persistent ischemia in the midmyocardial/subendocardial region. On the epicardium, electrodes recorded almost full recovery, suggesting that they sensed relatively healthy underlying tissue. An explanation for this apparent recovery is that the healthy subepicardial region masks the underlying subendocardial ischemic tissue, creating a false negative marker on the epicardial surface for the presence of ischemia within the myocardium.

This subepicardial recovery impacts all remote ischemic potentials recorded from the epicardial and torso surface and provokes exploration of why this region recovers so selectively. A promising mechanism was described by Penny [23] in studies in which guinea pig hearts were Langendorff perfused, and perfusate flow was modulated between no flow and partial flow (10%). Penny observed a peak followed by a significant reduction in ischemic epicardial and action potential changes only during partial flow ischemic episodes. Penny further investigated this phenomenon and isolated catecholamine release as a possible driver for the transient improvement of action potentials and reduced ischemic signals. Specifically, Penny noted a significant reduction in extracellular potassium concentration during the recovery phase of an acute ischemic episode, which was

present only during partial-flow ischemic events. Penny also showed, during an ischemic episode, catecholamine release reduced extracellular potassium concentration. He hypothesized this response was from catecholamines stimulating the sodium-potassium pump, whose activity is diminished during ischemia [23]. In his experiments, removing and blocking catecholamine release resulted in no paradoxical biphasic response on remote recording electrodes, which supports a hypothesis that catecholamine release is a necessary component of the transient ischemic response we observed. The time course of the observations by Penny was similar to our own, in which action potential morphology recovered at approximately 10 minutes into a partial flow ischemic event. We suspect the subepicardial recovery is driven by catecholamine release that restores the electrical state of cardiomyocytes.

5.5.3 Development of Clinical Subendocardial Ischemia

Current clinical dogma dictates the formation of subendocardial ischemia that is driven strictly by differentially reduced nutrient flow to the subendocardial region [11], [24]. This notion is substantiated by previous measurements of decreased blood flow to the subendocardial regions compared to the subepicardial regions, suggesting subendocardial regions will be more affected than subepicardial during an ischemic event. However, our studies over the past 6 years have shown that ischemia can initially develop in localized regions distributed throughout the myocardial wall, i.e., in the subepicardial, midmyocardial, or subendocardial regions [11]. This finding contradicts the clinical dogma and further blurs the notion that ischemia could be described as a simple, perfusion-only-based event.

In this study, we further examined the time course of ischemia development during a clinical cardiac stress test. We showed a preferential *recovery* of the subepicardial region compared to the subendocardium and midmyocardium. This finding suggests subendocardial ischemic development is not driven solely by regional differences in blood flow but requires another critical element. The combination of our results and previous studies highlights catecholamine release as a possible missing element to explain subendocardial ischemia development. In our ex-

tended mechanistic hypothesis, the regional differences in blood flow likely play a role. Subepicardial regions likely deplete the catecholamines quickly, which prevents their protective effect from reaching the subendocardial layers. Therefore, a lack of not only nutrients but also catecholamines reaching the subendocardial regions creates subendocardial ischemia.

Also of note is the finding that recovery of ischemic potentials in the subepicardial region does not mean the ischemic stress has ended or that the tissue is no longer ischemic. Catecholamines on the subepicardial region have been shown to change cardiomyocyte electrical function, not rescue them from ischemic stress [23]. Previous literature has shown that significant damage still occurs within the “recovered” ischemic tissue despite an absence of electrical indication of persistent ischemia [23]. This false recovery of ischemic potentials is another possible mechanism for developing “silent” myocardial ischemia, which is not detected by the epicardial or other remote electrodes, i.e., body-surface ECGs.

5.6 Limitations

This study has some limitations. We do not have direct intracellular conductance measurements for cell-to-cell connectivity; however, the plethora of previous literature has documented a clear correlation between significant conduction delays and cell-to-cell uncoupling [10]. We also were unable to measure catecholamine release directly within the experimental preparation. Furthermore, the natural sympathetic and parasympathetic responses that lead to catecholamine enhancement could have been altered by the deep anesthesia during the experiments.

5.7 Acknowledgments

We want to acknowledge the support from the Nora Eccles Treadwell Cardiovascular Research and Training Institute staff, including Jayne Davis, Ala Booth, Wilson Lobaina, and Bruce Steadman, for preparing and maintaining equipment and coordinating experiment logistics.

5.8 Grant Support

Support for this research came from the NIH NHLBI grant no. 1F30HL149327; NIH NIGMS Center for Integrative Biomedical Computing (www.sci.utah.edu), NIH NIGMS grants P41GM103545 and R24 GM136986; and the Nora Eccles Treadwell Foundation for Cardiovascular Research.

5.9 References

- [1] B. Safdar, P. Ong, and P. G. Camici, "Identifying myocardial ischemia due to coronary microvascular dysfunction in the emergency department: introducing a new paradigm in acute chest pain evaluation," *Clin. Therapeutics*, pp. 1–11, Nov. 2018. doi: <http://dx.doi.org/10.1016/j.clinthera.2018.09.010>.
- [2] F. A. Bhuiya, S. R. Pitts, and L. F. McCaig, "Emergency department visits for chest pain and abdominal pain: United States, 1999–2008," *NCHS Data Brief*, no. 43, pp. 1–8, Sep. 2010.
- [3] J. Cinca, M. J. Janse, H. Morena, J. Candell, V. Valle, and D. Durrer, "Mechanism and time course of the early electrical changes during acute coronary artery occlusion," *Chest*, vol. 77, no. 4, pp. 499–505, Apr. 1980. doi: <http://dx.doi.org/10.1378/chest.77.4.499>.
- [4] G.-X. Yan, A. Joshi, D. Guo, T. Hlaing, J. Martin, X. Xu, and P. R. Kowey, "Phase 2 reentry as a trigger to initiate ventricular fibrillation during early acute myocardial ischemia," *Circ.*, vol. 110, no. 9, pp. 1036–1041, Aug. 2004. doi: <http://dx.doi.org/10.1161/01.CIR.0000140258.09964.19>.
- [5] B. M. C. Noel, P. C. J., W. M. Norine, F. J. L., C. P. G., C. W. M., C. J. Austin, C. L. S., C. Filippo, D. C. Marcelo, D. P. S., G. Z. S., G. Paul, H. E. M., H. Ahmed, H. J. A., H. J. S., I. Erin, K. Ruth, L. G. N., L. Peter, L. Joao, M. Puja, D.-N. Patrice, O. Michelle, P. G. D., Q. A. A., R. Harmony, R. British, S. George, T. Viviany, W. Janet, and W. Nanette, "Ischemia and no obstructive coronary artery disease (INOCA)," *Circ.*, vol. 135, no. 11, pp. 1075–1092, Mar. 2017. doi: <http://dx.doi.org/10.1161/CIRCULATIONAHA.116.024534>.
- [6] J. Degroot and R. Coronel, "Acute ischemia-induced gap junctional uncoupling and arrhythmogenesis," *Circ. Res.*, vol. 62, no. 2, pp. 323–334, May 2004. doi: <http://dx.doi.org/10.1016/j.cardiores.2004.01.033>.
- [7] J. Cinca, M. Warren, M. Tresanchez, L. Armadans, P. Gomez, and J. Soler-Soler, "Changes in myocardial electrical impedance induced by coronary artery occlusion in pigs with and without preconditioning: Correlation with local ST-segment potential and ventricular arrhythmias," *Circ.*, vol. 96, pp. 3079–3086, Nov. 1997.
- [8] A. Kléber, M. Janse, F. van Capelle, and D. Durrer, "Mechanism and time course of ST- and TQ-segment changes during acute regional myocardial

ischemia in the pig heart determined by extracellular and intracellular recordings," *Circ. Res.*, vol. 42, pp. 603–613, May 1978.

- [9] A. Kléber, C. Riegger, and M. Janse, "Electrical uncoupling and increase of extracellular resistance after induction of ischemia in isolated, arterially perfused rabbit papillary muscle," *Circ. Res.*, vol. 61, pp. 271–279, Aug. 1987.
- [10] A. Kléber, M. Janse, F. Wilms-Schopmann, A. Wilde, and R. Coronel, "Changes in conduction velocity during acute ischemia in ventricular myocardium of the isolated porcine heart," *Circ.*, vol. 73, pp. 189–198, Jan. 1986.
- [11] K. Aras, B. Burton, D. Swenson, and R. MacLeod, "Spatial organization of acute myocardial ischemia," *J. Electrocardiol.*, vol. 49, no. 3, pp. 689–692, May 2016.
- [12] P. M. Okin, O. Ameisen, and P. Kligfield, "A modified treadmill exercise protocol for computer-assisted analysis of the ST segment/heart rate slope: Methods and reproducibility," *J. Electrocardiol.*, vol. 19, no. 4, pp. 311–318, Oct. 1986. doi: [http://dx.doi.org/10.1016/S0022-0736\(86\)81058-5](http://dx.doi.org/10.1016/S0022-0736(86)81058-5).
- [13] J. Bartunek, W. Wijns, G. R. Heyndrickx, and B. de Bruyne, "Effects of dobutamine on coronary stenosis physiology and morphology," *Circ.*, vol. 100, no. 3, pp. 243–249, Jul. 1999. doi: <http://dx.doi.org/10.1161/01.CIR.100.3.243>.
- [14] B. Zenger, W. Good, J. Bergquist, B. Burton, J. Tate, L. Berkenbile, V. Sharma, and R. MacLeod, "Novel experimental model for studying the spatiotemporal electrical signature of acute myocardial ischemia: a translational platform." *J. Physiol. Meas.*, vol. 41, no. 1, p. 015002, Feb 2020.
- [15] B. Zenger, J. A. Bergquist, W. W. Good, L. C. Rupp, and R. S. MacLeod, "High-capacity cardiac signal acquisition system for flexible, simultaneous, multidomain acquisition," in *2020 Computing in Cardiol.*, Sep. 2020. doi: <http://dx.doi.org/10.22489/CinC.2020.190>. pp. 1–4.
- [16] A. Rodenhauer, W. Good, B. Zenger, J. Tate, K. Aras, B. Burton, and R. MacLeod, "PFEIFER: Preprocessing framework for electrograms intermittently fiducialized from experimental recordings," *J. Open Source Software*, vol. 3, no. 21, p. 472, 2018.
- [17] J. A. Bergquist, W. W. Good, B. Zenger, J. D. Tate, and R. S. MacLeod., "GRÖMeR: A pipeline for geodesic refinement of mesh registration," in *Lecture Notes in Computer Science*, vol. 11504, Functional Imaging and Model of the Heart (FIMH). Springer Verlag, Jun. 2019, pp. 37–45.
- [18] A. Neic, F. O. Campos, A. J. Prassl, S. A. Niederer, M. J. Bishop, E. J. Vigmond, and G. Plank, "Efficient computation of electrograms and egs in human whole heart simulations using a reaction-eikonal model," *Journal of computational physics*, vol. 346, pp. 191–211, 2017.

- [19] J. Bayer, A. J. Prassl, A. Pashaei, J. F. Gomez, A. Frontera, A. Neic, G. Plank, and E. J. Vigmond, "Universal ventricular coordinates: A generic framework for describing position within the heart and transferring data," *J. Med. Img. Anal.*, vol. 45, pp. 83–93, 2018.
- [20] W. W. Good, K. Gillette, J. A. Bergquist, B. Zenger, L. C. Rupp, J. Tate, D. Anderson, G. Plank, , and R. S. MacLeod, "Estimation and validation of cardiac conduction velocity and wavefront reconstruction using epicardial and volumetric data," *IEEE Transactions in Biomedical Engineering*, p. In Preparation, 2020.
- [21] W. W. Good, B. Erem, J. Coll-Font, B. Zenger, J. A. Bergquist, D. Brooks, , and R. S. MacLeod, "Characterizing the transient electrocardiographic signature of ischemic stress using laplacian eigenmaps for dimensionality reduction," *IEEE Transactions in Biomedical Engineering*, p. In Preparation, 2020.
- [22] D. C. Russell, J. S. Lawrie, R. A. Riemersma, and M. F. Oliver, "Mechanisms of phase 1a and 1b early ventricular arrhythmias during acute myocardial ischemia in the dog," *Am. J. Cardiol.*, vol. 53, no. 2, pp. 307–312, Jan. 1984. doi: [http://dx.doi.org/10.1016/0002-9149\(84\)90444-2](http://dx.doi.org/10.1016/0002-9149(84)90444-2).
- [23] W. J. Penny, "The deleterious effects of myocardial catecholamines on cellular electrophysiology and arrhythmias during ischaemia and reperfusion," *Europ. Heart J.*, vol. 5, no. 12, pp. 960–973, Dec. 1984. doi: <http://dx.doi.org/10.1093/oxfordjournals.eurheartj.a061616>.
- [24] R. Holland and H. Brooks, "TQ-ST segment mapping: Critical review and analysis of current concepts," *Am. J. Cardiol.*, vol. 40, no. 1, pp. 110–129, Jul. 1977.

CHAPTER 6

CONCLUDING REMARKS

6.1 Development of a Translational Experimental Model

The first aim of this dissertation research was to refine the experimental model of partial occlusion acute myocardial ischemia in order to include torso surface recordings and thus simulate clinical cardiac stress tests. First, we had to modify and construct new intramural plunge needle arrays. These arrays had to be compact to limit contact with other thoracic organs during the chest closure. Furthermore, the chest closure had to be scrupulous to limit the damage to surrounding organs and remove artifacts from the air remaining in the torso. Following the experimental procedure, we then had to identify each recording electrode location within the heart, on the heart surface, and the torso surface. To do this, we incorporated postmortem whole-body MRI imaging. We could isolate the general location of electrodes on the torso surface, within the heart, and markers from the epicardial sock array from these images.

To support these new, comprehensive experiments, we have developed three *de novo* processing tools and created succinct pipelines based on six open-source software packages. Following each experiment, we had to process the experimental data, register geometries, and visualize results, tasks for which few standard tools available. We refined our signal processing and filtering approaches for our experiments, including automatic electrogram annotation and filtering [1]. We then developed a registration technique to link the *ex vivo* high-resolution imaging with the *in vivo* postmortem scans. Finally, we significantly improved the epicardial sock registration technique by incorporating nonrigid energy-based deformations [2]. The resulting pipeline was essential for the studies described here and also forms an enabling legacy for future studies and so marks a substantial

contribution.

Another essential facet of translational models is animal species selection. In our case, several differences between animals guided our selection. The two best species for our experimental preparation and scientific questions were dogs or pigs. Both species have similar cardiovascular systems compared to humans in terms of relative size, shape, and gross anatomy [3]. Pigs and dogs have several known cardiovascular differences, including the location of Purkinje fibers and collateral vessels [3]. Other important considerations for our application were species stability in the face of experimental stresses and torso anatomy in the context of re-closing the chest cavity. We have found that dogs provide significantly more stable animal models of ischemia than pigs and have lower complication and attrition rates. While incompletely characterized, we hypothesize that the lack of collateral blood flow and mid-wall Purkinje system make pigs significantly more vulnerable during acute myocardial ischemia. By switching from young, domestic pigs, to mature Yucutan minipigs, we reduced the impact of these liabilities and achieved similar attrition rates and stability compared to dogs throughout repeated episodes of ischemia. The increased age of the minipigs could explain these improvements. Another important difference between pigs and dogs is the torso anatomy. The body habitus of pigs makes the chest closure simpler than dogs, which have a large "barrel" chest and overlapping lungs that make it difficult to remove the residual air. Based on the stability and similar torso structure, we chose the Yucutan minipig species for our studies.

We also designed the experiments described here to have more focused and consistent protocols to answer a specific set of scientific questions than previous studies that improved general understanding of acute myocardial ischemia. In those previous studies, Aras et al. demonstrated the ability to accurately detect and localize ischemia within the myocardial wall throughout an ischemic episode [4]. Using these initial findings, we designed and developed focused questions that were repeatably tested using our experimental ischemia model. In this doctoral work, we repeated identical ischemic protocols across nearly all animal experiments, each designed to answer specific scientific questions. As a consequence,

the results can be easily compared and compiled to assess trends and provide statistical analysis power.

A challenge in any experiment preparation is developing strategies to reduce attrition, maximize stability, and ultimately reduce any unnecessary use of animals. To achieve these goals, we implemented an animal stability test at the beginning of each experiment, which allowed us to calibrate the maximum ischemic load each animal could survive without showing adverse effects such as excessive arrhythmias and even fibrillation. These tests were vital to ensure the animals survived the barrage of ischemic episodes that followed. These tests also helped us identify unique, animal-specific markers of ischemic instability that could be tracked throughout the experiment.

Another challenge of all experiments on living organisms is animal-to-animal variability. To reduce this variability, we selected a consistent species of pig, at similar weights and ages. Still, we found significant differences between the coronary anatomy, skin texture, and overall appearance of each animal. Any such variability, especially in coronary anatomy, is a significant confounding factor when comparing results across studies. To reduce the effects of these differences, we implemented several pipeline techniques to register and localize ischemic tissue in a normalized approach. Specifically, we implemented universal ventricular coordinates (UVCs) to compare ischemic sites and zones from one animal heart to another [5]. Furthermore, we selected metrics and statistics that would minimize the impact of variability across animals, e.g., using the UVCs to normalize locations of ischemia.

Finally, all large-scale animal models require extensive and elaborate experimental recording equipment. In our studies, we recorded from 1024 channels at 1 kHz sampling frequency. During this dissertation period, we replaced a custom-designed system based on 30-year-old technology [6] with a new system based on contemporary electronics and acquisition techniques [7]. We have several options to consider when designing experimental recording equipment. First, buying a full commercial system with integrated software and hardware would require the least initial design and prototype work. However, commercial systems can be

expensive because of their limited market, and usually have limited flexibility to sample signals outside of the predetermined purpose. In our case, we had to record samples from within the myocardium, on the heart surface, and on the torso surface, which created a wide range of signal amplitudes. Furthermore, commercial systems can be difficult to connect to custom electrode arrays and connectors. Therefore, our approach was to link a commercially available system for neural recordings combined with custom circuitry that included a step-down in amplitude, cardiac-specific filtering, and defibrillation protection. We performed several tests to compare the new system recordings to those from the previous system to verify signal quality and stability based on signals from a signal generator, ECGs, and animal experiments. We published our approach and findings in a recent conference proceeding [7].

6.2 Contributions to Knowledge of Acute Myocardial Ischemia Development

In this dissertation, we examined acute myocardial ischemia using translational models and made two critical findings that further our understanding of the nature of electrical effects during episodes of acute myocardial ischemia.

The first finding showed differences in ischemic zones and signatures that develop during dobutamine and simulated exercise stress. Current clinical standards already use 12-lead ECG measurements and ultrasound echocardiography for exercise and pharmacological stress tests, respectively. The fundamental reason for a test or stress type performing better than another was not clearly defined. The differences we observed in electric potentials appeared both within the myocardium and on the epicardial surface. Clinically, our findings do not indicate that one stress technique is superior to another. However, they suggest possible advantages to selecting the best observation modality for a given stress type. In our studies, we showed exercise testing produced more clinically detectable ischemia from ECG measurements than did dobutamine. Furthermore, we have novel evidence to suggest a unique physiological mechanism that may explain the differences we observed.

The second important observation from this dissertation provides a possible mechanistic explanation for the development of subendocardial ischemia. The previous reasoning for nontransmural ischemia being limited to the subendocardium is that this region is furthest downstream from the epicardial coronary vessels and hence experiences the most reduced perfusion when coronary flow is limited [8], [9]. The electrocardiographic result is the appearance of nonspecific ST-depressions during clinical stress tests [8], [9]. However, previous results from our group have demonstrated repeatedly that during the hyperacute phase, ischemic zones develop throughout the myocardium [4], [10], [11]. Although other authors have also described subendocardial ischemia in experimental models, the mechanism of development remains unclear [12]–[14].

In this dissertation, we propose an alternative explanation for the development of subendocardial ischemia formation. This mechanism is fully compatible with our previous results acquired during the very earliest phases of ischemia, and may also explain the largely subendocardial ischemia described by others. Our findings suggest that ischemia development is more complicated than a perfusion mismatch and hypothesize that catecholamines are more concentrated at the epicardial surface, which drives and apparent recovery of epicardial electrical activity. During a perfusion deficit, catecholamines cannot reach deeper parts of the heart; therefore, subendocardial tissue continues to generate injury currents. Under this hypothesis, the apparent recovery of subepicardial tissue is likely not from an increase in perfusion to the region but the cellular effects of catecholamines, which are known to hyperpolarize the resting potentials of cardiomyocytes. This cellular effect pulls the resting potentials of ischemic cells closer to normal resting values, enabling a restoration of voltage-gated ion channel function. These findings suggest that while the catecholamines reduce or eliminate injury currents (and the associated ST deviations), the subepicardial tissue is still ischemic [15].

6.3 Providing Meaningful Clinical Insights From Experimental Studies

Several elements of almost all experimental models challenge their translation to meaningful clinical insights. First, during experiments, one can control many confounders and reduce outside noise. In our case, detailed experimental planning and concrete repetition of experiments allow us to extract critical measurements accurately and reproducibly, and trends can emerge. However, examining experimentally identified trends in the context of the clinical questions is crucial to extrapolate information faithfully from animal models to humans. Such extrapolation may overstate the conclusions or trends isolated experimentally, often because of differences between human and animal physiology, some of which are known and others as yet unknown. Furthermore, in several circumstances, the observations may be interesting scientifically; however, the clinical result is almost entirely meaningless, i.e., it will not change the resultant diagnosis or treatment.

In experiments, measuring all the relevant parameters is impossible, so we also had to balance competing challenges and goals. We focused on the electrical changes of the heart during acute myocardial ischemia; therefore, our recording equipment and preparation were designed to measure electrical signals with the goal of achieving adequate sampling rates, densities, and coverage of the heart and thorax. We naturally relied on previous studies that correlated, associated, or mechanistically described the relationships among parameters and inferred plausible explanations. For example, our studies examined changes in electrical parameters such as conduction velocity and ischemic potential gradients as manifestations of cellular uncoupling or microvascular dysfunction, respectively. Although these are not direct measures of the underlying behavior, they suggest relationships built upon previous studies. This technique of performing translational research is one of the most fruitful and meaningful ways to quickly assess mechanistic changes in a translatable model to clinical medicine.

Finally, we consider fundamental role of interdisciplinary teams and collaborating across the scientific and clinical specialties. Since the beginning of my dissertation work, I was driven to test meaningful clinical hypotheses that would

directly affect patient care. However, after my doctoral training, I have changed my approach. Exploring for exploring's sake has immense value. These explorations may or may not immediately provide clinical impact but may develop future hypotheses that drive more studies in the long term. Direct clinical research is valuable to correlate and stratify patient risk. In an ideal world, these ideas and collaborations should flow back and forth with mechanistic studies feeding more clinical studies and clinical studies feeding mechanistic examination. As a dual-degree student, the ideas of both clinical evaluation and mechanistic determination should sit at the forefront of most of my projects in the future. The ability to dance between the two domains will drive significant scientific discovery and improve human health.

6.4 Future Work

6.4.1 Further Experimental Model Refinement

Several key elements could be improved in the current experimental preparation. First, the registration and modeling pipeline still suffers from errors related to the sock registration on the heart surface. Ideally, more MRI correspondence points from imaging would contribute to a better epicardial sock registration. Careful design of MRI compatible contrast markers could selectively increase the accuracy of these registrations. Another important change would be to the model of occlusion. In our protocols, we relieved occlusion after each ischemic episode and began recording immediately after occlusion at the start of each simulated episode. Future work could incorporate a progressive occlusion onset or an occlusion stabilization period before increasing the heart rate with drugs or pacing.

Another important experimental modification would be to measure mechanical changes during episodes of acute myocardial ischemia. Clinically, ultrasound echocardiography is used to identify myocardial tissue regions that are not contracting correctly during cardiac stress [16]–[18]. Incorporating echocardiography measurements into the experimental model while still recording electrical signals in high resolution would be a fruitful if technically challenging innovation. The potential artifacts generated from the intramural and epicardial recording arrays

may limit this application, so further studies must identify if the artifact is substantial and if different materials or array resolutions could be used to limit the presence of artifacts.

6.4.2 Detecting and Quantifying Microvascular Dysfunction

As we indicated in Chapter 4, we suspect differences in microvascular dysfunction drive the significant differences in electrical potentials seen between dobutamine and simulated exercise stress types. To test this hypothesis thoroughly, we would measure the coronary vascular resistance downstream from the occlusion site to determine if microvascular dysfunction exists in either stress type. Such measurements could also be coupled with measurements of the mechanical impact of varying levels of microvascular dysfunction. We hypothesize that echocardiographic resolution will be insufficient to detect microvascular dysfunction directly because regions of ischemic and healthy tissue are interspersed, and wall motion abnormalities will be blurred over large amounts of space. However, there may well be macroscopic affects visible with ultrasound-based approaches.

6.4.3 Detecting and Quantifying Catecholamine Release and Ischemic Recovery

As discussed Chapter 5, we suspect catecholamine release plays a role in the paradoxical recovery of ischemic potentials during a cardiac stress test. To test this hypothesis, we plan to measure the catecholamine release throughout the ischemic episode and relate ischemic changes to the relative concentrations of catecholamines in the blood. To perform this study, the sampling frequency required to accurately reconstruct catecholamine changes would need to be identified. Additionally, directly controlling catecholamine release through drug infusion is important to stimulate or inhibit catecholamine targets during an ischemic episode.

6.4.4 Determining Ischemic Load Function

We have previously attempted to create a function that predicts the amount of ischemia present based on several key physiological parameters, such as time, occlusion percentage, heart rate, etc. However, many of these studies have been

unsuccessful. To improve on previous examinations, future experimental studies must be designed to explore each physiological parameter space. Additionally, more recorded physiological parameters should be recorded and modulated, such as blood pressure, systemic pCO₂, and catecholamine concentration. Finally, multiple model types relating each physiological parameter (linear vs. piece-wise or others) should be tested to determine the ideal approach.

6.4.5 Arrhythmia Formation During Ischemic Episodes

Another important and active area of research is arrhythmias that develop during episodes of acute myocardial ischemia. Ischemia can create an ideal environment for cardiac arrhythmias to form. Specifically, ischemia changes the electrical substrate of the myocardium by slowing conduction, changing refractory periods, or blocking electrical function altogether. Furthermore, injury currents or other re-entry circuits can develop and create an electrical trigger. The combination of the electrical substrate and trigger is one of the necessary components for a cardiac arrhythmia to form.

In many cases, the resultant arrhythmia from an acute ischemic event is sudden cardiac death. However, our mechanistic understanding of how arrhythmias form during partial occlusion ischemic events is incomplete. The experimental model refined and discussed in this dissertation could provide further insights into arrhythmia development, including potential mechanistic drivers for arrhythmia formation during acute myocardial ischemia. We observed consistent time points when arrhythmias initiate most frequently. Future studies will examine these “vulnerable” periods for both trigger initiation and substrate changes. A combination of conduction velocity, wave propagation, tissue recovery, and injury currents could significantly improve our understanding of arrhythmias during acute myocardial ischemia.

6.5 References

- [1] A. Rodenhauer, W. Good, B. Zenger, J. Tate, K. Aras, B. Burton, and R. MacLeod, “PFEIFER: Preprocessing framework for electrograms intermittently fiducialized from experimental recordings,” *J. Open Source Software*,

vol. 3, no. 21, p. 472, 2018.

- [2] J. A. Bergquist, W. W. Good, B. Zenger, J. D. Tate, and R. S. MacLeod., "GRÖMeR: A pipeline for geodesic refinement of mesh registration," in *Lecture Notes in Computer Science*, vol. 11504, Functional Imaging and Model of the Heart (FIMH). Springer Verlag, Jun. 2019, pp. 37–45.
- [3] B. Zenger, W. W. Good, J. A. Bergquist, B. M. Burton, J. D. Tate, L. Berkenbile, V. Sharma, and R. S. MacLeod, "Novel experimental model for studying the spatiotemporal electrical signature of acute myocardial ischemia: A translational platform," vol. 41, no. 1, p. 15002, Dec. 2020. doi: <http://dx.doi.org/10.1088/1361-6579/ab64b9>.
- [4] K. Aras, B. Burton, D. Swenson, and R. MacLeod, "Spatial organization of acute myocardial ischemia," *J. Electrocardiol.*, vol. 49, no. 3, pp. 689–692, May 2016.
- [5] J. Bayer, A. J. Prassl, A. Pashaei, J. F. Gomez, A. Frontera, A. Neic, G. Plank, and E. J. Vigmond, "Universal ventricular coordinates: A generic framework for describing position within the heart and transferring data," *J. Med. Img. Anal.*, vol. 45, pp. 83–93, 2018.
- [6] P. Ershler, R. Lux, and B. Steadman, "A 128 lead online intraoperative mapping system," in *Proceedings of the IEEE Engineering in Medicine and Biology Society 8th Annual International Conference*. IEEE Press, Jan. 1986, pp. 1289–1291.
- [7] B. Zenger, J. A. Bergquist, W. W. Good, L. C. Rupp, and R. S. MacLeod, "High-capacity cardiac signal acquisition system for flexible, simultaneous, multidomain acquisition," in *2020 Computing in Cardiol.*, Sep. 2020. doi: <http://dx.doi.org/10.22489/CinC.2020.190>. pp. 1–4.
- [8] R. Holland and H. Brooks, "Spatial and nonspatial influences on the tq-st segment deflection of ischemia," *J. Clin. Invest.*, vol. 60, no. 1, pp. 197–214, Jul. 1977.
- [9] —, "TQ-ST segment mapping: Critical review and analysis of current concepts," *Am. J. Cardiol.*, vol. 40, no. 1, pp. 110–129, Jul. 1977.
- [10] K. Aras, D. Swenson, and R. MacLeod, "The origin of myocardial ischemia is not limited to the sub-endocardium," in *International Society for Computerized Electrocardiology (ISCE)*, 2011.
- [11] —, "Heterogeneous electrographic myocardial response during ischemia," *J. Electrocardiol.*, vol. 44, no. 6, p. 748, 2011.
- [12] J. Degroot and R. Coronel, "Acute ischemia-induced gap junctional uncoupling and arrhythmogenesis," *Circ. Res.*, vol. 62, no. 2, pp. 323–334, May 2004. doi: <http://dx.doi.org/10.1016/j.cardiores.2004.01.033>.

- [13] J. Cinca, M. Warren, M. Tresanchez, L. Armadans, P. Gomez, and J. Soler-Soler, "Changes in myocardial electrical impedance induced by coronary artery occlusion in pigs with and without preconditioning: Correlation with local ST-segment potential and ventricular arrhythmias," *Circ.*, vol. 96, pp. 3079–3086, Nov. 1997.
- [14] A. Kléber, M. Janse, F. van Capelle, and D. Durrer, "Mechanism and time course of ST- and TQ-segment changes during acute regional myocardial ischemia in the pig heart determined by extracellular and intracellular recordings," *Circ. Res.*, vol. 42, pp. 603–613, May 1978.
- [15] W. J. Penny, "The deleterious effects of myocardial catecholamines on cellular electrophysiology and arrhythmias during ischaemia and reperfusion," *Europ. Heart J.*, vol. 5, no. 12, pp. 960–973, Dec. 1984. doi: <http://dx.doi.org/10.1093/oxfordjournals.eurheartj.a061616>.
- [16] S. Stern, "State of the art in stress testing and ischaemia monitoring." *Card. Electrophysiol. Rev.*, vol. 6, no. 3, pp. 204–208, Sep. 2002.
- [17] B. Safdar, P. Ong, and P. G. Camici, "Identifying myocardial ischemia due to coronary microvascular dysfunction in the emergency department: introducing a new paradigm in acute chest pain evaluation," *Clin. Therapeutics*, pp. 1–11, Nov. 2018. doi: <http://dx.doi.org/10.1016/j.clinthera.2018.09.010>.
- [18] J. Knuuti, H. Ballo, L. E. Juarez-Orozco, A. Saraste, P. Kolh, A. W. S. Rutjes, P. Jüni, S. Windecker, J. J. Bax, and W. Wijns, "The performance of non-invasive tests to rule-in and rule-out significant coronary artery stenosis in patients with stable angina: A meta-analysis focused on post-test disease probability," *Europ. Heart J.*, vol. 39, no. 35, pp. 3322–3330, Sep. 2018. doi: <http://dx.doi.org/10.1093/eurheartj/ehy267>.